FOR REFERENCE

NOT TO BE TAKEN FROM THIS ROOM

ANALYSIS OF MODE III INTERLAMINAR FRACTURE TOUGHNESS OF COMPOSITE MATERIALS

by

M. Gökhan GÖKÇEN

B.S. in M.E., Boğaziçi University, 1996

Submitted to the Institute for Graduate Studies in

Science and Engineering in partial fulfillment of

the requirements for the degree of

Master of Science

in

Mechanical Engineering

Bogazici University Library

39001100544900

Boğaziçi University

1999

ACKNOWLEDGMENTS

I would like to express my sincere gratitude to Assoc. Prof. Vahan Kalenderoğlu, who has supervised my thesis.

I would also like to thank to Prof. Öktem Vardar and Prof. Gülay Altay for their interest.

ABSTRACT

The demand for advanced materials stimulates the research on composite materials, which provide high stiffness accompanied with high toughness. One major failure type of fiber-reinforced composite materials is delamination or interlaminar fracture, which can be analyzed in three modes employing fracture mechanics. Although testing of mode I and mode II fracture toughnesses are well established, the characterization of mode III fracture toughness is still to be refined. The edge crack torsion (ECT) specimen seems to be the most promising configuration.

In this thesis a three dimensional finite element model of the edge crack torsion (ECT) specimen having a stacking sequence of $[90/(\pm 45)_3/(\mp 45)_3/90]_s$ is developed. Using virtual crack closure technique, distribution of the individual components of strain energy release rate along the crack front is obtained and the percentage of mode III component of strain energy release rate, G_{III}, is determined. Several finite element models are constructed to investigate the effect of specimen dimensions on the percentage of mode III component of strain energy release rate, G_{III}, intending to contribute to the optimization of the edge crack torsion (ECT) specimen.

The results of finite element analysis revealed that the percentage of mode III component of strain energy release rate, G_{III}, extends up to 98 per cent with increasing length and decreasing width. The corresponding length is 133.4 mm and the width is 19.1mm. The proposed dimensions will provide necessary data to redesign the fixture for the interlaminar fracture toughness in mode III using edge crack torsion (ECT) specimen.

ÖZET

TABAKALI LAMİNATLARIN MOD III KIRILMA ANALİZİ

İleri malzemelere duyulan ihtiyaç, yüksek tokluk ile beraber yüksek esneklik sağlayan kompozit malzemelerin araştırılmasını teşvik etmektedir. Fiber-destekli kompozit malzemelerin önemli bir hasar tipi de kırılma mekaniği ile üç mod halinde incelenebilen delaminasyondur veya tabakalar arası kırılmadır. Mod I ve mod II kırılma tokluğu testleri kesinleşmesine rağmen, mod III kırılma tokluğunun karakterize edilmesi daha fazla araştırılmalıdır. Kenardaki çatlak burulma (ECT) numunesi en fazla ümit vaad eden konfigrasyon olarak gözükmektedir.

Bu tezde, tabaka düzeni $[90/(\pm 45)_3/(\mp 45)_3/90]_s$ olan kenardaki çatlak burulma (ECT) numunesinin üç boyutlu sonlu eleman modeli geliştirilmiştir. Sanal çatlak kapanma metodu ile her bir gerinim enerjisi açığa çıkma hızı, G, komponenti çatlak boyunca hesaplanmıştır ve gerinim enerjisi açığa çıkma hızının mod III komponentinin, G_{III}, yüzde olarak oranı bulunmuştur. Birkaç sonlu eleman modeli kurularak numune boyutlarının; gerinim enerjisi açığa çıkma hızının mod III komponentinin, G_{III}, yüzde olarak oranına etkisi incelenerek, kenardaki çatlak burulma (ECT) numunesinin optimizasyonuna katkıda bulunma hedeflenmiştir.

Sonuçlara bakıldığında gerinim enerjisi açığa çıkma hızının mod III komponentinin, G_{III}, yüzde olarak oranı artan uzunluk ve azalan en ile yüzde 98'lere varmaktadır. Buna karşılık gelen uzunluk 133.4 mm ve genişlik 19.1 mm'dir. Önerilen boyutlar, tabakalı laminatların mod III kırılma testinin kenardaki çatlak (ECT) numunesi kullanılarak yapılabilmesi için deney düzeneğinin yeniden tasarlanmasına imkan verecektir.

TABLE OF CONTENTS

LIST OF FIGURES

LIST OF TABLES

1. INTRODUCTION

Search for advanced materials is the search for materials which provide the prescribed properties. The development of composite materials was a response to the needs of high technology. Opposite materials -regarding their properties- are combined as a compliant matrix reinforced with stiff and strong elements. This idea was borrowed from nature -the leaves and stalks of plant, human and animal bones are anisotropic materials reinforced by fibers, i.e., composite materials.

They can be defined as the macroscopic combination of two or more distinct materials, which have a recognizable interface. The main use of composite materials is due to their structural properties. Common reinforcement materials are glass, carbon, boron, aramid, siliconcarbide, aluminumoxide, etc. As matrix materials polyester, vinylester, epoxy, bismaleimide, polyimide and thermoplastic resins such as (PEEK) are widely used.

One simple classification of composite materials is to divide them according to their reinforcement types:

(a) particulate-reinforced composite materials,

(b) fiber-reinforced composite materials, and

(c) laminated composite materials.

Fiber-reinforced composite materials can be further separated into those containing continuos or discontinuous fibers.

If the reinforcement has all of its dimensions almost equal, than it is called particulate-reinforced composite material. The particles may have the shape of a sphere, rod, flake, etc. The reinforcement may be structural or the particles may improve nonstructural properties such as fire resistance, thermal conductivity etc. The materials that

are produced by adding of filling particles to polymers in order to decrease cost are generally not considered as particulate composite materials.

A reinforcement is called to be fiber if its length is much greater than their cross-sectional dimensions. A composite material having such a reinforcement is considered to be discontinuous fiber or short fiber composite if its properties vary with fiber length. If the properties of the fibers do not change with length than these composite materials are considered to be continuous fiber composites. Most continuous fiber composites, in fact, contain fibers that are comparable in length to the overall dimensions of the composite part.

Laminated composite materials are those composed of two or more layers with two of their dimensions being much more greater than their third dimension. Complicating the definition of a composite material as having both continuous and discontinuous phases is the fact that in a laminated composite material, neither of these phases may be regarded as truly continuous in three dimensions.

The advanced fibrous composite materials are heterogeneous anisotropic materials. The elasticity and the inelasticity of fibrous composites are governed by the type of the fiber-reinforcement (glass, boron, carbon and organic) and matrix (polymer, carbon, metallic and ceramic), the extend of their interaction in composite materials, and also by the angle of load application relative to the reinforcement directions. Composite materials have heterogeneities at two levels:

(a) micro-heterogeneities; a single ply composed of fibers and matrix

(b) macro-heterogeneities; laminate composed of plies with an arbitrary lay-up through the thickness of the laminate.

High-performance composite materials will become much important in the applications because they have superior performance compared to conventional structural materials such as steel and aluminum alloys. They were developed because no single, homogeneous structural material could be found that had all the desired attributes for a given application. For example, aluminum alloys replaced steel especially in aerospace

industry because they provide high strength and high stiffness at low weight. But they suffered from corrosion and fatigue. This lead to the development of fiber-reinforced composites. Although recent improvements of metallic materials have led to some solutions of their problems, fiber-reinforced composite materials still provide other substantial benefits to engineers and manufacturers.

Almost all high-strength/high-stiffness materials fail because of the propagation of cracks. A fiber of such a material is inherently stronger than the bulk form, because the size of a crack is limited by the small diameter of the fiber. Moreover, if equal volumes of fibrous and bulk material are compared, it is found that even if a crack does produce failure in a fiber, it will not propagate to fail the entire assemblage of fibers, as would happen in the homogenous material. In addition, preferred orientation may be used (as in aramid and carbon fibers) to increase the modulus in a specific direction, and perhaps strength, well above isotropic values. When this material is also lightweight, there is a tremendous potential advantage in strength-to-weight and/or stiffness-to-weight ratios over conventional materials. Favorable fiber properties can be carried into practical applications when the fibers are embedded in a matrix that binds them together, transfers load to and between the fibers, and provides protection against environment and handling. Furthermore, fiber-reinforced composite materials are ideally suited where weight is critical. The high strengths and moduli of these composite materials can be tailored to the high load directions, with little material wasted on needles reinforcement (Reinhart, 1987).

2. DAMAGE OF COMPOSITE MATERIALS

Like metals, composite materials are also notch sensitive and loose much of their structural integrity when damaged. Damage can be introduced during manufacturing or during service. The manufacturing defects may be in the form of delamination and voids due to improper lamination and curing or damage may be introduced while machining the components for fastener holes and design cutouts etc. Also the damages during manufacture or maintenance may be caused by even dropping tools accidentally. The service damage may result from various kinds of impacts.

Composite materials failure mode characterization is complicated by the number and complexity of fracture mechanisms exhibited by composites. By definition composite materials are heterogeneous. Furthermore, the individual lamina that constitute a laminated continuous fiber reinforced composite are anisotropic. Therefore the damage of a composite component is quite different from the damage of a metallic component. There is no single, self similar propagating crack as in metals, but rather, the damage zone is characterized by matrix cracking, fiber breakage, and delamination, which ultimately combine to yield component failure.

The failure may initiate from interlaminar stresses created by impacts, eccentricities in structural load paths or from discontinuities in the structure. Besides mechanical loads, the moisture and temperature also may cause interlaminar stresses in a laminate.

One approach to classify composite material failure is to separate them into two major types, but it is sure that these two mechanisms interact,

(a) in-plane failure: failure that is due to in-plane stresses

(b) out-of-plane failure: failure that is due to out-of-plane or interlaminar stresses (Masters,1987).

2.1. In-Plane Failure

2.1.1. Compression

Although tension plays a predominant role in fracture of metals, in-plane compression loading is even more severe and limiting in the case of laminated composite materials. Because of the weakness of the matrix and the fiber-matrix interface, compared to the high strength of the fibers, unidirectional composite materials can fracture along the fibers when loaded in compression by a transverse tensile failure mode, as shown in figure 2.1. Transverse tensile stresses can develop in the matrix because of Poisson's ratio differences between the matrix and the fiber (Masters,1987).

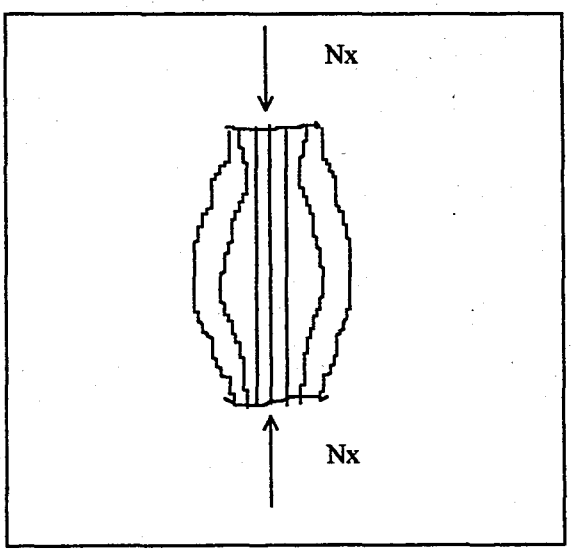

FIGURE 2.1. Induced transverse tensile failure under compressive loading.

If a fiber buckles, the fiber-matrix interface may fracture in shear and lead to ultimate failure, as shown in figure 2.2.

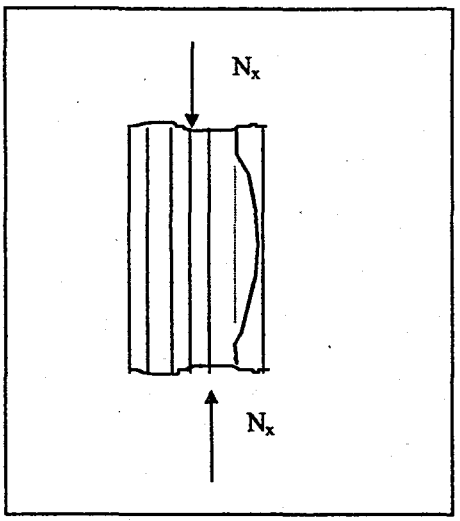

FIGURE 2.2. Compressive delamination failure of composite materials.

If the matrix is ductile and the interface is strong enough, the fiber can bend without fracture, in this case the failure will be at higher loads due to buckling, as in figure 2.3.

Another type of failure of unidirectional laminates is shear crippling caused by fiber microbuckling and fiber kinking. This looks like a shear failure at the macroscopic scale (Figure 2.4).

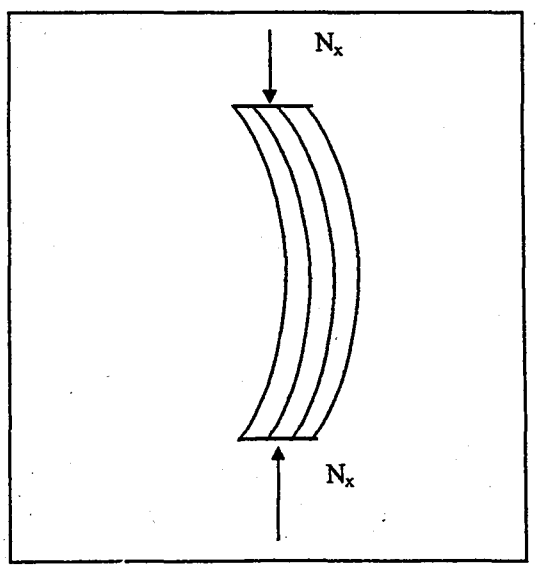

FIGURE 2.3. Euler failure, buckling.

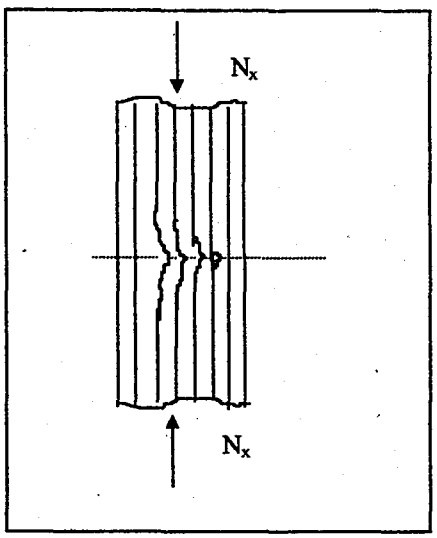

FIGURE 2.4. Microbuckling.

There is also the possibility of the fracture of the fiber due to pure compression, in unidirectional laminates. This failure creates a fracture surface at usually 45° to the direction of the load application, like the ultimate shear failure of isotropic materials (Figure 2.5).

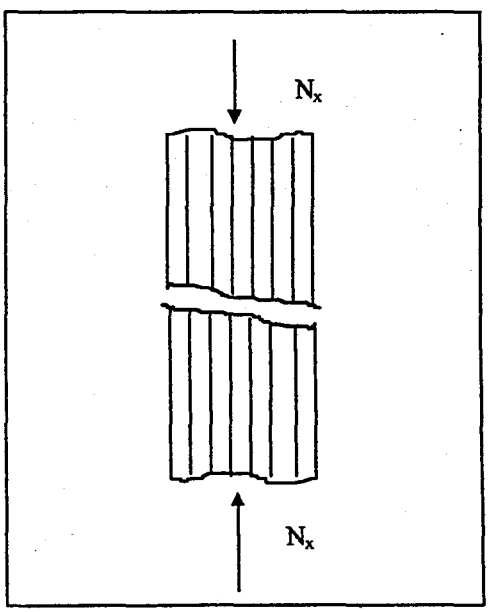

FIGURE 2.5. Strength failure of composite materials under compression.

2.1.2. Tension

The strength of a lamina in in-plane tensile loading depends mainly on the behavior of the fibers in the direction of the load, i.e. at 0°. The analysis of unidirectional laminates will give enough information about the tensile failure characteristics of laminated composites.

In tension the load is carried by fibers. That is why they are constituted the composite material, but they are usually brittle. If individual fibers break, the remaining fibers can still carry the load. If the amount of broken fibers increases complete rupture may take place (Masters,1987). Three types of failure modes can be developed in tensile loading, as can be seen in figure 2.6.

(a) brittle fracture caused by the stress concentrations accumulated at the ends of broken fibers. (figure 2.6 a)

(b) brittle fracture with fiber pull-out occurs if the matrix-fiber interface or bonding is stronger. (figure 2.6 b)

(c) brittle fracture with debonding and/or matrix failure is caused by different cracks initiated independently and the load on the matrix is increased due to decrease in "active" fibers. As a result, either or both of matrix-fiber interface debonding or matrix shear failure can be observed. (figure 2.6 c)

For the case of transverse tensile loading the basic failure modes are matrix tensile failure and debonding.

2.2. Out-of-Plane Delamination Failure

A major asset of composite laminates is the ability to orient fibers to achieve directional strength and stiffness properties that match the requirements. However, interlaminar stresses may develop because of the mismatch in engineering properties between individual lamina within the laminate.

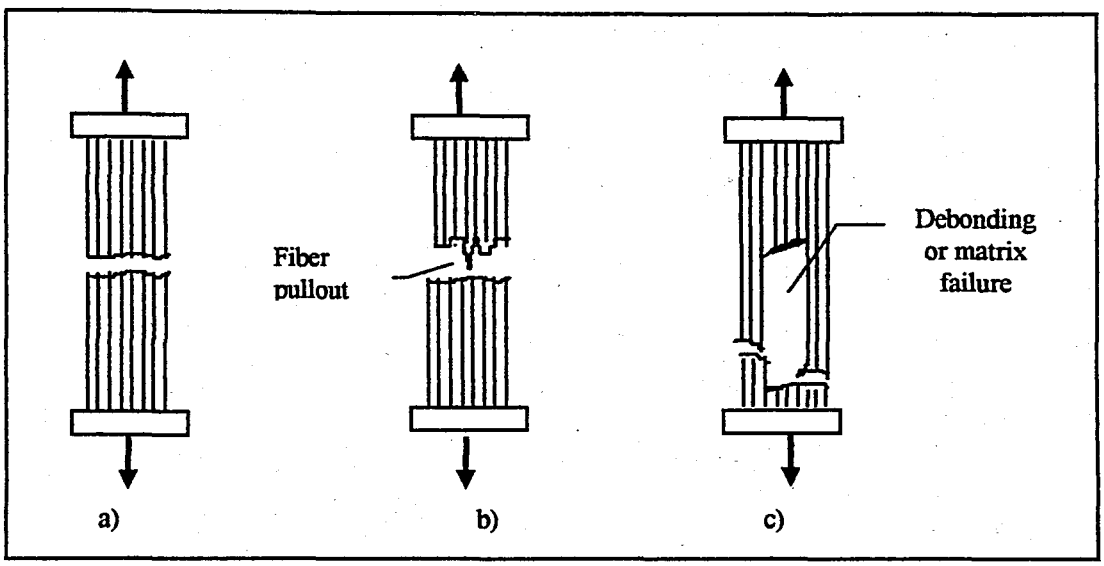

FIGURE 2.6. Failure modes of unidirectional composite subjected to longitudinal tensile loading. a)Brittle fracture, b) Brittle fracture with fiber pull-out, c) Brittle fracture with debonding and/or matrix failure.

Delamiantion is the matrix crack development at the lamina interface. In general the causes of delamination can be attributed to the existence of out-of-plane stresses. The out-of-plane stresses can develop as a result of 0° ply failure and the subsequent internal load redistribution under in-plane compression loading.

If the laminate is composed of laminae at different orientations, and also if the stacking sequence is not symmetric with respect to the midplane than the bending and stretching is coupled. That is, any tensile (or compressive) force will induce bending moments and vice versa.

In addition to that, the out-of-plane stresses are also introduced at variety of design features involving local discontinuities. The most common types of design details are shown in figure 2.7 (Reinhart,1987). These are straight or curved free edges, ply termination or ply drop for tapering the thickness, bonded or co-cured joints and bolted joints.

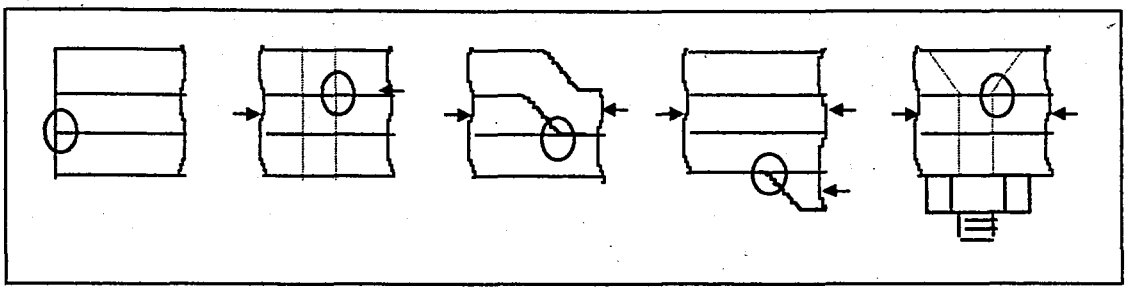

FIGURE 2.7. Sources of out-of-plane loads (Masters,1987).

2.3. Delamination Caused by Impact

When a laminate is hit by a projectile or impactor the materials directly under the projectile are compressed. The deformation is highly localized. This may cause large transverse shear and normal stresses which can lead to damages to propagate and even failure of the laminate.

Another effect of impact is the creation of a compression stress wave which travels from the impact surface through the thickness of the laminate. This wave is reflected from the back surface as a tension wave which can cause failure at the first weak interface, resulting in chipping or splintering of the parts of the rear ply(Garg, 1988).

2.4. Delamination Caused by Other Effects

Besides mechanical loads, the moisture and temperature also may cause interlaminar stresses in a laminate. These may be result from residual thermal stresses due to cool down of the laminate from the elevated curing temperature or due to the difference between test and stress free temperatures, residual stresses created by the moisture absorption in the laminate and moisture gradient through the thickness of the laminate.

3. FRACTURE MECHANICS RESUME

3.1. Fracture of Composite Materials

The objective of fracture mechanics analysis is the prediction of the critical load initiating crack growth in a body containing a crack of a given size and under a set of applied loads. Fracture mechanics has actually been developed for simple fractures of homogeneous, isotropic materials, like metals. However its methods are equally applicable to failures of inhomogeneous, anisotropic materials such as composite materials.

The most common mode of failure in laminated composite materials is delamination. Delamination may be regarded as a propagation of an interlaminar crack. Laminated composite materials are manufactured to give high stiffness and strength in the plane of the sheet and the occurrence of delamination is a problem because it can give a significant decrease in the flexural stiffness of the composite material. Delamination of composite materials is generally constrained to grow in layers because of the presence of continiuos fibers above and below of each interface. In this sense, the composite delamination process is analogous to debonding of adhesive joints (Hashemi et al. 1990). Interlaminar fracture is governed by the toughness of the matrix material. The interlaminar plane is the most weak part, having the lowest resistance to failure. Hence, the fracture plane is usually known.

As a result, fracture mechanics schemes can be applied to the problem of delamination. Moreover, composite materials can be analyzed using linear elastic fracture mechanics principles because they are designed to be stiff and elastic. Therefore they can be treated as linear elastic, avoiding the problems of plastic deformation analysis (Williams, 1989).

The characterization of delamination behavior or fracture toughness will bring many benefits:

(a) it will provide a fail-safe approach to design primary structures,

(b) it will integrate available inspection techniques with proof testing to define the minimum flaw that can exist in a structure without failure,

(c) it can be used to predict the useful life of a structure.

3.2. Linear Elastic Fracture Mechanics

Linear elastic fracture mechanics (LEFM) has been found useful for certain types of cracks in composites: interlaminar cracks or in-plane cracks in unidirectional composites. This approach adequately describes delamination propagation since it fulfills the two major requirements for the applicability of LEFM to composite materials: the crack must lie in a plane of material symmetry and it must propagate in a collinear or self-similar fashion (Kim and Dharan, 1989).

In linear elastic fracture mechanics analysis, the following is assumed (Kim and Dharan, 1989) :

(a) the material behavior is linear elastic and exhibits little plasticity at the crack tip,

(b) there is a single dominant flaw in the material,

(c) the crack growth of this flaw is self-similar,

(d) the material is homogenous along the plane of crack.

In linear elastic fracture mechanics analysis, when a flaw is aligned parallel to the direction of minimum fracture resistance, critical values of stress intensity factor, K, or strain energy release rate, G, are sufficient to characterize the behavior of the material under given loading conditions. The relation between K and G can be computed. All the possible stress fields around the crack tip can be resolved into three basic modes of fracture, which are (Figure 3.1.)

(a) mode I, where the crack surfaces move directly apart,

(b) mode II, where the crack surfaces slide over one another in a direction perpendicular to the edge of the crack,

(c) and mode III, where the crack surfaces move relative to each other in the direction parallel to the leading edge of the crack.

For each mode stress intensity factor, K, and strain energy release rate, G, can be defined separately as K_I, G_I, K_{II}, G_{II}, K_{III}, G_{III}.

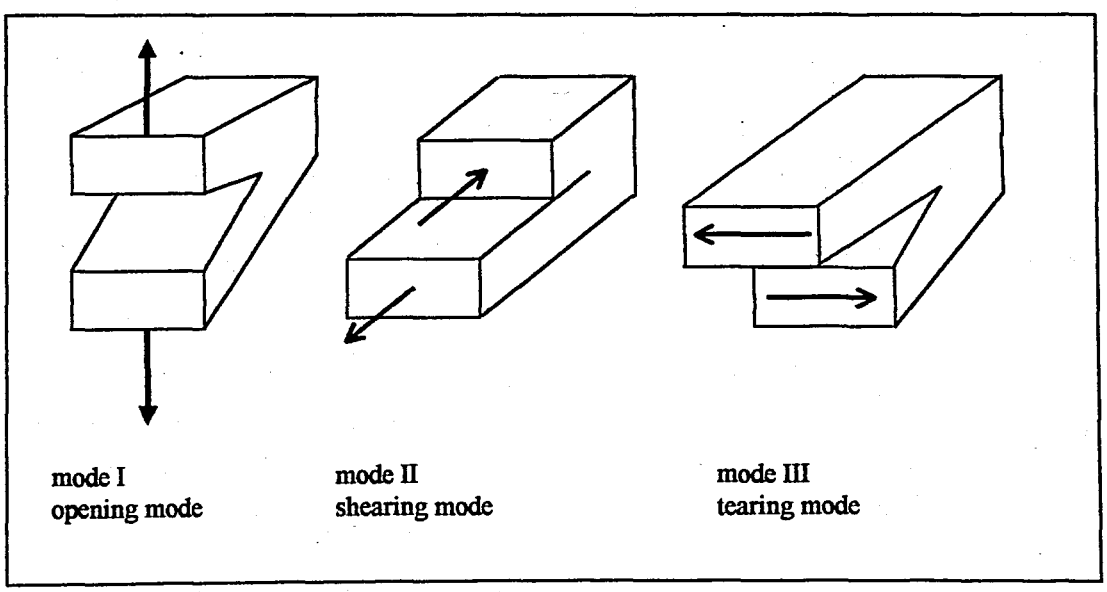

FIGURE 3.1. The modes of interlaminar fracture.

3.3. Stress Intensity Factor

The stress intensity factor, K, indicates the strength or the intensity of the stress singularity at the crack tip, that is, how fast the stresses go to infinity as the crack tip is approached. This factor can be found as a by-product, when the stress distribution near the crack tip is solved by the methods of elasticity (Vardar, 1988).

In general, it is not possible to define the components of the stress intensity factor, K_I, K_{II}, and K_{III}, for a crack between dissimilar anisotropic composite layers in the same manner as for cracks in an homogeneous material. While the overall stress intensity factor may be used to designate the maximum amplitude of crack tip stress and to correlate crack extension, accurate description of asymptotic stress field at the composite delamination crack tip requires detailed knowledge of individual stress intensity factors. Because of the complexities involved in the problem, numerical methods are generally required to obtain this information (Wang, 1983).

3.4. Strain Energy Release Rate

Strain energy release rate, G, is based on energy criterion. A body having a crack can release a specific amount of energy into the crack tip in a stress field. This is the available energy for the creation of an incremental crack surface. The amount of the surface energy required to extend the existing crack is the critical value. For fracture process to occur, the energy release rate must at least be equal to the critical energy release rate, G_c, which is also called fracture toughness.

The strain energy release rate approach is more popularly used in the analysis of interlaminar fracture. It is based on energy considerations and is mathematically well defined as well as physically measurable in experiments. The energy approach, which stems from the

original Griffith treatment, is based on a thermodynamic criterion for fracture by considering the energy, available for crack growth, of the system on one hand and the surface energy required to extend an existing crack on the other hand. For a cracked body shown in figure 3.2, a potential H may be defined as

$$H=W-U \tag{3.1}$$

where W is the work done by the external forces, and U is the elastic strain energy stored in the body.

If the critical strain energy release rate, G_c, is the work required to create a unit crack area, it is possible to formulate a criterion for crack growth,

$$\delta H \geq G_c \delta A \tag{3.2}$$

where δA is the increase in crack area.

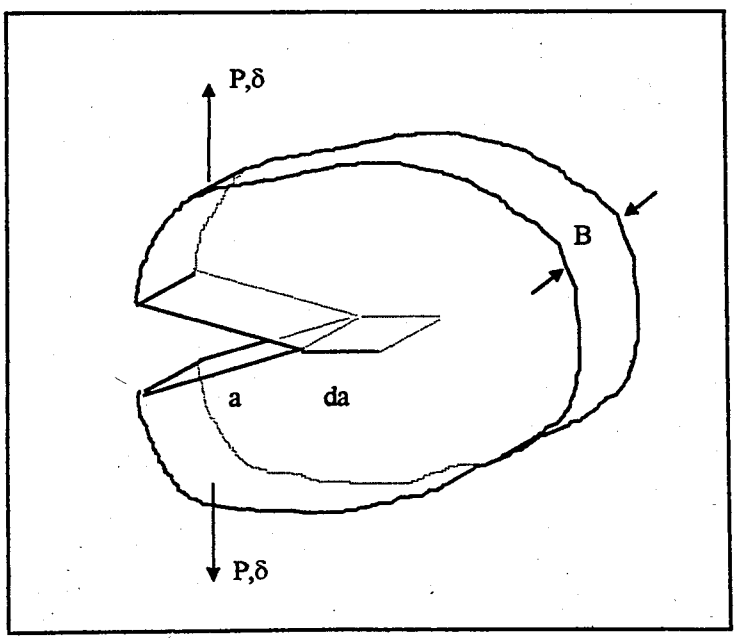

FIGURE 3.2. General loading on a cracked body.

The strain energy release rate is defined as

$$G = \frac{\partial H}{\partial A} \tag{3.3}$$

In terms of G, the fracture criterion may thus be formulated as

$$G \geq G_c \tag{3.4}$$

This concept is illustrated for a linear elastic body containing a crack of length a and a+δa, respectively. Figure 3.3 shows the load, P, versus displacement, u, behavior for the cracked body where crack growth is assumed to occur either at constant load (fixed load) or at constant displacement (fixed grip).

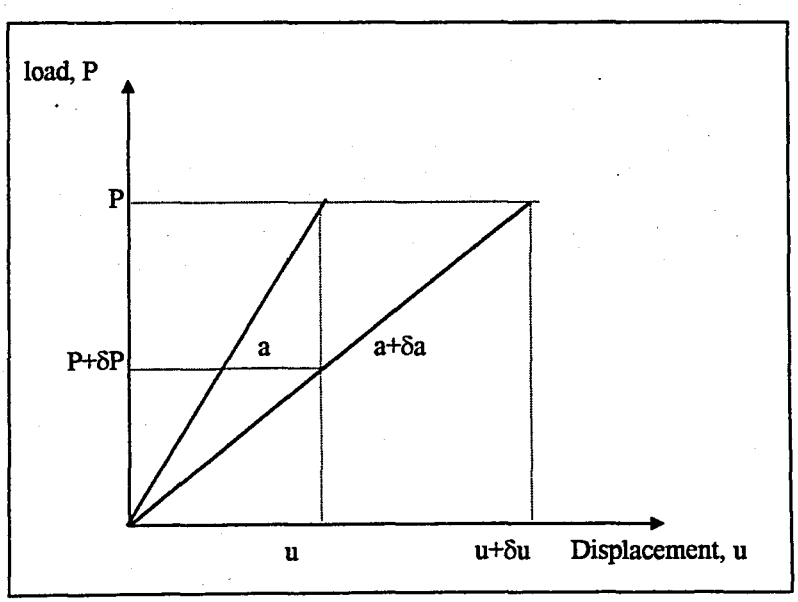

FIGURE 3.3. Load-displacement behavior for a cracked body.

For the fixed load case,

$$\delta U = \frac{P \delta u}{2} \tag{3.5}$$

$$\delta W = P \delta u \tag{3.6}$$

Equation (3.1) gives

$$\delta H = P\delta u - P\delta u/2 = P\delta u/2 \tag{3.7}$$

and equation (3.3) gives

$$G = \frac{P}{2} \frac{\delta u}{\delta A} \tag{3.8}$$

For the fixed grip case, the work term vanishes and

$$\delta U = \frac{u \delta P}{2} \tag{3.9}$$

Note that δP is negative because of the loss in stiffness is followed by crack extension, and G is

$$G = -\frac{u}{2} \frac{\delta P}{\delta A} \tag{3.10}$$

For a linear elastic body, the relation between load and displacement may be expressed as

$$u=CP \tag{3.11}$$

where C is the compliance of the specimen. Substitution into equation (3.8) (fixed load case) gives

$$G = \frac{P^2}{2}\frac{\delta C}{\delta A} \tag{3.12}$$

and substitution of P=u/C into equation (3.10) (fixed grip case) gives

$$G = \frac{u^2}{2C^2}\frac{\delta C}{\delta A} = \frac{P^2}{2}\frac{\delta C}{\delta A} \tag{3.13}$$

Consequently, both cases reduce to the same expression. This expression is convenient for the experimental determination of strain energy release rate, G and fracture toughness, G_c (Carlsson and Pipes, 1987). This method requires an expression relating compliance to crack length. That is why it is also called compliance method.

3.4.1. Direct Energy Methods

An alternative to the compliance methods is the direct energy method. Such an approach is used by Whitney et al. (1982). The crack extension is related directly to the area enclosed between the loading and the unloading curves in figure 3.4.

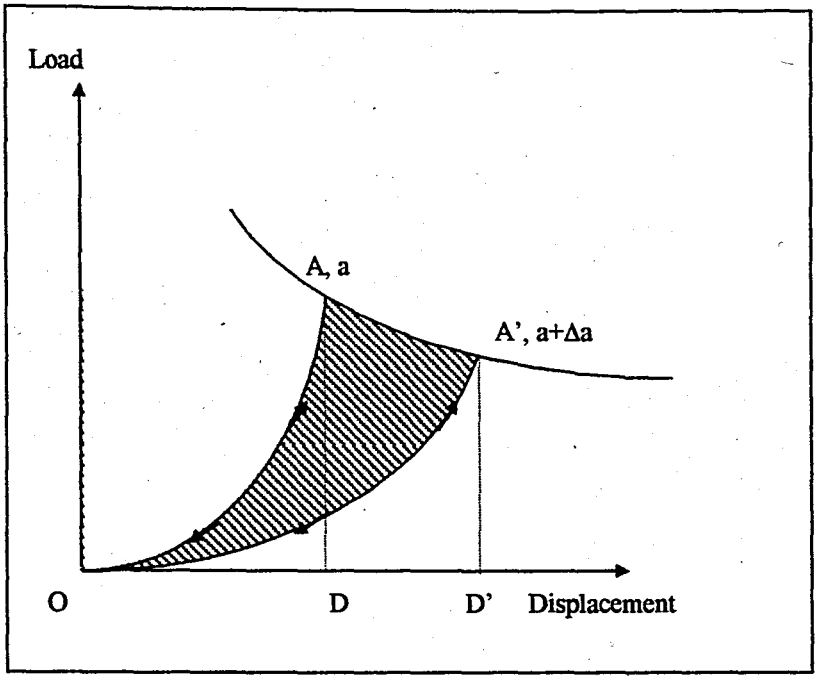

FIGURE 3.4. Definition of strain energy release rate, G, and area method.

For a crack of width B and length a, the fracture condition is:

$$G = G_c = \frac{1}{B}\left[\frac{\Delta U_e}{\Delta a} - \frac{\Delta U_s}{\Delta a}\right] = \frac{\Delta U}{B\Delta a} \tag{3.14}$$

where U_e is external work, U_s is strain energy and Δa is the associated increment of crack growth.

From the figure 3.4

$$\Delta U_e = ADD'A' \tag{3.15}$$

$$\Delta U_s = OA'D' - OAD \tag{3.16}$$

So critical strain energy release rate, G_c, becomes,

$$G_c = \frac{shaded\ area}{B\ x\ crack\ growth} = \frac{\Delta U}{B\Delta a} \tag{3.17}$$

This is an exact definition of strain energy release rate, G, but it is imprecise because what is, in effect, a derivative must be determined from two finite measurements (Hashemi et al., 1990).

4. ANALYSIS OF DELAMINATION

4.1. Testing and Analysis of Mode I Delamination

Over the years the double cantilever beam (DCB) test emerged as the preferred configuration for measuring the opening mode I interlaminar fracture toughness, G_{Ic} (Figure 4.1).

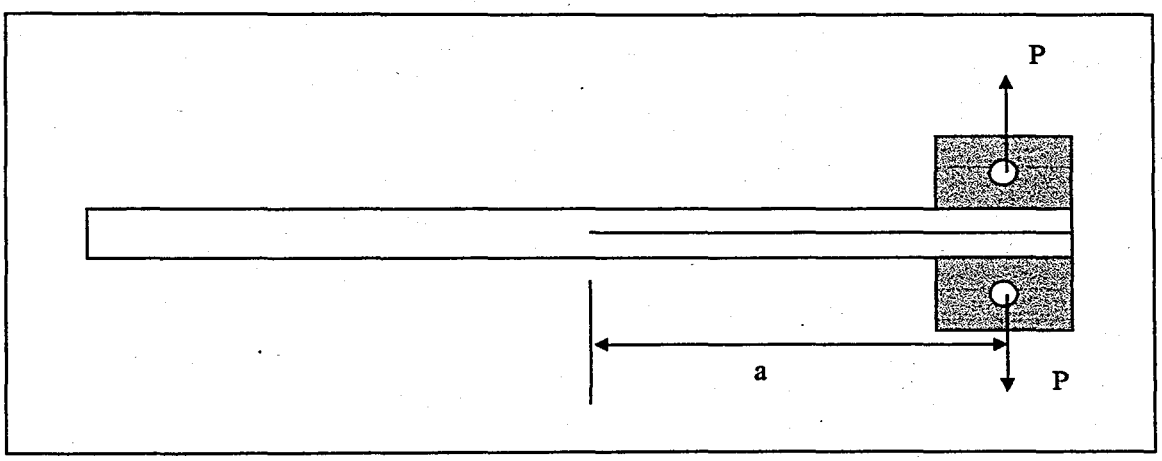

FIGURE 4.1. Double cantilever beam (DCB) specimen.

The DCB test consists of a composite laminate loaded normal to the thickness through attached load blocks, or piano hinges, at the end of the laminate containing a thin non-adhesive insert. The specimen contains a starter crack usually in the form of a Teflon film placed in the midplane during manufacturing. Early studies within ASTM in the 1970s identified problems with delamination branching in this test if angle ply laminates bordered the midplane containing the insert. Hence, a zero degree unidirectional laminate has become the most common lay-up for this test. However, because of the nesting inherent in unidirectional composites, fibers above and below the midplane tend to bridge the

delamination growth reflected in a crack growth resistance curve (R curve). However, fiber bridging is an artifact of the unidirectional double cantilever beam (DCB) specimen and does occur in structural composite laminates where delaminations typically form between plies of dissimilar orientation. Hence, emphasis has been placed on measuring delamination onset from the insert to obtain a generic measure of G_{Ic}. In 1994, as a result of round robin tests double cantilever beam (DCB) test became a ASTM standard test method: D5528-94a (O'Brien, 1998).

As it has been discussed in the previous chapter, critical strain energy release rate (or fracture toughness), G_c, can be calculated by compliance methods:

$$G_c = \frac{P_c^2}{2B}\frac{dC}{da} \tag{4.1}$$

where P_c is the critical load, B is the width, C is the compliance and a is the crack length. These methods require an expression relating compliance to crack length.

Davies and Benzeggah (1989), present some of the popular analytical models. The first one presented is proposed by Gilman,

$$C = \frac{8a^3}{EBh^3} \tag{4.2}$$

$$G_{Ic} = \frac{12P_c^2a^2}{EB^2h^3} \tag{4.3}$$

where a is the crack length, E the tensile modulus, B the width, h the thickness and P_c the critical load. This expression takes account of strain energy due to bending moment.

To include the effect of shear, the expression was modified by Timoshenko as

$$C = \frac{8a^3}{EBh^3}\left[1 + \frac{3}{10}\frac{E}{G}\left(\frac{h}{a}\right)^2\right] \tag{4.4}$$

$$G_{Ic} = \frac{12P_c^2a^2}{EB^2h^3}\left[1 + \frac{1}{10}\frac{E}{G}\left(\frac{h}{a}\right)^2\right] \tag{4.5}$$

where G is the shear modulus.

Ripling, Mostoyov and Patrick proposed a similar expression,

$$G_{Ic} = \frac{12P_c^2a^2}{EB^2h^3}\left[(a + 0.6h)^2 + \tfrac{1}{3}h^2\right] \tag{4.6}$$

Kanninen has proposed an analytical model for the shear, rotation and crack-tip response, using the theory of beams on elastic foundations. It yielded the following expression for the compliance:

$$C = \frac{4a^3}{EBh^3}\left[1 + 1.92\frac{h}{a} + 1.22\left(\frac{h}{a}\right)^2 + 0.39\left(\frac{h}{a}\right)^3\right] \tag{4.7}$$

4.2. Testing and Analysis of Mode II Delamination

Characterization of the sliding mode II interlaminar fracture has been investigated by two main groups preferring different test configurations. ASTM prefers the end-notched flexure test (ENF) which consists of the same unidirectional specimen used in the double cantilever beam (DCB) test but loaded in three point bending, shown in figure 4.2. It has been standardized under the standard ASTM D-30. The simplicity of load introduction makes this configuration to be selected. However, the delamination growth is unstable. The European Structural Integrity Society (ESIS) prefers the end-loaded split beam (ELS) configuration illustrated in figure 4.3 where the specimen is fixed on the uncracked end to maintain a zero slope and loaded as a cantilever on the insert end. This configuration is stable, but requires a complicated fixture to ensure the clamped end condition (O'Brien,1998).

4.2.1. End Notched Flexure (ENF) Specimen

The mechanics of the ENF geometry is quite complex because of the presence of a crack in a finite domain. Therefore approximate analytical models have been derived.

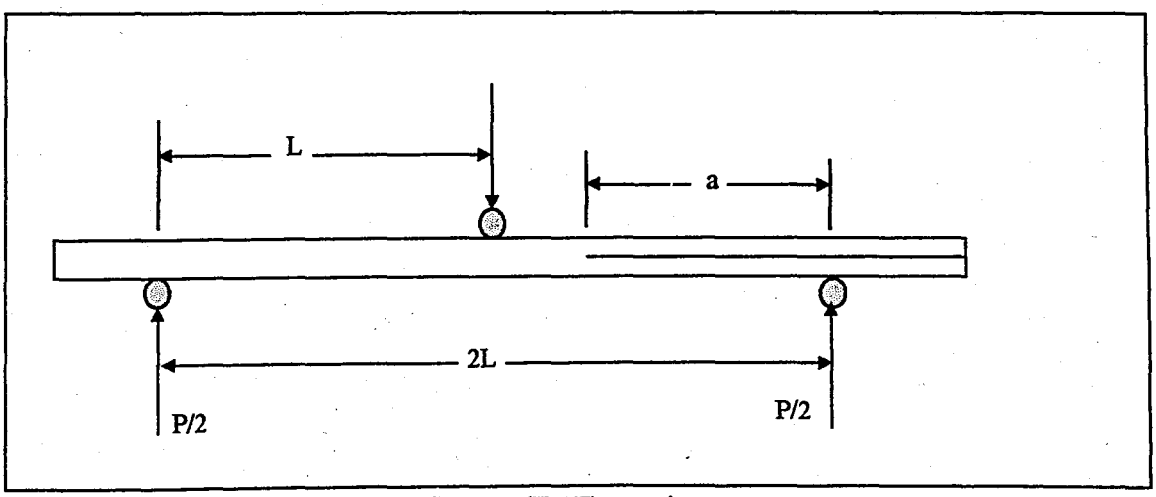

FIGURE 4.2. End notched flexure (ENF) specimen.

ÜNİVERSİTESİ KÜTÜPHANESİ

The classical beam theory expression for compliance given by Russel and Street (1982) is:

$$C = \frac{2L^3 + 3a^3}{8E_{11}Bh^3} \tag{4.8}$$

where L is the half span length, a is the crack length, E_{11} is the elastic modulus in the fiber direction, B is the width and h is the half thickness.

Including the effect of shear provides a more realistic model for advanced composites that typically have low interlaminar shear stiffness. The analysis using shear deformation beam theory gives the following expression for compliance (Carlsson et al., 1983).

$$C = \frac{2L^3 + 3a^3}{8E_{11}Bh^3}\left[1 + \frac{2(1.2L + 0.9a)h^2E_{11}}{(2L^3 + 3a^3)G_{13}}\right] \tag{4.9}$$

and

$$G_{II} = \frac{9a^2P^2}{16E_1B^2h^3}\left[1 + 0.2\left(\frac{E_1}{G_{13}}\right)\left(\frac{h}{a}\right)^2\right] \tag{4.10}$$

where G_{13} is the out-of-plane shear modulus which is approximately equal to in-plane shear modulus, G_{12}, in most of the advanced composite systems (Ersoy, 1994).

The accuracy of these equations are to be established by methods that do not use simplifying assumptions of beam theory. Attempts were made to analyze the end-notched flexure (ENF) specimen by two-dimensional finite element analysis. The results of Trethewey et al. (1986), Gillespie et al. (1986), Salpekar et al. (1988) and Lokman (1997) are close to the results obtained from beam theory considering shear deformations.

However Whitney (1988) states that the reported finite element results display a long discrepancy from the theoretical results. Therefore develops a higher order beam theory and obtains the following expression for the mode II component of strain energy release rate:

$$G_{II} = \frac{9P^2\bar{a}^2}{16E_1b^2h}\left\{1+\frac{1}{\lambda^2\bar{a}^2}\left[1+\frac{\lambda^2}{60}\left(\frac{E_1}{G_{13}}\right)\right]+\frac{1}{\sinh^2\lambda(2\bar{L}-\bar{a})}(1\right.$$

$$+\frac{2}{\lambda\bar{a}}\left(\sinh\lambda(2\bar{L}-\bar{a})-\sinh\lambda\bar{L}\right)\cosh\lambda(2\bar{L}-\bar{a})$$

$$-\frac{2}{\lambda^2\bar{a}^2}\sinh\lambda(2\bar{L}-\bar{a})\sinh\lambda\bar{L})+\left(\frac{E_1}{G_{13}}\right)\frac{\lambda^2\sinh\lambda\bar{L}}{396\bar{a}^2}\left[\lambda\bar{a}\cosh\lambda(2\bar{L}-\bar{a})\right.$$

$$\left.\left.+\sinh\lambda\,(2\bar{L}-\bar{a})-2\sinh\lambda\,\bar{L}\right]\right\} \tag{4.11}$$

with

$$\lambda = 4\sqrt{\frac{14}{5}\left(\frac{G_{13}}{E_1}\right)} \quad , \quad \bar{L} = L/h, \quad \bar{a} = a/h \tag{4.12}$$

4.2.2. End-Loaded Split Beam (ELS) Specimen

The end loaded split beam (ELS) specimen shown in figure 4.3 can be used for the determination of the delamination resistance of unidirectional fiber-reinforced laminates. Shear loads (mode II) are applied through a load-block under displacement control at a constant rate. Stable delamination growth (propagation) from a non-adhesive insert (starter film) and from a mode I or mode II precrack both at the laminate midplane is monitored, and delamination initiation and propagation readings (both from insert and precrack) are recorded on the load-displacement curves. Data reduction yields the critical strain energy release rates, G_{IIC}, for initiation and propagation of a mode II delamination that may be presented in the form of R-curves (critical strain energy release rate G_{IIC} versus delamination length a) (ESIS, 1995).

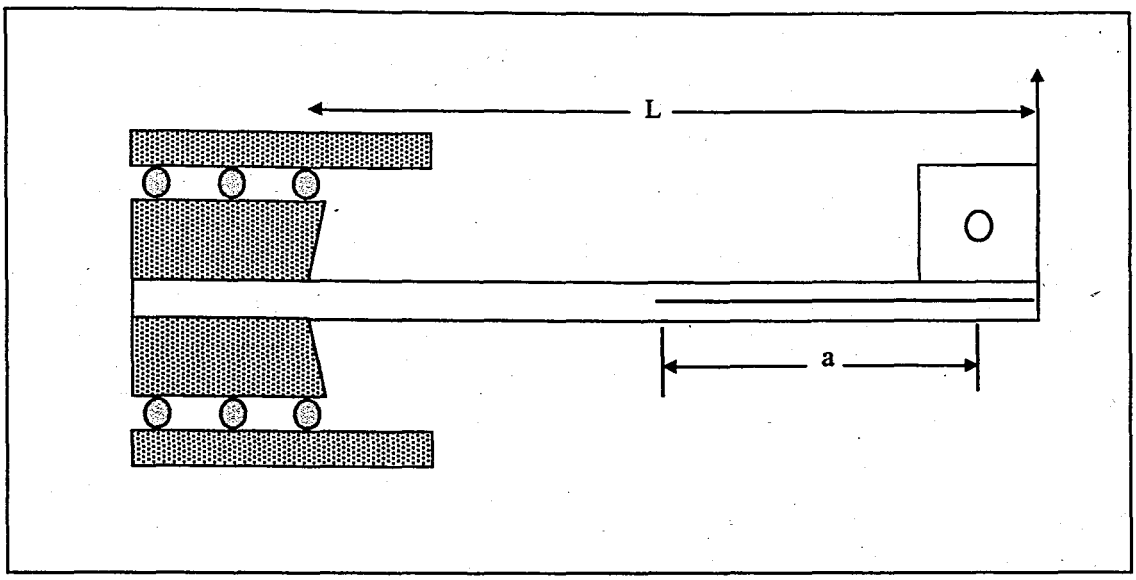

FIGURE 4.3. End-loaded split beam (ELS) specimen.

A corrected beam theory taking the rotation at the crack tip into account is used in the analysis of ELS specimen. It results in:

$$G_{IIC} = \frac{3P_c^2\left(a + \Delta_{II}\right)^2}{16BEI} \tag{4.13}$$

where P_c is the critical load, a the delamination length, Δ_{II} the crack tip rotation correction determined from mode I tests using the double cantilever beam (DCB) specimen, B the width of the specimen, the value of EI shall be directly determined (E the modulus from a flexural test) and I is the moment of inertia of the beam.

4.3. Testing and Analysis of Mixed-Mode I and II Delamination

In order to generate a delamination failure criteria, information is needed on the resistance to delamination under combined loadings at the delamination front. Hence, in addition to the pure mode tests, mixed-mode characterization tests are also needed. Ideally, a mixed-mode test would allow characterization over a very large range of mode ratios and would maintain a fairly constant ratio as the delamination grows. The mixed-mode bending (MMB) configuration satisfies these conditions using the same specimen as mode I and mode II tests. It has become the candidate for measuring mixed mode I and II fracture toughness.

The mixed-mode bending (MMB) test applies a bending load through a lever to a pseudo three point bending rig to grow the delamination from the insert, shown in figure 4.4. The lever position determines the ratio of mode I and mode II loading at the delamination front. The mixed-mode bending (MMB) test is essentially a combination of the double cantilever (DCB) and end notched flexure (ENF) tests, with the same issues that must be resolved. Hence, standardization of this test will likely follow the publication of the pure mode I and mode II test standards (O'Brien, 1998).

The best known analysis of this test is proposed by Reeder and Crews (1988), based on beam theory, which was subsequently checked by finite element calculations. Ducept et al. (1997) conclude that a modified beam theory method including crack tip corrections gives the best correlation with finite element calculations.

Taking into account the equations for pure mode and the beam theory analysis, Reeder and Crews (1990) propose expressions for the energy release rate components in mode I and II loading:

$$P_I = \left(\frac{3c - L}{4L}\right)P \tag{4.14}$$

$$P_{II} = \left(\frac{c+L}{L}\right)P \tag{4.15}$$

$$G_I = \frac{12a^2P_I^2}{b^2h^3E} \tag{4.16}$$

$$G_{II} = \frac{9a^2P_{II}^2}{16b^2h^3E} \tag{4.17}$$

where P is the load, P_{II} is the mode I component of the load, P_{II} is the mode II component of the load, a is the crack length, b is the width, h is the thickness, E is the elastic modulus, c and L are lengths on the specimen as shown in figure 4.4.

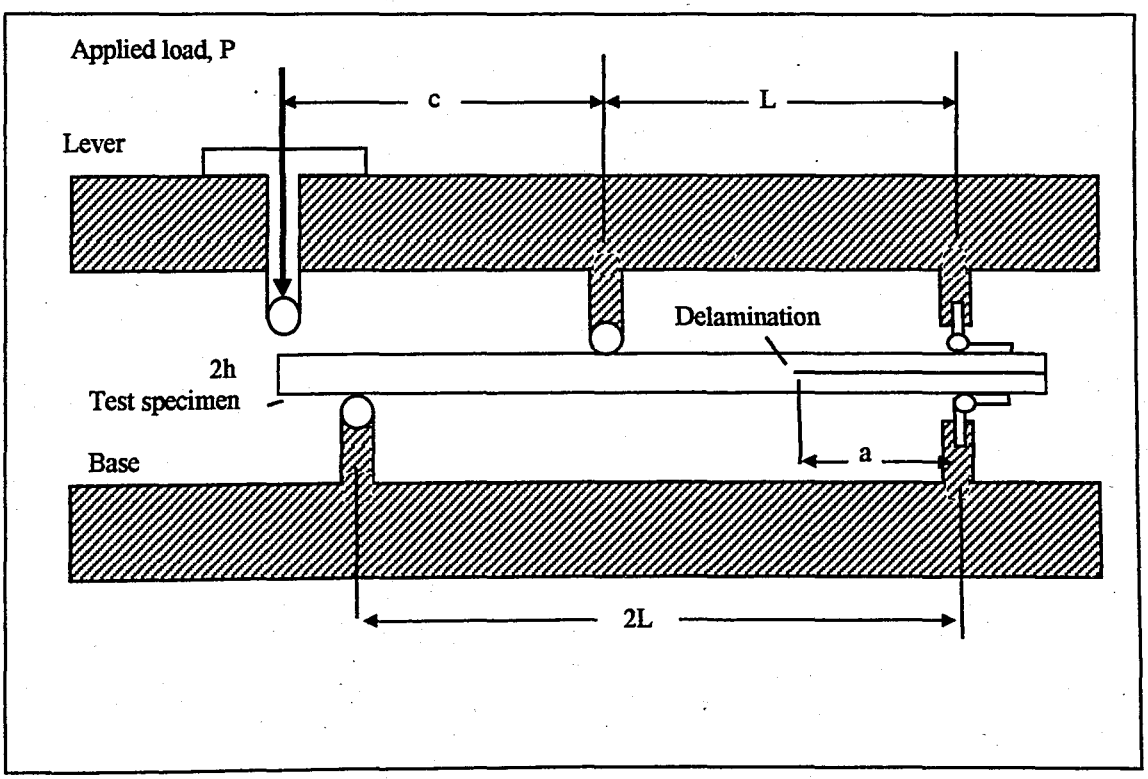

FIGURE 4.4. : Mixed mode bending (MMB) specimen.

4.4. Previous Work on Mode III Delamination

The development of a standard test method for mode III interlaminar fracture toughness has lagged behind the others due to the difficulty in identifying a configuration that exhibits pure mode III at the delamination front. Variations of the split cantilever beam (SCB) were first examined. However, this configuration had difficulty with mode II failures at the surfaces. Although this problem may be resolved by applying a moment to the beam ends, all SCB test configurations had problems with data reduction because of small change in compliance with delamination growth.

The next method, crack rail shear (CRS) test configuration is adapted from standard rail shear tests. This method also suffers from the same problem like split cantilever beam (SCB) test, besides the fixture is complicated.

4.4.1. Split Cantilever Beam (SCB) Specimen

The split cantilever beam test was first proposed by Donaldson (1988) as a test method to characterize mode III delamination in composite materials. The split cantilever beam (SCB) specimen is shown in figure 4.5. It is similar to the mode I double cantilever beam (DCB) specimen, except that the loading directions were parallel to the crack plane. The composite laminate is adhesively bonded between two aluminum bars to give the specimen torsional stiffness as the delamination grew and the bars are loaded in opposite directions. As the crack extends the aluminum bars act as cantilevers.

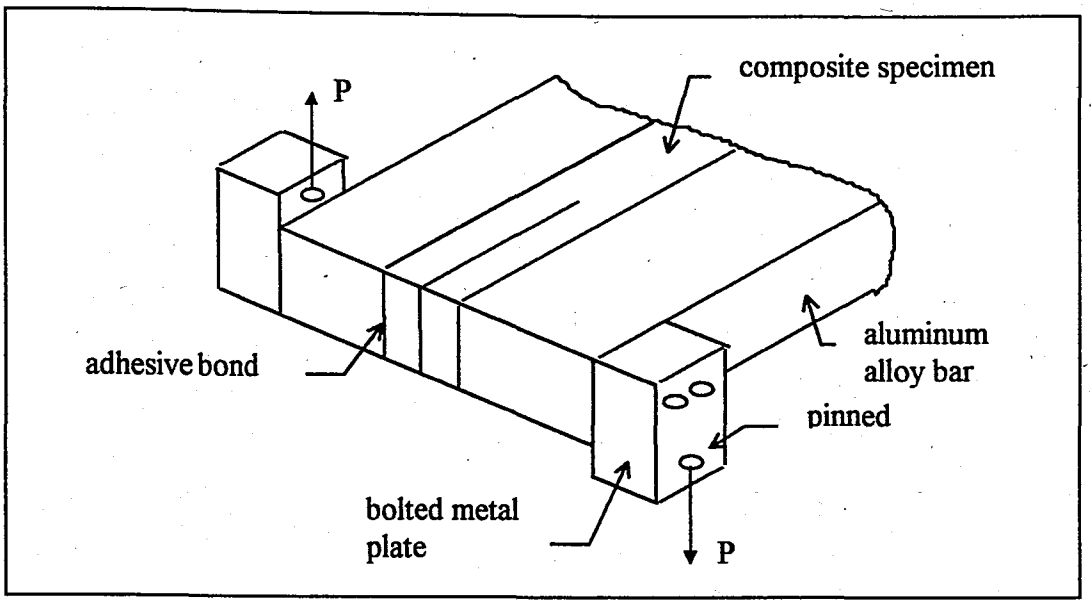

FIGURE 4.5. Split cantilever beam (SCB) specimen.

In the experimental study (Donaldson, 1988), two types of carbon fiber reinforced composite materials are used: One of them is a brittle epoxy reinforced with carbon fiber, AS4/3502, and the other is a thermoplastic resin reinforced with carbon fiber, AS4/PEEK. In order to investigate the effects of laminate thickness and beam depth on mode III critical strain energy release rate (fracture toughness), G_{IIIc}, unidirectional laminates are tested. Experiments using angle ply laminates showed the effect of local fiber orientations.

The data reduction techniques used were similar to those developed for mode I double cantilever beam (DCB) test. Beam theory is used to analyze the split cantilever beam (SCB) test. It was assumed that the beam is loaded at one end, and fixed at the opposite end. The beam length was assumed to be equal to the crack length. The resulting expression is

$$G_{IIIC,i} = \frac{\left(3P_i\delta_i\right)}{2b_i} \tag{4.19}$$

where b is the beam depth, P_i is the load, and δ_i is the total end displacement (Donaldson, 1988).

Alternatively, calculation of G_{IIIc} with a compliance determined empirically yields:

$$G_{IIIc,i} = \frac{nP_i\delta_i}{2ba_i} \tag{4.20}$$

where a_i is the i th crack length measured from the loading axis.

The results of the experimental study can be summarized as follows (Donaldson, 1988):

As the laminate thickness decreased, a considerable aluminum to composite debonding and a significant scatter in the test results were observed. Specimens having 16 plies and more yielded nearly identical results, indicating no thickness dependence in this range.

As the beam depth decreased, fiber bridging was observed. Specimen having depth above 1.27 cm had negligible fiber bridging.

The results of the tests conducted with multidirectional $[+\theta_4//-\theta_8/+\theta_4]$ (// indicates the position of initial crack) laminates showed that the toughness values for θ=15 and θ=75 degrees are somewhat higher than the unidirectional results. This may be due to thermal residual stresses.

Tests conducted with laminates $[+\theta_{16}]$ and $[+\theta_{24}]$ were unsuccessful. Bonding failures are observed.

Consequently, in split cantilever beam (SCB) test configuration the problem of adherent bonding prevents the determination of fracture toughness for tougher materials. One solution to this debonding problem was proposed by Martin (1991). He made laminates

sufficiently thick to provide their own torsional stiffness (Figure 4.6.). Moreover, Martin (1991) changed the loading set-up consisting of bonded aluminum bars bolted to the loading bars and developed a loading nose system, which enables the determination of loading point accurately.

The most important problem of split cantilever beam (SCB) specimen is that there is mode II failure at the edge of the specimen due to rotation of the beam. Using finite element analysis Martin (1991) showed that at the edge of the delamination front, G_{II} was significantly higher than G_{III} for all beam depths and delamination lengths. As the delamination length increased, the ratio of G_{II}/G_{III} along the delamination front increased. The examination of the surfaces of the failed specimen confirmed the analysis. The failure in mode II results in surfaces having hackles without fiber bridging, whereas the surfaces of the specimen failed in mode III exhibit fiber bridging. So, it can be concluded that the split cantilever beam (SCB) test configuration does not represent a pure mode III test.

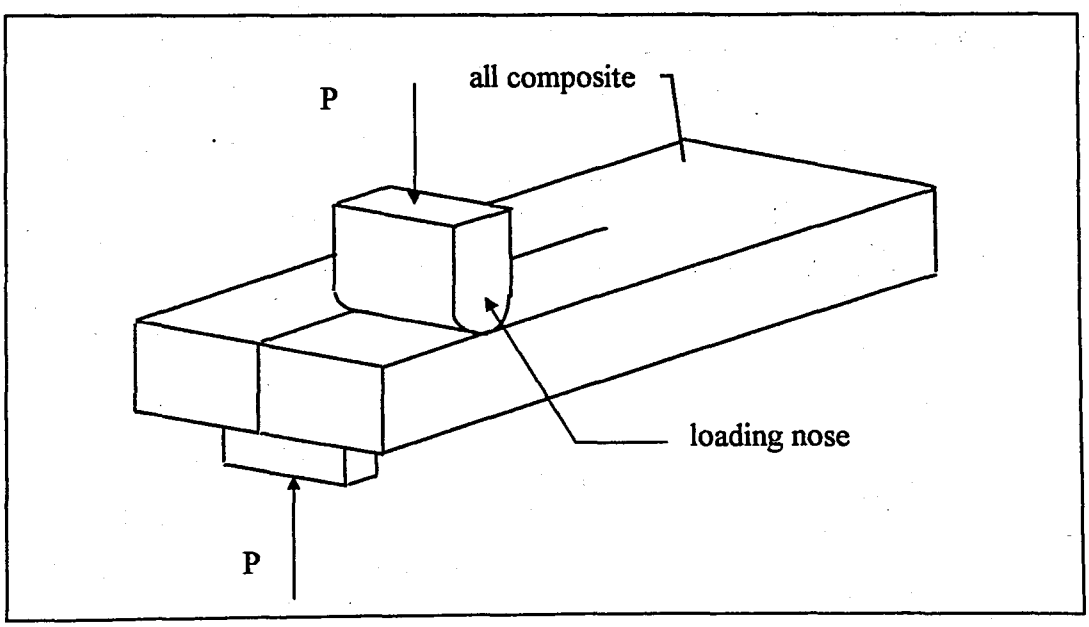

FIGURE 4.6. The improved split cantilever beam (SCB) specimen.

In order to overcome the problems of the split cantilever beam (SCB) test Robinson and Song (1992) proposed a modified SCB test. The problem of standard split cantilever beam (SCB) specimen arises from the tensile and compressive stresses producing mode II components. Therefore Robinson and Song (1992) tried to reduce the moment at the crack front to zero, suggesting a different loading pattern illustrated in figure 4.7. They prepared a test jig that enables to apply the required loads accordingly.

The finite element analysis (Robinson and Song, 1994) shows that the unwanted mode II component diminishes as expected. The analysis also tells that the results of the modified split cantilever beam (SCB) test are insensitive to mispositioning and to variations in material properties. However, the longitudinal mispositioning and variations in the though thickness shear modulus, G_{23}, produce the most significant errors.

The experimental study (Robinson and Song, 1994) uncovered that split cantilever beam (SCB) testing method is not suitable for compliance calibration technique due to very small displacements.

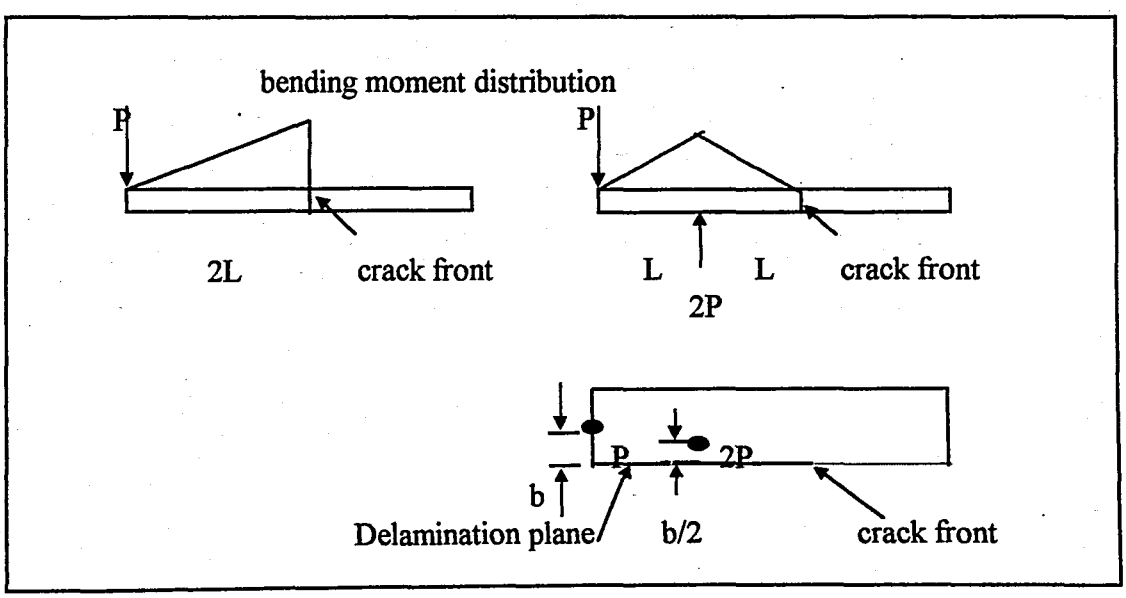

FIGURE 4.7. a)Bending moment distribution in one arm of the SCB specimen. b)Bending moment distribution in one arm of the modified SCB specimen. c)Top view showing loading on a single arm of the modified SCB specimen.

4.4.2. Crack Rail Shear (CRS) Test

The crack rail shear (CRS) specimen was first proposed by Becht and Gillespie (1988) to characterize the mode III interlaminar fracture toughness of continuous fiber-reinforced composite materials. The double and single crack versions of the crack rail shear specimen are shown in figure 4.8. The specimen geometries are very similar to the two rail shear tests (ASTM standard guide D4255-83) for measuring the in-plane shear properties of composite laminates. The Kapton film placed between appropriate plies serves as the starter cracks for subsequent fracture testing.

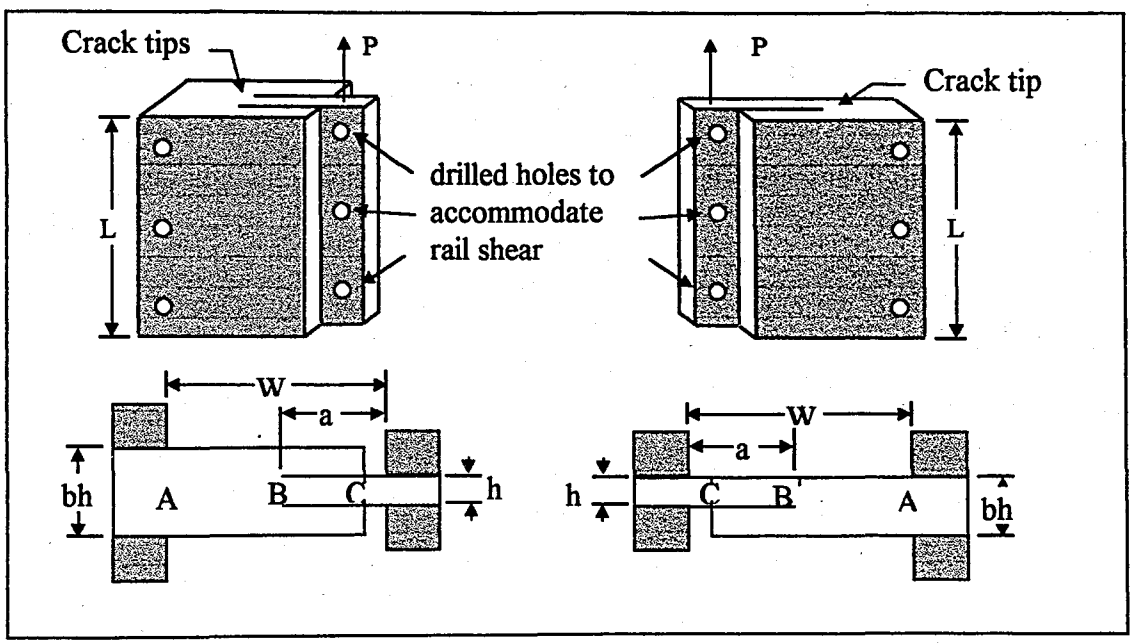

FIGURE 4.8. Crack rail shear (CRS) specimen, double and single crack versions.

The analysis of crack rail shear (CRS) specimen (Becht and Gillespie, 1988) assuming pure shear stress state and neglecting the crack tip singularities, yields the following expressions for the compliance and the strain energy release rate of the specimen:

$$C = \frac{1}{Lh}\left[\frac{w-a}{bG_{AB}} + \frac{a}{G_{BC}}\right] \tag{4.21}$$

$$G = \frac{P^2}{4L^2h}\left[\frac{G_{AB}b - G_{BC}}{G_{AB}G_{BC}b}\right] \tag{4.22}$$

where L is length, h is thickness of the strap section, w width of specimen, b is the total laminate thickness, a is the crack length, G_{AB} is the shear modulus of section AB and G_{BC} is the shear modulus of section BC (Figure 4.8.).

The crack rail shear (CRS) specimen is a quasi-stable (strain energy release rate, G, is independent of crack length) under fixed load conditions and crack growth is stable for all crack lengths under fixed grip conditions. The work on the sizing of the specimen showed that the composite materials exhibit a large degree of non-linearities.

The crack rail shear (CRS) test is modeled using a quasi three dimensional linear elastic finite element code. The analysis assumed that the specimen is infinitely long and therefore all cross sections deform in the same manner, which means that free edge and bending effects are not present. Deformation of the model showed that only the out-of-plane displacement is non-zero, indicating that a pure mode III fracture state does indeed exist within the constraints of the above assumption. Compliance and strain energy release rate predictions are in good agreement with the analytical model.

A further numerical analysis, a fully three dimensional finite element analysis using NASTRAN has been performed. (Becht and Gillespie, 1988). This analysis showed that the mode III energy release rate is dominant and distributed parabolycally along the crack front. Mode I and mode II components are present but are relatively small and are confined to a small area adjacent to each of the crack front. Increasing the length of the crack rail shear (CRS) specimen reduces the total percentages of mode I and mode II component in the total strain energy release rate.

Becht and Gillespie (1989), performed an experimental study to measure mode III interlaminar fracture toughness, G_{IIIC}, of two graphite/epoxy systems, AS4/3501-6 and IM7/8551-7. However, they encountered some problems:

The compliance of the crack rail shear (CRS) specimen was very low. This means that very high loads are to be applied. Moreover the deflection is very small to measure accurately.

Multiple delaminations were observed and the delamination growth deviated from the starter crack plane.

A high coefficient of variation (up to 24 per cent) is reported. The repeatability of the experiments was low.

The double crack specimens did not delaminate symmetrically.

As a result the crack rail shear (CRS) test is not suitable for measuring mode III interlaminar fracture, since the set-up is complex and the low compliance prevents to apply compliance calibration technique.

5. ANALYSIS OF EDGE CRACK TORSION (ECT) SPECIMEN

The edge crack torsion (ECT) specimen proposed by Lee (1993), consists of a $[90/(\pm 45)_n/(\mp 45)_n/90]_s$ laminate with a delamination introduced by a non-adhesive film at the mid-plane along one edge and loaded in a special fixture to create torsion along the length of the laminate (Figure 5.1). The edge crack torsion specimen is tested in a fixture with three fixed support points and one loading point which induces a pair of counteracting torques.

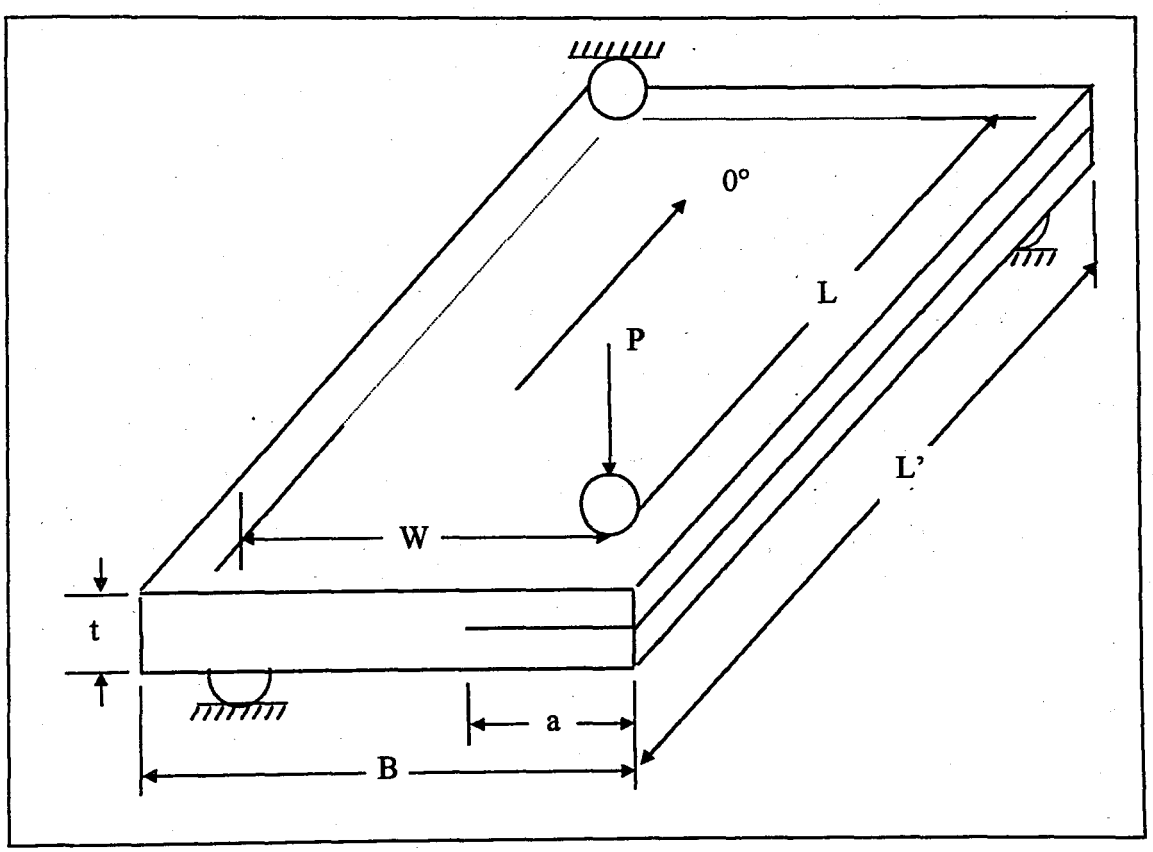

FIGURE 5.1. The edge crack torsion (ECT) specimen.

5.1. Analysis of Loading Mode

In the beginning of the analysis (Lee, 1993), a pure mode III loading is deduced to exist theoretically in the edge crack torsion (ECT) specimen under the given loading conditions. The loading condition of the edge crack torsion (ECT) specimen can be approximated to be a torque T (=PW) applied through the ends (Figure 5.2). Based on the superposition principle, one can equate an orthotropic plate (without crack) under torsional loading, to a plate with crack under torsional loading and its crack surfaces are subjected to shear stresses parallel to the crack front.

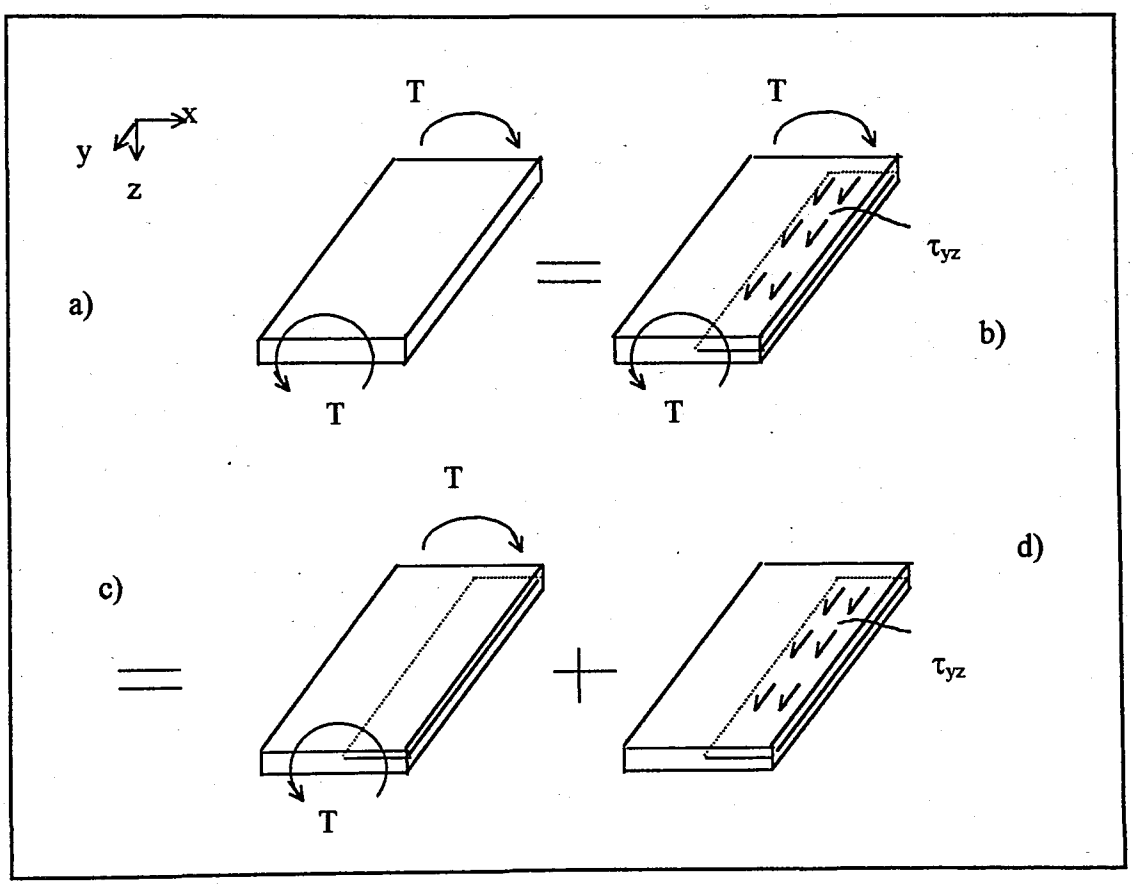

FIGURE 5.2. Equivalence of the loading of an uncracked plate under torsion to a cracked plate under torsion plus the shear forces at the crack surface.

For the orthotropic plate without crack subjected to a torque T, the only nonvanishing stress component along the midplane (xy) is τ_{yz} (Lekhinitski, 1963). This is equal to a plate with a crack subjected to torque T and the corresponding shear forces at the crack surfaces .

It is clear that d) is pure mode III and $K_c \neq 0$, and for the uncracked plate $K_a=0$. Hence,

$$K_a=0=K_c+K_d \tag{5.1}$$

and

$$K_c= -K_d. \tag{5.2}$$

Lee (1993) concludes that edge crack torsion (ECT) loading induces pure mode III loading at the crack front.

5.2. Classical Laminate Theory Analysis

Using the classical lamination theory the edge crack torsion (ECT) specimen can be analyzed. The compliance, C, is obtained as (Lee, 1993)

$$C = \frac{\delta}{P} = \frac{W^2 L}{4(B - (1 - 2s)a)(D_{66})_I} \tag{5.3}$$

with

$$s = \frac{(D_{66})_{II}}{(D_{66})_{I}} \tag{5.4}$$

where W is the moment arm, L is the distance between the loading points in the longitudinal direction, B is the specimen width, a is the crack length. D_{66} is the resultant in-plane shear stiffness of the laminate. The subscripts I and II denote the uncracked region and the cracked region, respectively.

G_{III} can be evaluated as follows:

$$G_{III} = \frac{P^2 C(1-2s)}{2LB(1-(1-2s)(a/B))} \tag{5.5}$$

This analysis assumes that the specimen is subjected to uniform twisting moment. But the deformation state of pure torsion can reproduced by four concentrated loads at the corners. The loading points are not exactly at the corners, but it can be shown from Saint Venant's principle that loading is equivalent to pure torsion except at the small areas from the loading points to the edges. Also the localized loads at the contact points and possible friction may have additional effects. The crack front stress intensity should therefore not appreciably affected by these loads except when the crack is short and only in areas close to the loading points (Lee, 1993).

5.3. Testing of Edge Crack Torsion (ECT) Specimen

In the experimental part of the study (Lee, 1993), epoxy systems R914, R922, R6376 reinforced with T500 or IM6 carbon fibers are used. Several laminates with lay-ups of $[\ 90/(\pm 45)_n/(\mp 45)_n/90]_s$, n=1,2,3, and 4, were tested to optimize specimen design. The (±45) plies in the specimen were introduced to provide sufficient torsional stiffness to the specimen. Since each half of the specimen is symmetric about its own midplane, each half of the laminate remained flat after the test. A Teflon film was inserted in the midplane to provide the initial crack. Since a large resin accumulate at the initial crack tip around the Teflon film a sharp mode I precrack was introduced.

Experimental results showed that for laminates $[\ 90/(\pm 45)_n/(\mp 45)_n/90]_s$, n=1 and 2, the behavior is highly nonlinear. For higher values of n (three and four) the specimen behavior is linear and the minimum thickness is achieved for n=3, corresponding to 28 plies.

All the edge crack torsion (ECT) specimens studied (Lee, 1993) had high compliance to allow the compliance calibration method to be used. Lee (1993) could find the relation between compliance, C, and crack length. The result of R6376/IM6 (28 ply) studies is expressed in the form of (1/C) vs a using linear regression:

$$\frac{1}{C} = 2.253\ 10^3\left(1 - 0.806(a/B)\right) \tag{5.6}$$

To compare the theoretical and experimental work, the properties of the considered composite (Table 5.1) can be substituted into the equation (5.3).

TABLE 5.1. Material properties used in the analysis

E_x=165 Gpa	G_{xy}=5.5 Gpa	Pr_{xy}=0.28
E_y=10.3 Gpa	G_{yz}=5.5 Gpa	Pr_{yz}=0.28
E_z=10.3 Gpa	G_{xz}=5.5 Gpa	Pr_{xz}=0.28

The theoretical curve is

$$\frac{1}{C} = 2.797\ 10^3\left(1 - 0.794(a/B)\right) \tag{5.7}$$

Clearly there is a gap between the two lines obtained from the classical lamination theory and from the experimental data although their slopes are very close.

An additional experimental work is performed by Li et al. (1997). For this purpose G40-800/R6376 graphite/epoxy laminates were manufactured and tested monotonically to failure in the ECT fixture (Li et al., 1997). Li et al. (1997) obtained the following results from the tests.

A load- displacement (P-δ) curve linear up to the delamination onset is obtained.

The experiments with the specimen having small initial delaminations were unsuccesful. The specimen having small crack lengths 2.5 mm and 5 mm are discarded, since mode III delamination is not achieved.

Dye penetrant enhanced X-radiograph of failed specimens revealed that the delamination initiated at the middle of the specimen length and propagated in a self-similar manner along the laminate mid-plane.

Unfortunately, for the edge crack torsion (ECT) configuration it is not possible to generate a compliance curve from a single edge crack torsion (ECT) specimen using the methods utilized for mode I and mode II, because of (1) the unstable delamination growth and (2) it is not possible to shift the specimen in the fixture and change the initial delamination length. Using a set of specimen, 1/C as a function of a/b is obtained. So, G_{IIIc} can also be obtained using the following equation

$$G_{IIIc} = \frac{P_c^2}{2B}\frac{dC}{da} \tag{5.8}$$

Crack propagation is non-uniform along the crack front, peaking at the middle. This may effect the measurement of a, but the error associated is negligible. The crack length is measured after the experiment, opening the specimen taking the mean of six measurements made at equally spaced locations. In case of large variations (>1mm) the results are discarded.

The mean of G_{IIIc} for nine specimen is 1.42kJm^{-2} with a coefficient. of variation of eight per cent (Li et al, 1997).

In order to compare the magnitude of mode III fracture toughness with the mode I and mode II fracture toughnesses of the same material, G40-800/R6376 graphite/epoxy, double cantilever (DCB) and end notched flexure (ENF) tests are performed.

Mode II Fracture Toughness:

G_{IIc}=1.04 kJm^{-2} with a coefficient of variation of 10 per cent.

Mode I Fracture Toughness:

G_{Ic}=322 Jm^{-2} with a coefficient of variation of 7.6 per cent.

5.4. Shear Deformation Theory Analysis

To overcome the deviation of classical lamination theory from test results the edge crack torsion (ECT) specimen is analyzed using a shear deformation theory developed by Li and Wang (1994). Shear deformation is important not only because the shear modulus of composites is relatively small in comparison with in-plane modulus but also because the out-of-plane warping due to torsional loading is predominant in rectangular cross-sectioned laminates.

The laminate is assumed under torsional loading at its ends only and the stress tensor does not vary along the x-axis (longitudinal direction). Such a laminate is under a generalized plane deformation (Lekhinitski, 1963). The displacement field is assumed as

$$u(x,y,z) = \kappa x(z + h/2) + U(y) + z\beta_x(y) \tag{5.9}$$

$$v(x,y,z) = V(y) + z\beta_y(y) + \theta_x(z + h/2) \tag{5.10}$$

$$w(x,y,z) = -\tfrac{1}{2}\kappa x^2 - \theta x(y + \rho) + W(y) \tag{5.11}$$

where u, v and w denote displacements relative to the x-, y- and z-axes, respectively. The bending curvature in the x-z plane is denoted by κ. The angle of rotation per unit length about the x-axis, or twist, is denoted by θ. The constant ρ is the distance between the twisting center and the delamination tip. Shear deformation is recognized through the rotations β_x and β_y. U, V, W, β_x and β_y are functions of y only.

Li and Wang (1994) derive the solutions for the rotations β_{x1} and β_{x0} as:

$$\beta_{x1} = 2\theta H_1 e^{s_1 y} + 2\theta H_2 e^{-s_1 y} - \theta (y + \rho) \tag{5.12}$$

$$\beta_{x0} = 2\theta I_1 e^{s_0 y} + 2\theta I_2 e^{-s_0 y} - \theta (y + \rho) \tag{5.13}$$

where

$$s_1 = \sqrt{\frac{A_{55} - \frac{(A_{45})^2}{A_{44}}}{\xi_3^1}} \tag{5.14}$$

$$s_0 = \sqrt{\frac{A_{55} - \frac{(A_{45})^2}{A_{44}}}{\xi_3^0 \frac{h}{2} + \xi_6^0}} \tag{5.15}$$

the integration constants H_1, H_0, I_1 and I_0 are functions of crack length a and the vectors $\{\gamma^1\}, \{\xi^1\}, \{\gamma^0\}$ and $\{\xi^0\}$ are functions of the components in the stiffness matrix A_{ij}, B_{ij} and D_{ij} of the laminate.

The parameters $\alpha_{11}, \alpha_{21}, \alpha_{12}$ and α_{22} are functions of the components in the stiffness matrix A_{ij}, B_{ij} and D_{ij} of the laminate and the specimen geometry (a, b, h).

$$\alpha_{11} = \xi_3^1 a + \left(\xi_3^0 \frac{h}{2} + \xi_6^0\right)(b - a) + \xi_3^1 f_1 + \left(\xi_3^0 \frac{h}{2} + \xi_6^0\right) f_2 \tag{5.16}$$

$$\alpha_{21}=\left(\xi_1^1\frac{h}{2}\xi_2^1\right)a+\left(\xi_1^0\frac{h}{2}+\xi_4^0\right)(b-a)+\left(\xi_1^1\frac{h}{2}+\xi_2^1\right)f_1+\left(\xi_1^0\frac{h}{2}+\xi_4^0\right)f_2 \quad (5.17)$$

$$\alpha_{12}=\gamma_3^1 a+\left(\gamma_3^0\frac{h}{2}+\gamma_6^0\right)(b-a)+\xi_3^1 f_3+\left(\xi_3^0\frac{h}{2}+\xi_6^0\right)f_4 \quad (5.18)$$

$$\alpha_{22}=\left(\gamma_1^1\frac{h}{2}\gamma_2^1\right)a+\left(\gamma_1^0\frac{h}{2}+\gamma_4^0\right)(b-a)+\left(\xi_1^1\frac{h}{2}+\xi_2^1\right)f_3+\left(\xi_1^0\frac{h}{2}+\xi_4^0\right)f_4 \quad (5.19)$$

where

$$f_1=-\left(H_{11}+H_{10}\right)\left(1-e^{s_1 a}\right)^2+\frac{1}{s_1}\left(1-e^{s_1 a}\right) \quad (5.20)$$

$$f_2=\left(I_{11}+I_{10}\right)\left(1-e^{-s_0(b-a)}\right)^2+\frac{1}{s_0}\left(e^{-s_0(b-a)}-1\right) \quad (5.21)$$

$$f_3=-\frac{\gamma_{31}^1}{\xi_3^1}H_{11}+\frac{\gamma_3^0\frac{h}{2}+\gamma_6^0}{\xi_3^0\frac{h}{2}+\xi_6^0}H_{10}(1-e^{s_1 a})^2+\frac{1}{s_1}\frac{\gamma_{31}^1}{\xi_3^1}(1-e^{s_1 a}) \quad (5.22)$$

$$f_4=-\frac{\gamma_3^1}{\xi_3^1}I_{11}+\frac{\gamma_3^0\frac{h}{2}+\gamma_6^0}{\xi_3^0\frac{h}{2}+\xi_6^0}I_{10}(1-e^{-s_0(b-a)})^2+\frac{1}{s_0}\frac{\gamma_3^0\frac{h}{2}+\gamma_6^0}{\xi_3^0\frac{h}{2}+\xi_6^0}(e^{-s_0(b-a)}-1) \quad (5.23)$$

Li and Wang (1994) obtained the following expression for compliance:

$$C = \frac{ed^2}{8\left(\alpha_{11} - \dfrac{\alpha_{12}\,\alpha_{21}}{\alpha_{22}}\right)} \tag{5.24}$$

For both cases n=3 and n=4, the total strain energy release rate increases as the crack length increases and reaches a plateau. As the crack continues to increase, the total strain energy release rate, G_{total}, drops and reaches zero before the crack runs through the entire laminate. For a valid toughness test, the value obtained should be independent of specimen configuration (Figure 5.3). The toughness can be obtained through experiments provided that the crack size falls within the plateau region.

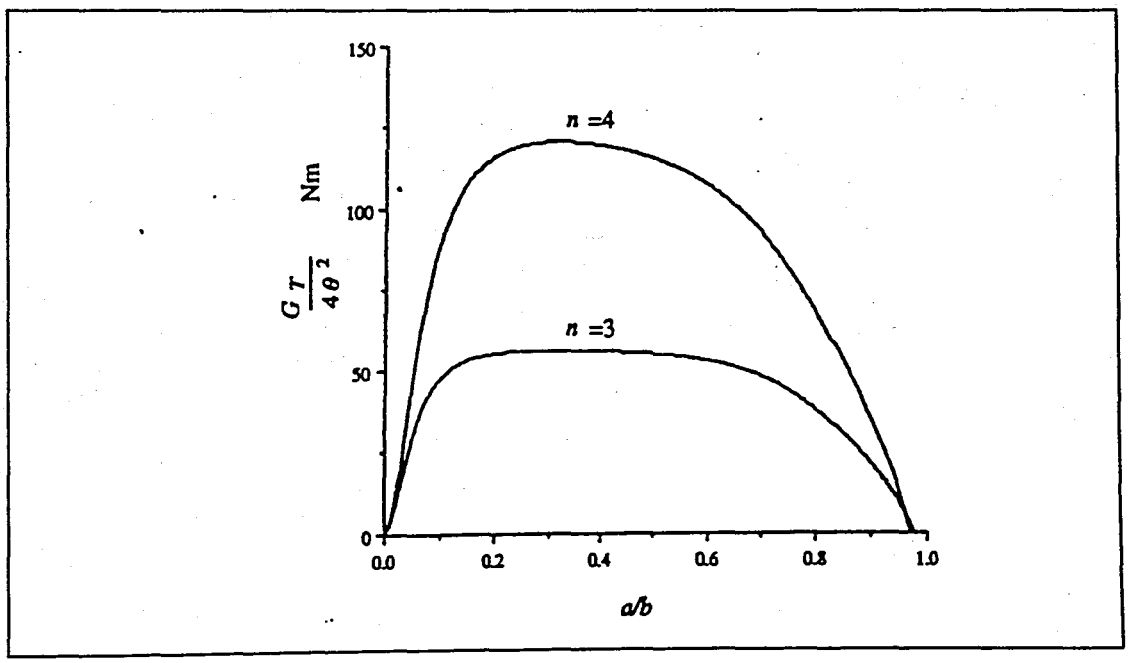

FIGURE 5.3. Total strain energy release rate as a function of normalized crack length a/b for $[90/(\pm 45)_n(\mp 45)_n/90]_s$ lay-up (Li and Wang, 1994).

The predictions of Li and Wang (1994) for the inverse of the compliance, 1/C, are compared with the test data (Lee, 1993) and the classical lamination theory (CLT) solutions (Lee, 1993) as shown in Figure 5.4. Excellent agreement between the test predictions and the test data is found for both n=3 and 4. The CLT solution tends to overestimate the inverse of the compliance and the error can be as high as 50 per cent. Obviously, the classical lamination theory (CLT) cannot accurately predict the torsional behaviour of the edge crack torsion (ECT) specimen. However, it can be seen from figure 5.4. that the classical lamination theory (CLT) can provide an upper bound for the inverse of the compliance, or a lower bound for the compliance.

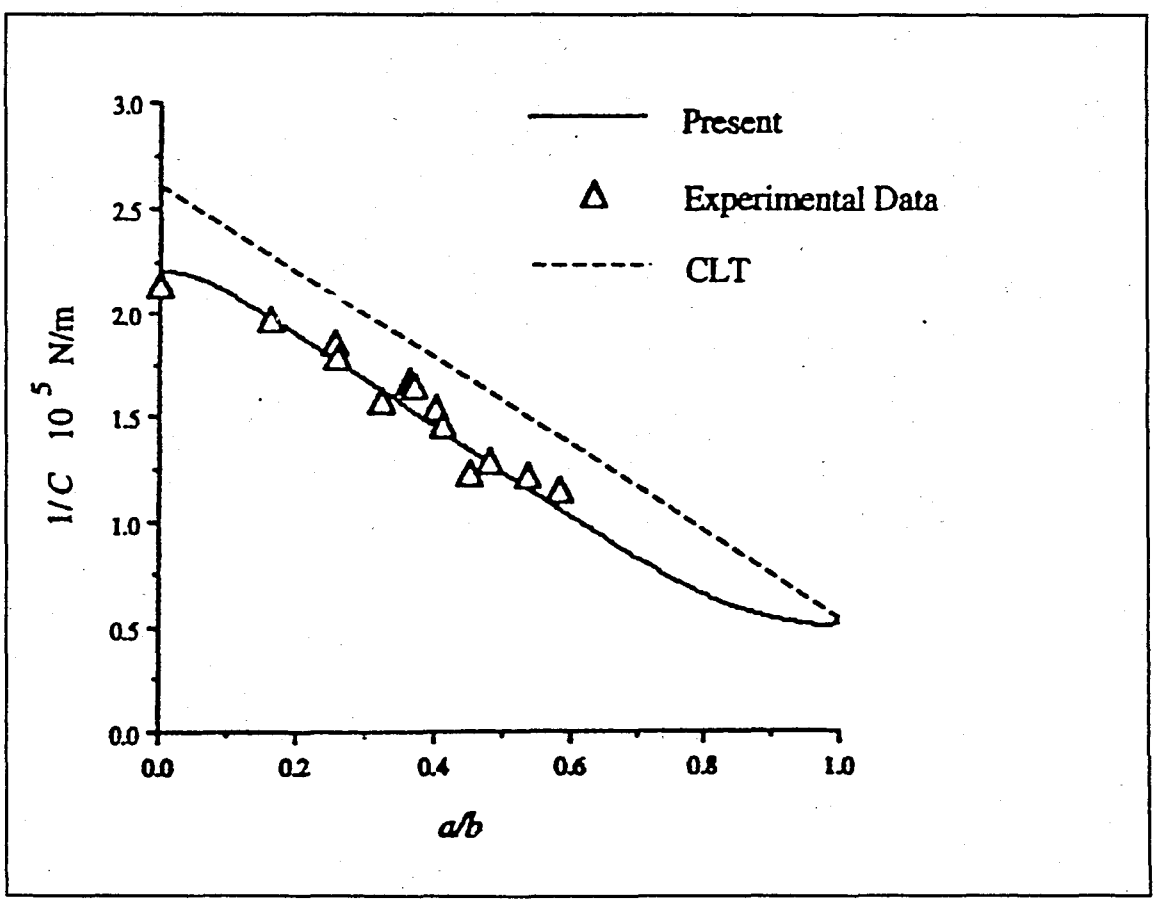

FIGURE 5.4. Inverse of the compliance as a function of normalized crack length a/b for $[\ 90/(\pm 45)_n(\mp 45)_n/90]_s$ layup (Li and Wang, 1994).

Mode III fracture toughness calculated by the shear deformation theory and from the compliance calibration method used in the experiment (Lee, 1993) are 1.18 kJ m^{-2} and 1.14 ±0.22 kJ m^{-2}, respectively. The only parameters needed from experiment in the shear deformation theory for fracture toughness calculation are the critical load, P_c and the corresponding crack length, a (Li and Wang,1994).

A further study on the simplification of the data reduction methods for the edge crack torsion test was presented by Li and O'Brien (1996). By taking advantage of the special lay-up for mode III testing using ECT specimen, the lengthy expression for compliance is simplified. The simplified expressions are in terms of parameters with well-known physical meanings.

Since for the proposed lay-up bending-twisting coupling can be neglected, the coefficients α_{21} is negligible. In addition, the sublaminates above and below the delamination plane should be symmetric about their own midplanes to eliminate any residual thermal stress contributions to strain energy releas rate for delamination growth.

The simplified expression for the inverse of the compliance is:

$$\frac{1}{C} = \frac{P}{\delta} = \frac{8}{ld^2}\left\{\left(D_{66} + \frac{h^2}{4}A_{66}\right)b - \frac{h^2}{4}A_{66}a + D_{66}f_1 + \left(D_{66} + \frac{h^2}{4}A_{66}\right)f_2\right\} \quad (5.25)$$

where f_1 and f_2 are the same parameters derived by Li and Wang (1994), equations (5.20) and (5.21).

5.5. The Effect of Transverse Shear Modulus

Moreover, Li and O`Brien (1996) have investigated the effect of transverse shear modulus, G_{23}, because in the analysis of Li and Wang (1994) the transverse shear modulus G_{23} is to be known. However, the transverse shear modulus G_{23} is much more difficult to determine than in-plane properties, such as E_{11}, E_{22} and G_{12}.

To asses the effect of G_{23}, two extreme values of G_{23} are examined (Li and O'Brien,1996); $G_{23}=0$ and $G_{23}=G_{12}$. The theoretical predictions of the inverse of the load point compliance 1/C for both the $G_{23}=0$ and $G_{23}=G_{12}$ cases are plotted in figure 5.5.

$G_{23}=0$ yields a lower value for 1/C and $G_{23}=G_{12}$ gives a higher value for 1/C. In conclusion the appoximation of $G_{23}=G_{12}$ appears to give a good conservative prediction of the mode III toughness.

5.6. Finite Element Analysis

A three-dimensional finite element analysis was performed (Li et al, 1997) using ANSYS sotfware package, that indicated that a pure mode III delamination exists at the middle of the specimen length away from both ends. The model is constructed using an arbitrary specimen tested successfully. To model the edge crack torsion (ECT) specimen and the crack plane, 34048 eigth-noded solid elements (SOLID45) and 4669 contact elements (CONTAC49) are used.

The model was supported in z direction at three nodes where the nodal locations are equivalent to the position of the three supporting pins of the edge crack torsion (ECT) fixture. The remaining two translational rigid body motions were prevented. A critical test load is applied.

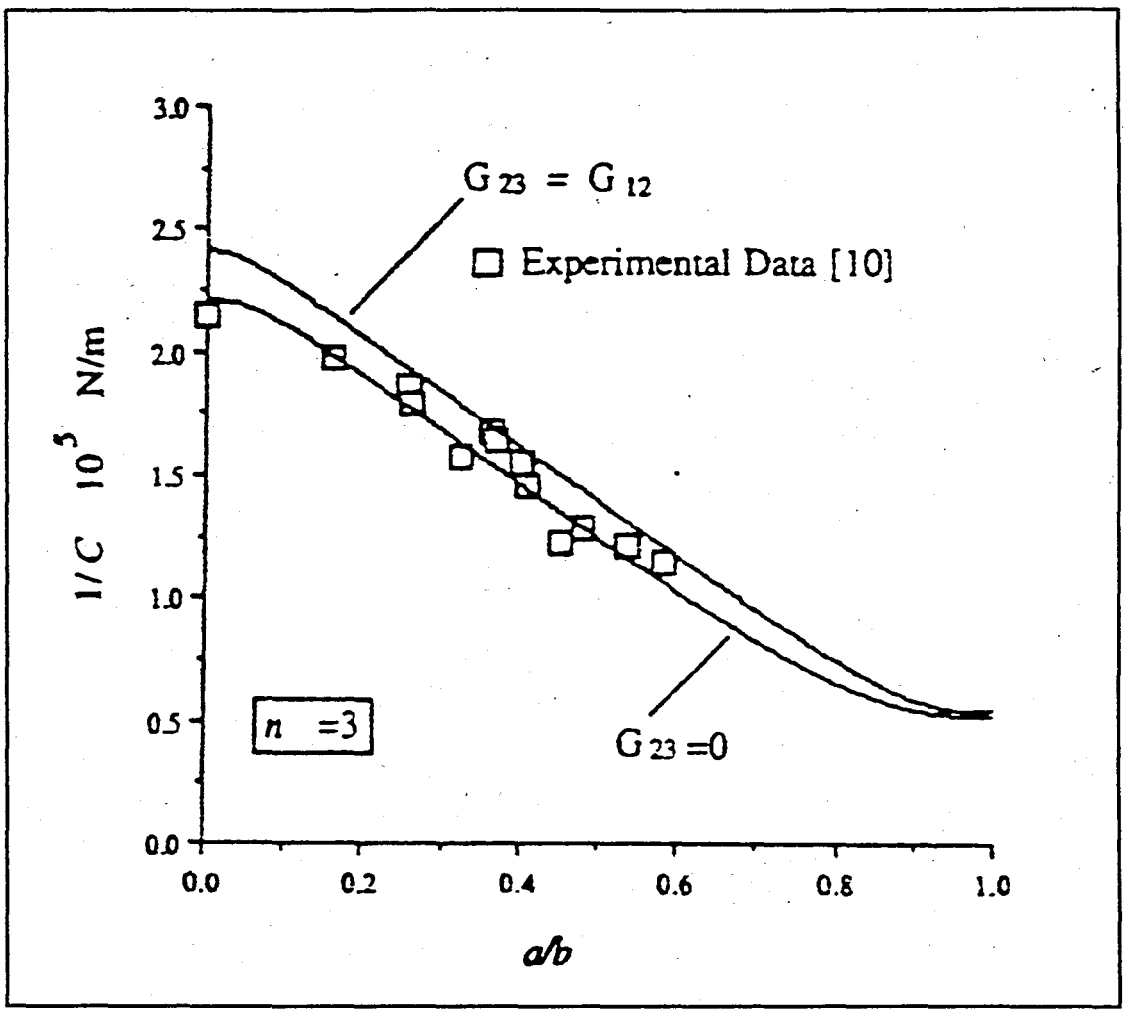

FIGURE 5.5. Inverse of the compliance 1/C for both the G_{23}=0 and G_{23}=G_{23} case (Li and O'Brien,1996).

The mode I, mode II and mode III strain energy release rate components are calculated using virtual crack closure technique. Virtual crack closure technique uses the stresses/nodal forces ahead of the delamination front and the displacements behind the front to determine the strain energy release rate components (Figure 5.6.). The expressions are as follows (Li et al, 1997):

$$G_I = \frac{F_{zj}\delta_{zi}}{2\Delta a \Delta x} \tag{5.26}$$

$$G_{II} = \frac{F_{yj}\delta_{yi}}{2\Delta a\Delta x} \tag{5.27}$$

$$G_{III} = \frac{F_{xj}\delta_{xi}}{2\Delta a\Delta x} \tag{5.28}$$

where Δx is the sum of one-half the element lengths on either side of node j in the x direction.

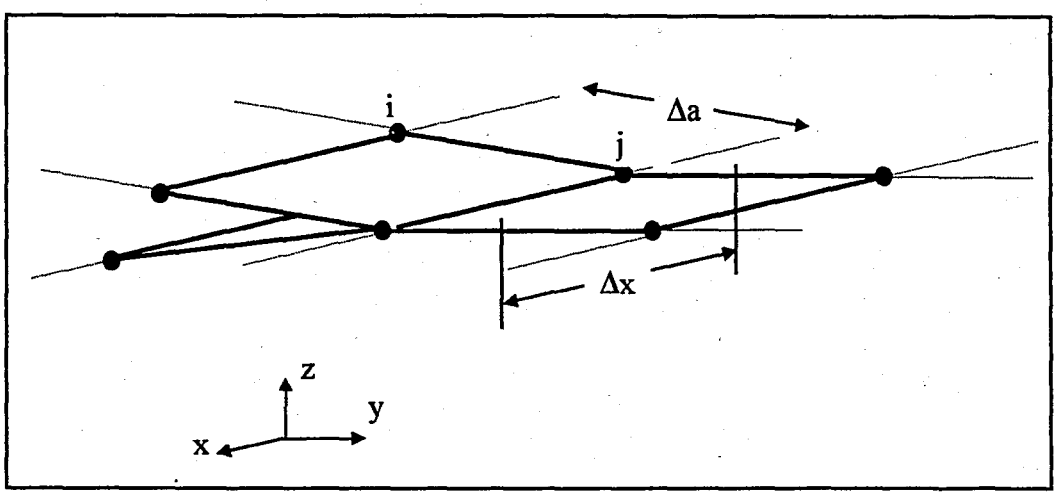

FIGURE 5.6. Virtual crack closure for three dimensional eigth node solid elements.

The numerical results of Li et al. (1997) revealed the distribution of strain energy release rate components along the length of the delamination front shown in figure 5.6. The mode I component is negligibly small. A finite mode II component is observed near the loading points, but decreases away from the loading points. The finite element analysis shows that the delamination will grow in pure mode III at the middle of the specimen length away from both ends. The average total strain energy release rate and mode III component computed from the finite element model are 1.35 kJ m^{-2} and 1.24 kJ m^{-2}, respectively, which indicates the critical total strain energy release rate, integrated along the delamination front at the insert, is 92 per cent mode III.

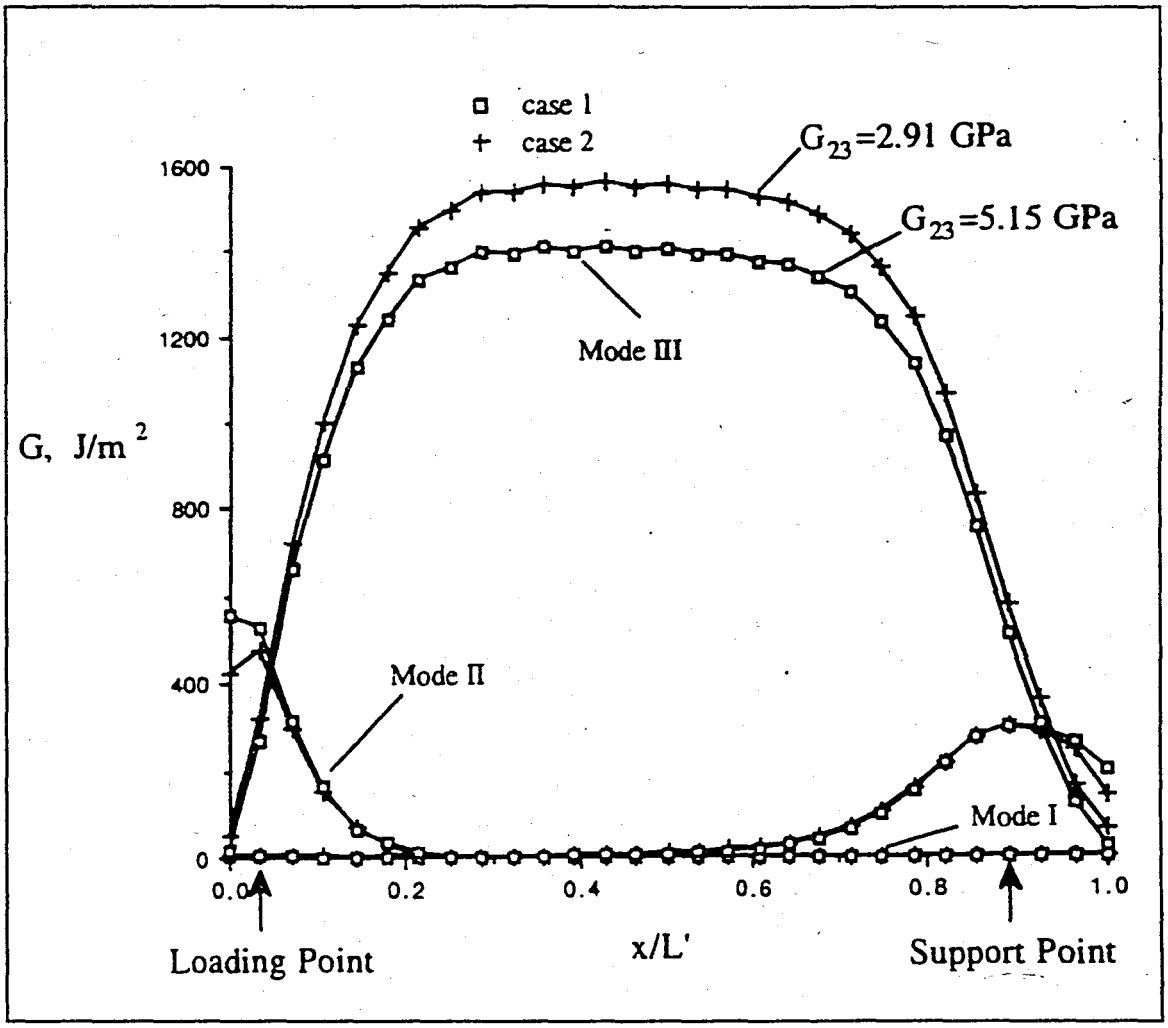

FIGURE 5.7. The distribution of strain energy release rate components along the length of the delamination front (Li et al., 1997)

6. FINITE ELEMENT ANALYSIS AND OPTIMIZATION OF ECT SPECIMEN

A three dimensional finite element model is constructed in order to analyze the edge crack torsion (ECT) specimen for mode III interlaminar fracture testing. The same model is used to investigate the optimum dimensions of the specimen.

The analysis is carried out using ANSYS® finite element software package version 5.2. on a Hewlett Packard workstation model 712-60 operated with Hp-Unix version 10.20.

The presented study covers the construction of the finite element model and the validation of the model by comparing and reconstructing analyses reported in the literature (Lee 1991, Li and Wang 1994, Li et al. 1997).

At the end, a series of finite element analyses are carried out to optimize the edge crack torsion (ECT) specimen for mode III interlaminar fracture.

6.1. The Finite Element Model

The solid model of the ECT specimen is constructed using 24 volumes (Figure 6.1). The smaller volumes near the edges are used to exactly locate the loading and supporting points. Therefore the corners of the volumes coincide with the locations of the loading and supporting points. One set of 12 volumes is located on top of the other set. The crack is modeled joining all the volumes except the volumes above and below the crack surface (Figure 6.2).

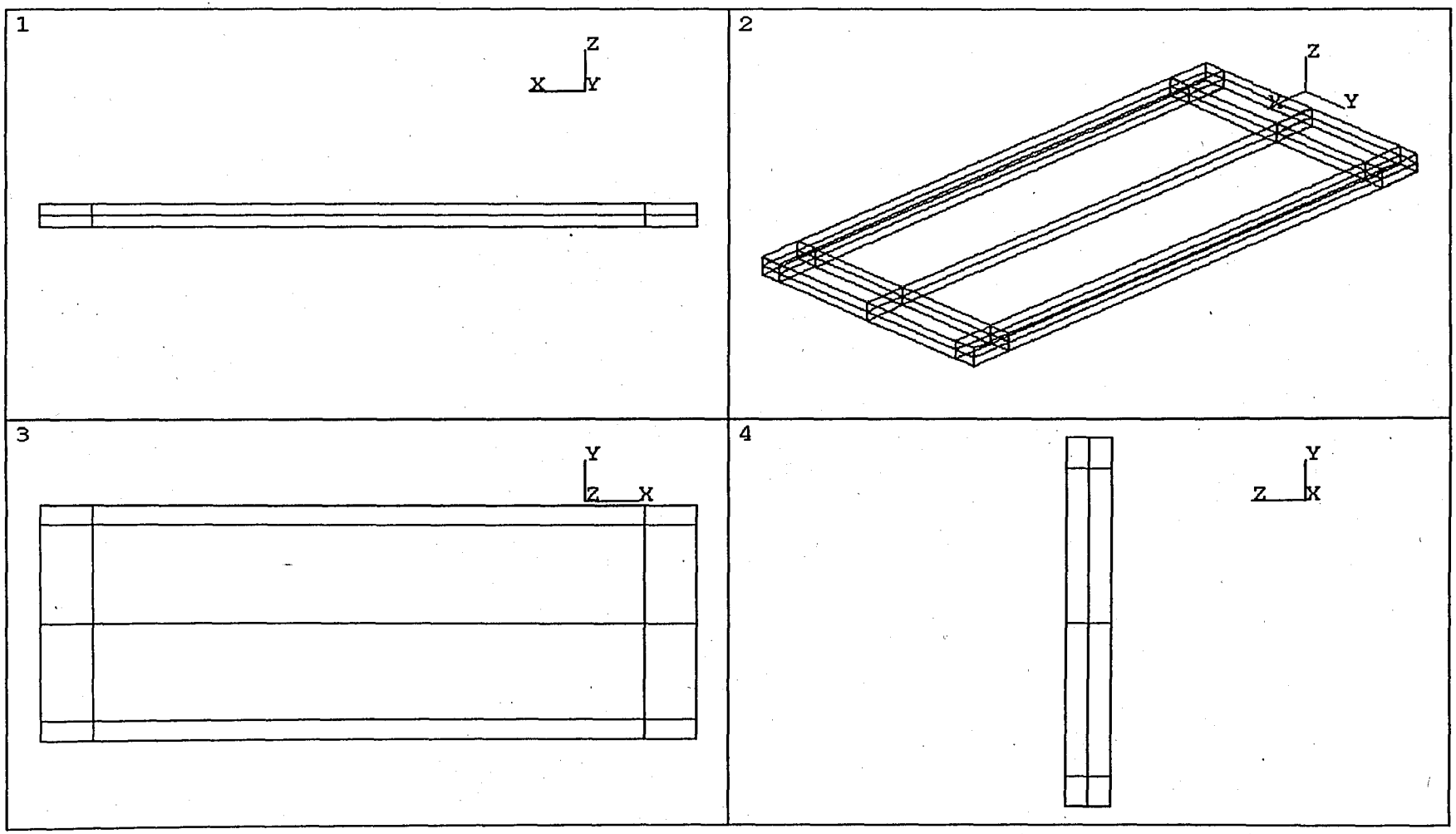

FIGURE 6.1. The solid model of edge crack torsion (ECT) specimen, crack to width ratio (a/B) is 1/2.

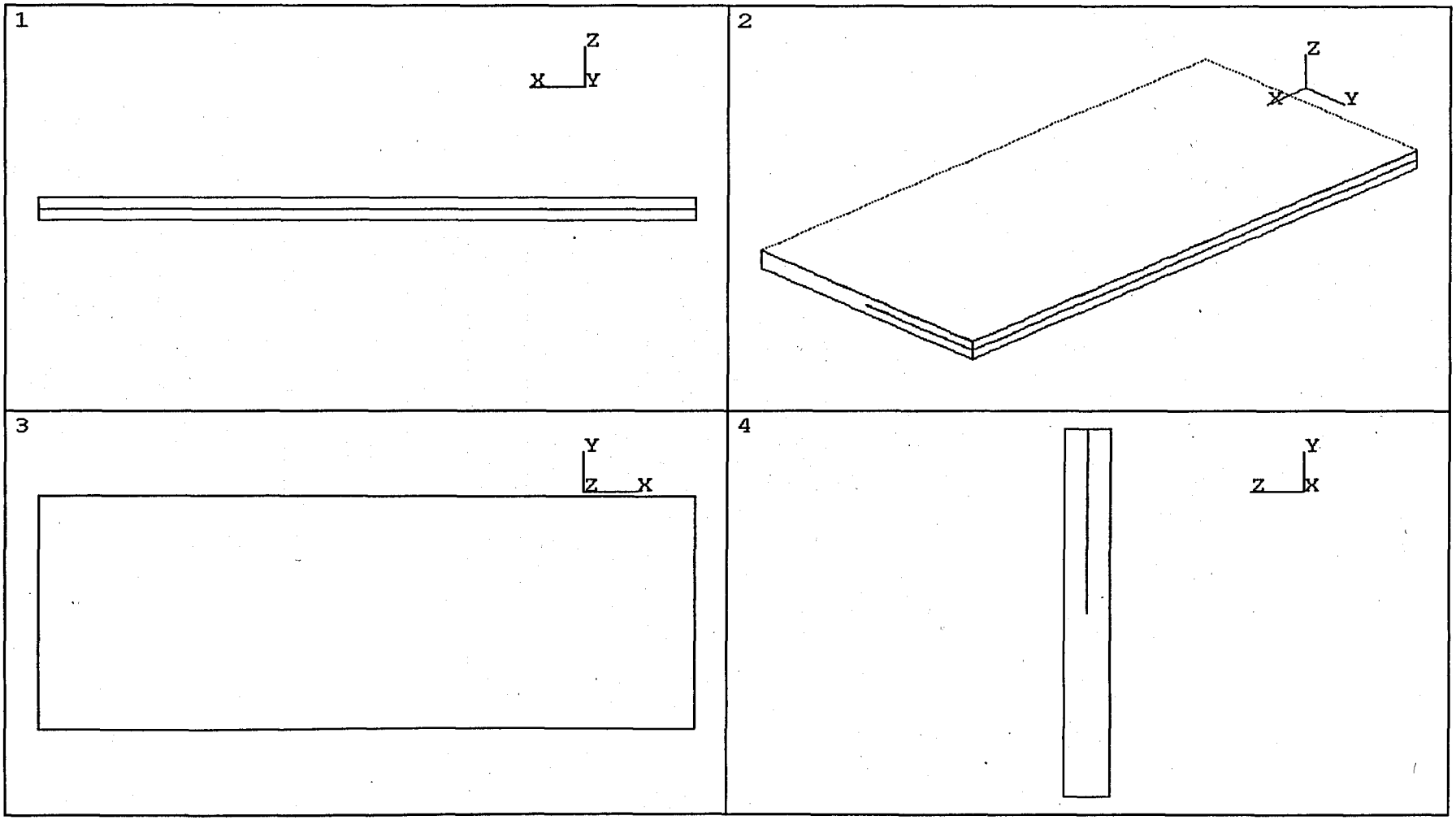

FIGURE 6.2. The modelling of the crack in a edge crack torsion (ECT) specimen.

Several material properties are used at various analyses (Table 6.1):

(a) properties of G40-800/R6376 are used to reproduce the finite element analysis of Li et al. (1997),

(b) properties of R6376/IM6 are used to model the experimental work of Lee (1991) and to compare the results with the analytical work of Li and Wang (1994) and

(c) properties of R6376/IM6 are used to optimize the ECT specimen.

TABLE 6.1. Material properties of different composite materials which are used in the finite element analyses.

	R6376/IM6	G40-800/R6376
	(Lee, 1993)	(Li et al, 1997)
E_x	165 GPa	151 GPa
E_y	10.3 GPa	8.97 GPa
E_z	10.3 GPa	8.97 GPa
G_{xy}	5.5 GPa	5.15 GPa
G_{yz}	5.5 GPa	5.15 GPa
G_{xz}	5.5 GPa	5.15 GPa
ν_{xy}	0.28	0.325
ν_{yz}	0.28	0.325
ν_{xz}	0.28	0.325

The solid model of the specimen is meshed with eight-noded-hexahedral layered elements (labeled as SOLID46 in ANSYS®) and with point-to-surface elements (labeled as CONTAC49). The "real constants" of the layered elements requested by the software are arranged such that the desired lay-up, $[90/(\pm 45)_3/(\mp 45)_3/90]_s$, is modeled.

The length is meshed with equilength elements. The thickness is meshed with four SOLID46 elements, which are designed for the analysis of composite laminates, each one of them representing seven layers. The width is meshed with elements, whose size decreases near the crack tip providing finer mesh (Figure 6.3). At the crack surface there are two nodes at the same location, one of them belonging to the upper elements and the other to the lower elements.

To prevent that the upper and lower surfaces penetrate into each other, which is physically meaningless, non-linear point to surface contact elements (CONTAC49) are introduced between surfaces at the region where the contact would start first, i.e. around the loading and supporting points (Figure 6.4).

The boundary conditions, constrain the displacement of the nodes at the support points in the z direction as in the edge crack torsion (ECT) fixture. The displacement loading in z direction is introduced at the loading point or node. The applied displacement loading may have a convenient value if the only concern is to calculate the compliance. In the case of determination of fracture toughness the value should be the critical displacement corresponding to critical load measured by an experiment or obtained from the literature. To prevent rigid body motion of the model the following restraints in x and y direction are applied (Figure 6.5).

At node one: ux=uy=uz=0

At node two: uz=uy=0

At node three: uz=ux=0

At node four: uz=(the displacement loading)

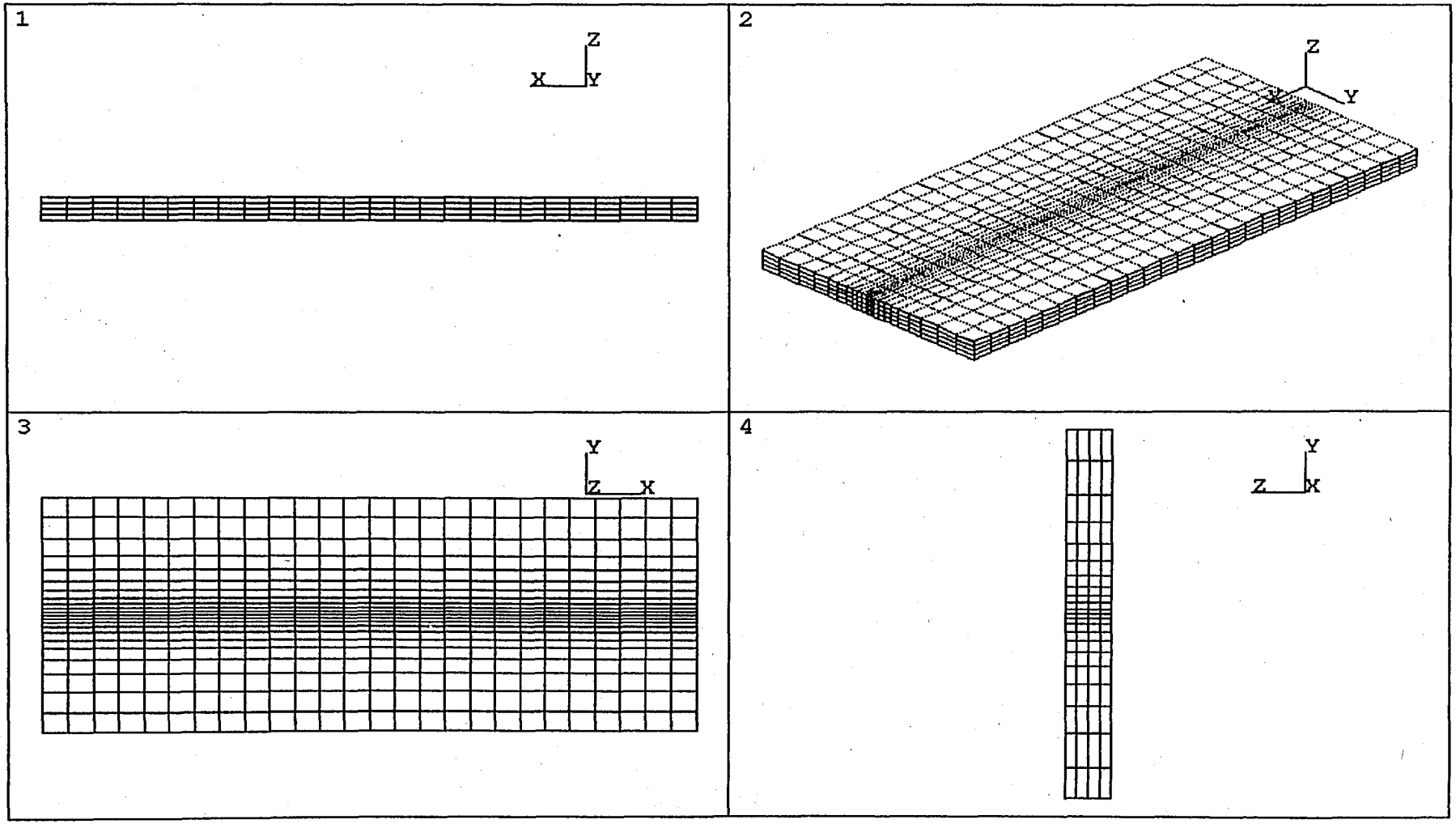

FIGURE 6.3. The meshed model of edge crack torsion (ECT) specimen.

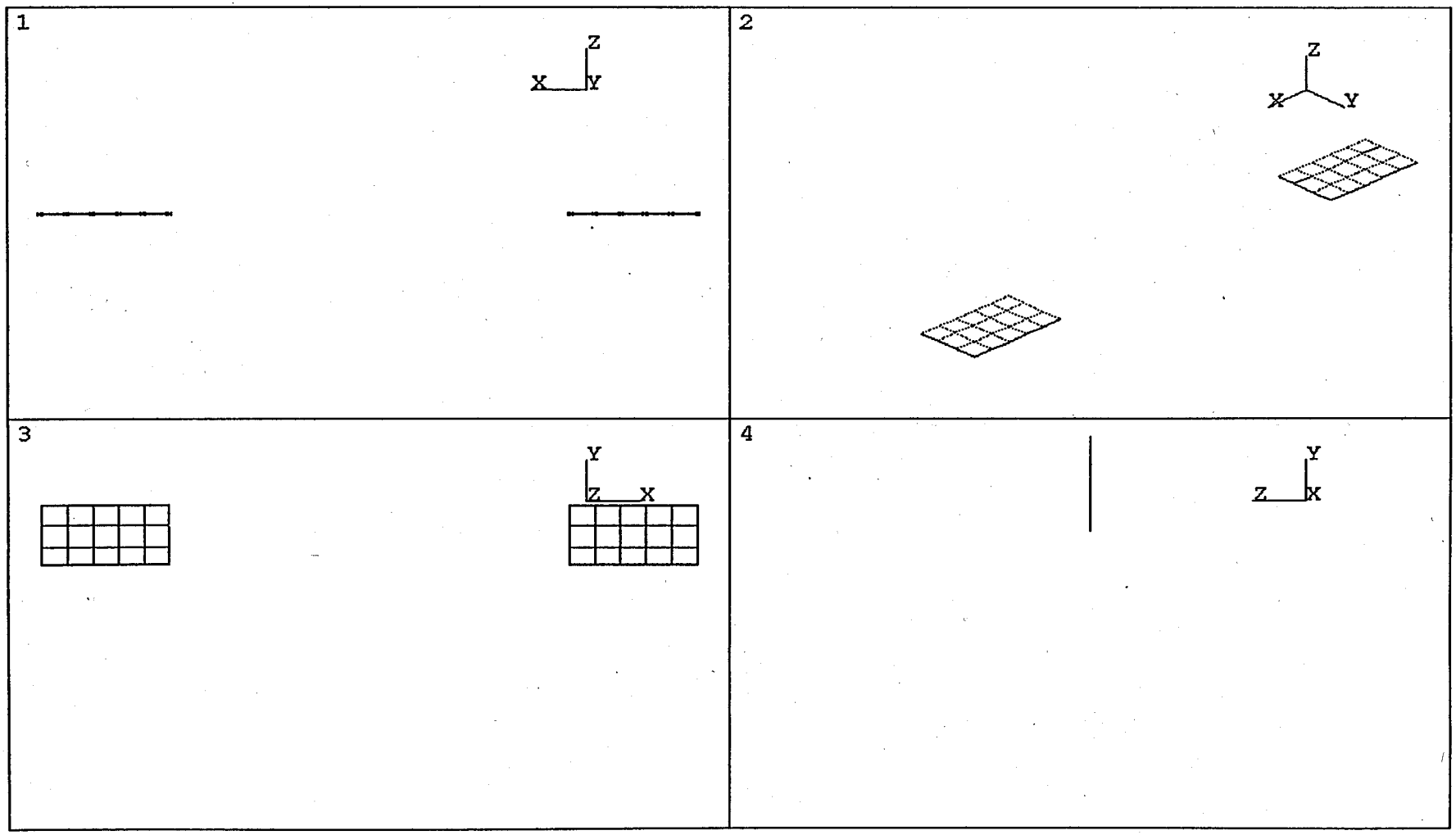

FIGURE 6.4. The contact elements used in the finite element analysis of ECT specimen.

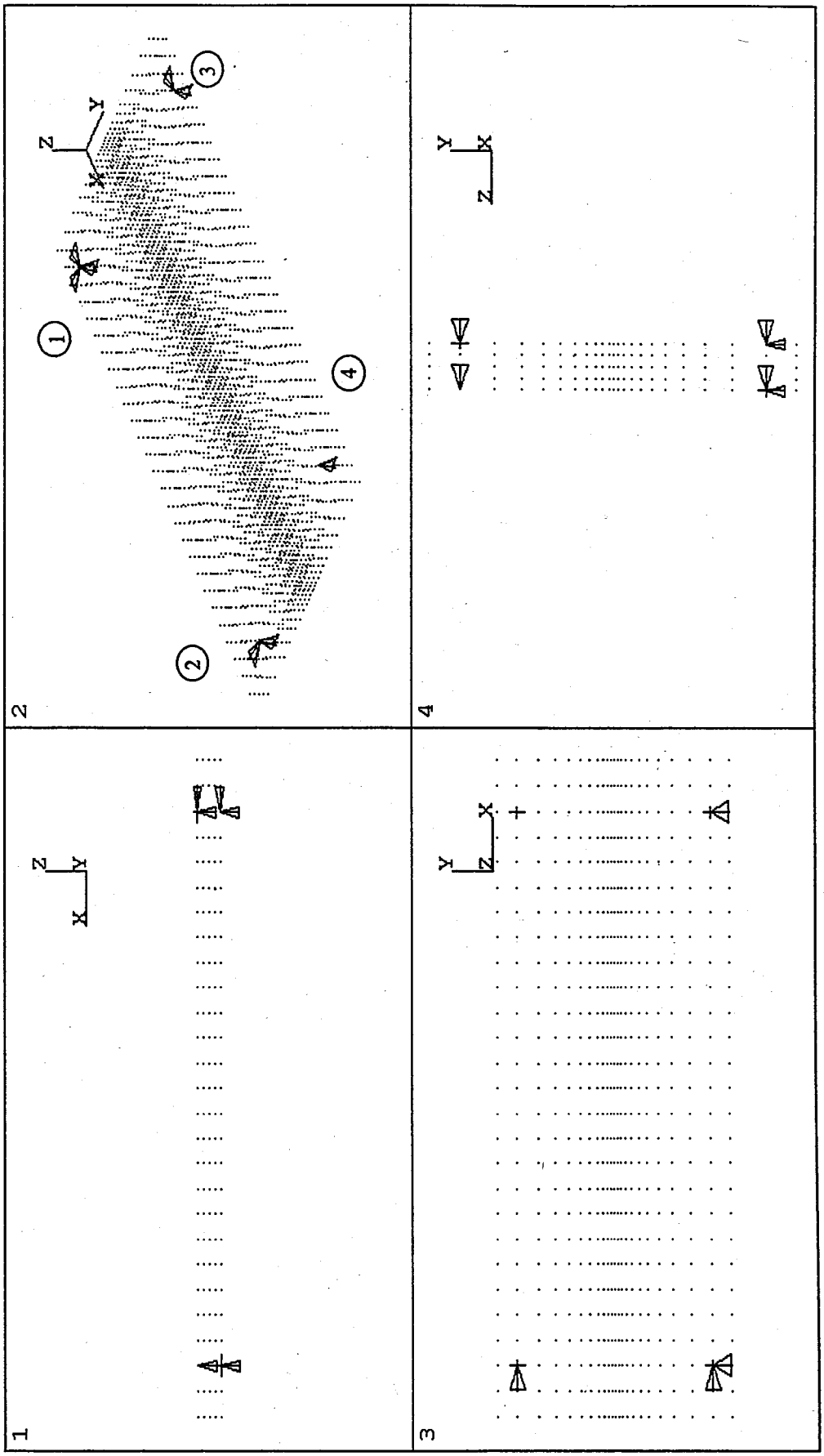

FIGURE 6.5. The boundary conditions applied to the finite element model of ECT specimen.

For the software to utilize the contact elements a KN value should be provided. Unfortunately the contact elements are non-linear and the value of KN should be determined by iterative methods, starting with a guess suggested in the manual of the software (ANSYS, 1995).

$$KN \approx fEH, \quad \text{with } f=1 \tag{6.1}$$

where E is the elastic modulus, h is the characteristic contact "length" (usually the typical element length)

During the iterations the following problems are encountered:

(a) the solution did not converge if KN is high.

(b) penetration of surfaces is observed if KN is low.

After some iterations KN=592000 is accepted and is used in the analyses.

The analysis is non-linear and the Full Newton-Rapson method with default options is selected in the software.

6.2. The Validation of The Model

To verify the model, the finite element analysis of Li et al. (1997) is reproduced and the testing of Lee (1993) is examined using finite element analysis.

6.2.1. Reproduction of The Finite Element Analysis of Li et al. (1997)

Since the presented finite element model is based on the model of Li et al. (1997) both models are similar. The differences are in the mesh pattern along the thickness and in the contact element parameters.

In the finite element analysis eigth-noded-hexahedral layered elements (SOLID46) are used whereas Li et al. (1997) used ordinary eight-noded-hexahedral elements (SOLID45). Since layered element can handle multiple laminate plies, a great reduction in element number can be achieved. Li et al. (1997) had to model each ply. Therefore they used 32 elements along the thickness. In the presented model 4 layered elements were enough.

The other difference lies in the properties of the contact elements. However this difference arises only due to the lack of information in the paper of Li et al. (1997). In the finite element analysis the contact elements are only placed around the loading points between the crack surfaces. Li et al.(1997) placed the contact elements everywhere in the crack surface. However they concluded that this excessive use of contact elements were needles (Li et al. 1997).

Due to the modelling with layered elements and elimination of needles contact elements the model could be contructed with 4340 elements instead of 38048 elements. The properties of the model are :

(a) length=89mm,

(b) width=38mm,

(c) height=4.8mm,

(d) lay-up: $[90/(\pm 45)_3/(\mp 45)_3/90]_3$,

(e) crack length=19mm,

(f) elements: 4256 SOLID46 and 84 CONTAC49,

(g) material : G40-800/R6376,

(h) the displacement loading= 4.63mm.

The resulting deformed shape obtained from the analysis is shown in figure 6.6 and figure 6.7.

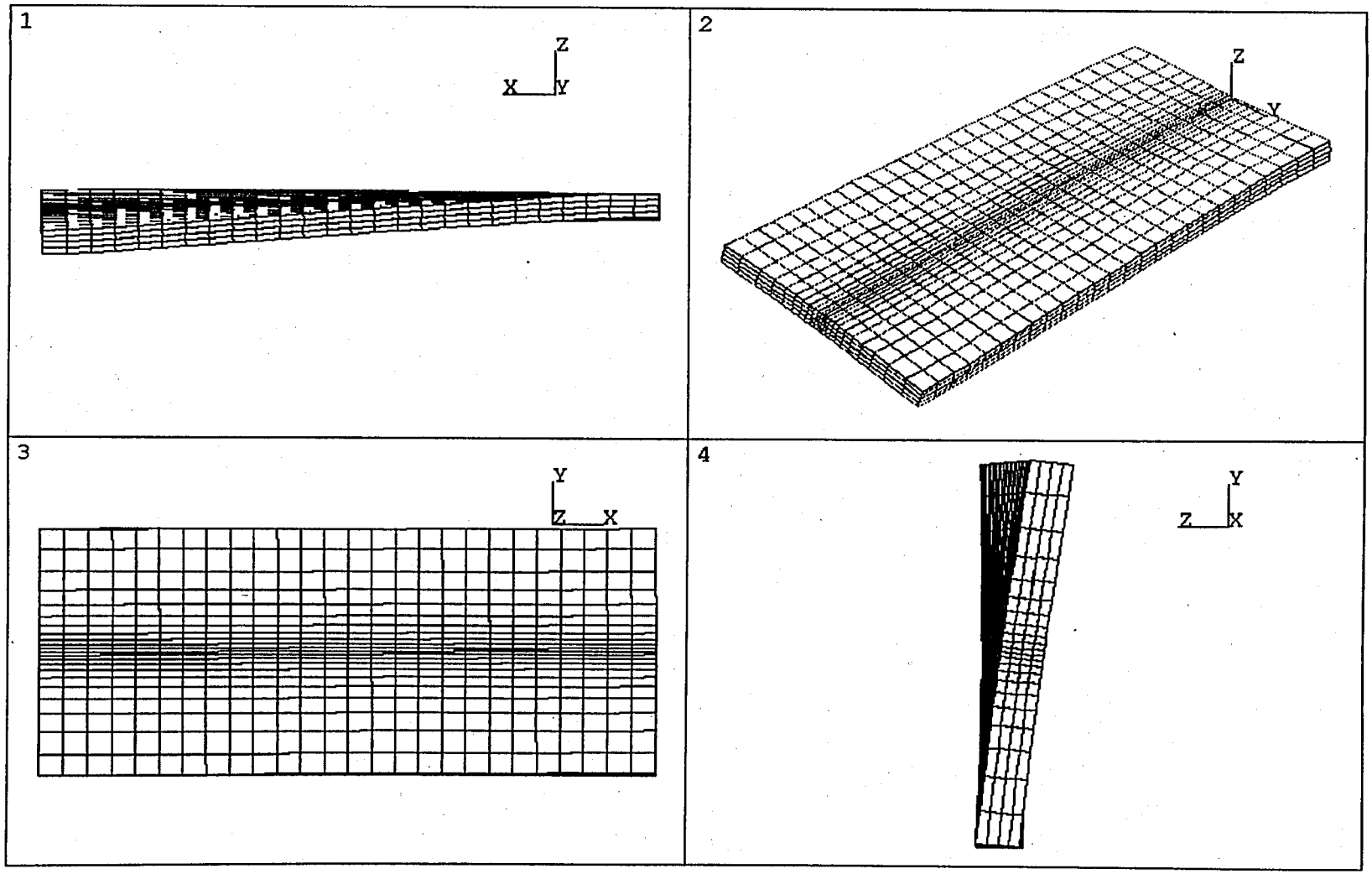

FIGURE 6.6. Deformed shape obtained from the finite element analysis of ECT specimen, the elements.

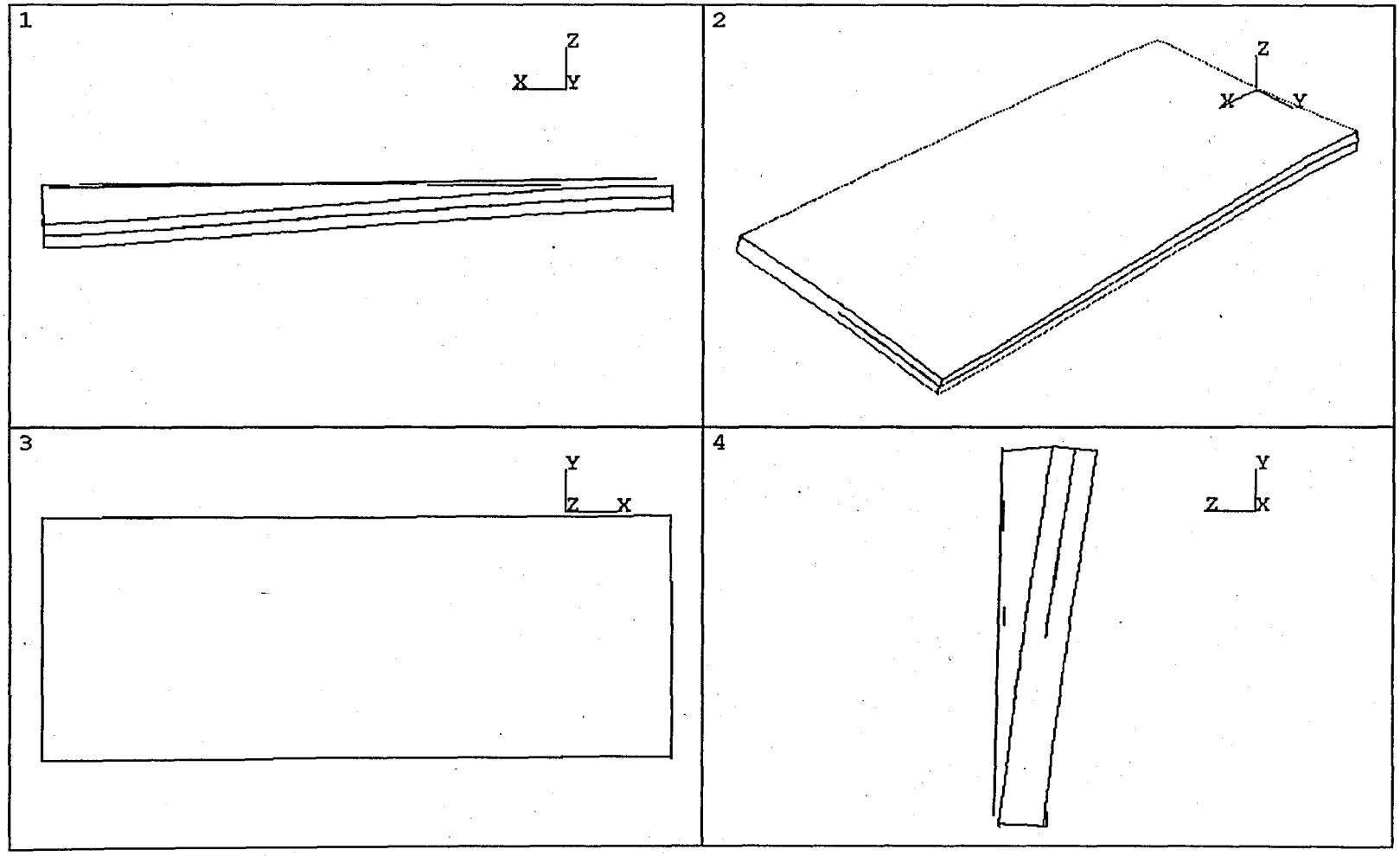

FIGURE 6.7. Deformed shape obtained from the finite element analysis of ECT specimen, the volumes.

Using the deformed specimen output, strain energy release rate at every node on the crack front is calculated using virtual crack closure technique.

As an example strain energy release rate is calculated for an arbitrary node. Consider 17th node from the right (Figure 6.8).

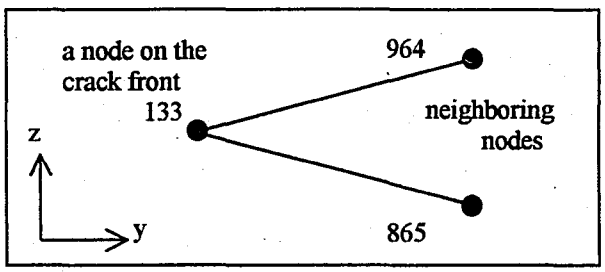

FIGURE 6.8. The nodes near the crack front, required to apply virtual crack closure technique (The x direction is perpendicular to plane of the nodes).

The output for the considered nodes (Figure 6.8) is

at node 133: F_x=360.0673 N

at node 964: u_x=0.2292 10^{-4}m

at node 865: u_x=0.26909 10^{-4}m

$dx=u_{x,865}-u_{x,964}$=0.03989 10^{-4}m

Δx=0.003179m

Δa=0.000161m

Substituting the values into the equation (5.28):

$$G_{III} = \frac{F_x d_x}{2\Delta x \Delta a} = 1403.141 \, J/m^2 \qquad (6.2)$$

the corresponding result of Li et al. (1997) is

G_{III}=1406.15 J/m^2

The error is 0.2 per cent. The strain energy release rate distribution at every node on the crack front is listed in table 6.2. and is plotted in figure 6.9. The results are in good agreement with the results of Li et al. (1997). The distribution of strain energy release rates reveal that the dominant component is in out-of-plane shearing mode, i.e. mode III.

TABLE 6.2. The strain energy release rate distribution along the crack front.

node	G_{III} (J/m^2)
1	9.401
2	398.324
3	792.116
4	1128.438
5	1257.439
6	1410.495
7	1423.703
8	1481.361
9	1453.518
10	1477.067
11	1441.526
12	1455.083
13	1423.373
14	1435.513
15	1409.784
16	1423.450
17	1403.268
18	1420.904
19	1404.714
20	1421.665
21	1384.997
22	1343.362
23	1190.720
24	993.698
25	694.530
26	438.927
27	211.656
28	90.917
29	1.447

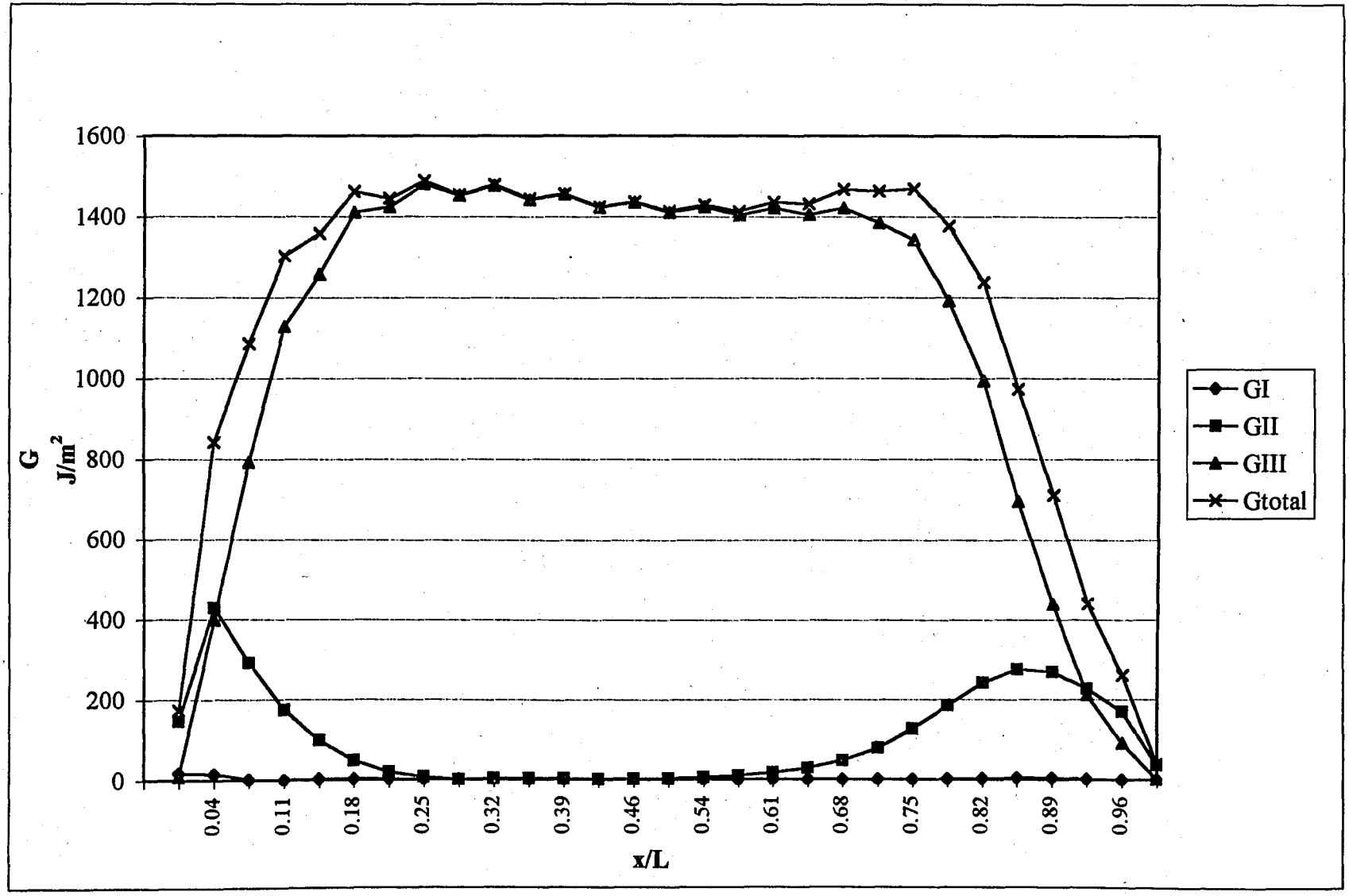

FIGURE 6.9. Distribution of the strain energy release rate components along the crack front.

The average strain energy release rate can be calculated by integrating the mode III component over the effective region, i.e. the region between the support/loading points, along the delamination front and divided by the effective length of the ECT specimen. If the average total strain energy release rate is calculated similarly, the percentage of mode III component of strain energy release rate can be obtained.

The percentage of G_{III} is found to be 91.9 per cent whereas Li et al. (1997) found 92 per cent. Similarly average G_{tot} and average G_{III} corresponding to a critical load are 1.38 and 1.27 kJ/m^2 , respectively and Li et al. (1997) report as 1.35 and 1.24 kJ/m^2 , respectively. Tests of Li et al. (1997) yielded a fracture toughness of 1.42 kJ/m^2. Knowing that the value of G_{23} is an approximation (Li and O'Brien, 1996) and the value is closer to the results of the experimental data, the model can be said to be validated.

6.2.2. Finite Element Analysis of the Test of Lee (1993)

A further verification is carried out by modeling the test of Lee (1993). The finite element model is the same. The material properties are changed to the properties of R6376/IM6 and the applied displacement loading is set to 0.001m.

Li and Wang (1994) developed an analytical model to calculate the compliance of the specimen proposed by Lee (1993). If the compliance is known, the load corresponding to the specified displacement can be found. The force values for a/B=1/2 and for a displacement input of 0.001m is calculated using the expression of Li and Wang (1991) and using the presented finite element analysis are:

$F_{\text{Li and Wang}}$=124.1448 N

$F_{\text{finite element}}$=124.143 N

The associated error is 0.001 per cent. This very small error justifies that the constructed finite element model is validated.

6.3. Optimization of Edge Crack Torsion (ECT) Specimen

In the Lokman's thesis (1997) it is suggested that the percentage of mode III component of strain energy release rate, G_{III}, would increase if the specimen length increases. Although the proposed configuration (Lee, 1993) provides already a high percentage of G_{III}, that is, 92 per cent, for a better geometry the percentage of G_{III} should become closer to 100 per cent.

A series of finite element analyses are carried out to investigate the effect of specimen size on the percentage of G_{III}. Therefore, batch files are developed which enable to model specimens with various dimensions. The batch files are written in ANSYS parametric design language (APDL) (ANSYS, 1995) and are presented in the appendix.

The individual and simultaneous effects of specimen length and width are investigated. The effect of thickness has already been examined by Lee (1993). The analyses are carried out with specimens having a crack-to-width ratio (or normalized crack length) (a/B) of 1/2. Additional set of analyses are done with models having a crack-to-width ratio (a/B) of 1/3. This few analyses are only used to support the behaviour obtained from the main analyses.

The constructed model for the specimen having crack-to-width ratio (a/B) of 1/3 can be summarized in figures 6.10. and 6.11. It can be seen that the model is very similar to the previous model, the only change is the position of the crack front. The mesh pattern is adapted accordingly.

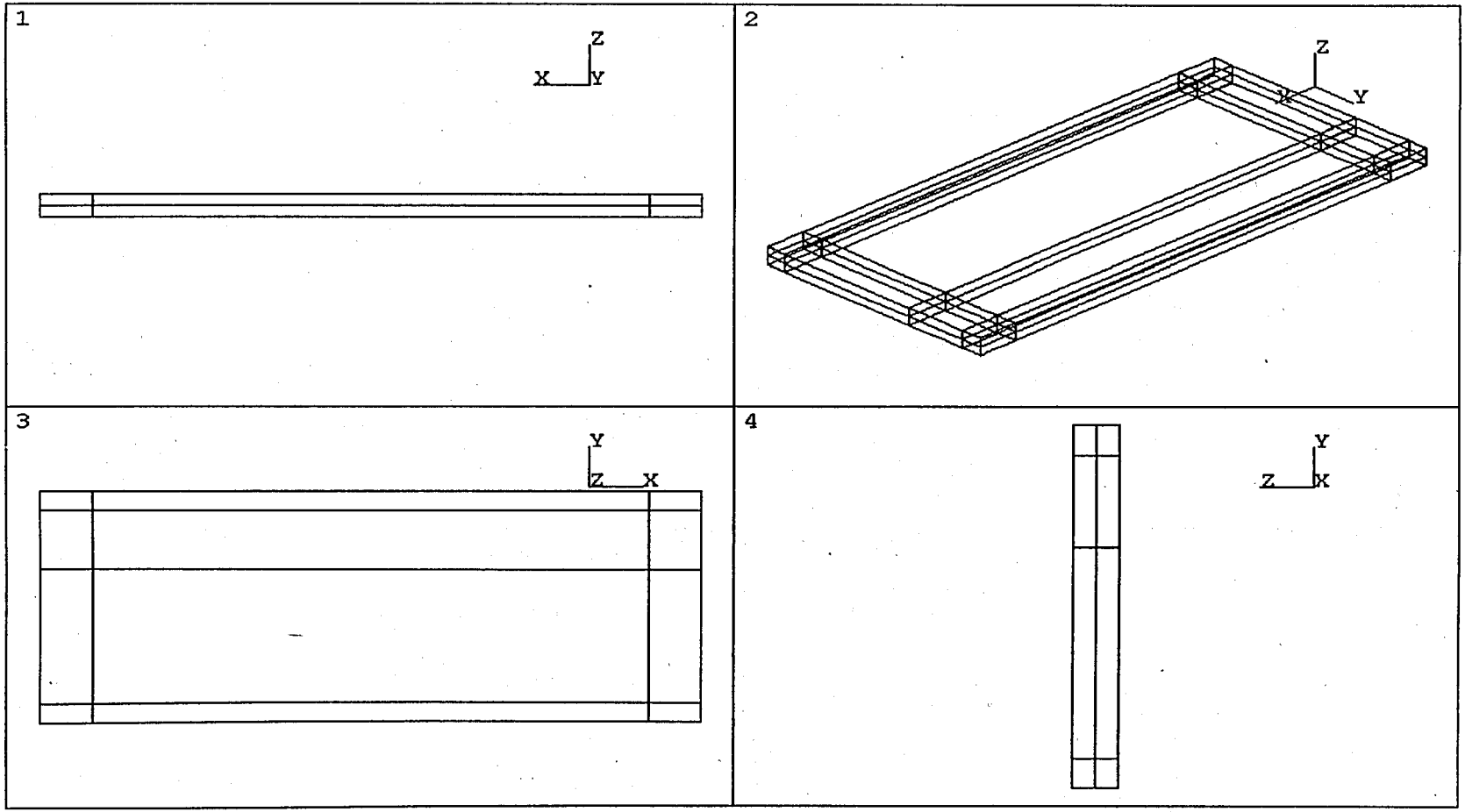

FIGURE 6.10. Solid model of Edge crack torsion specimen with a crack to width ratio of 1/3

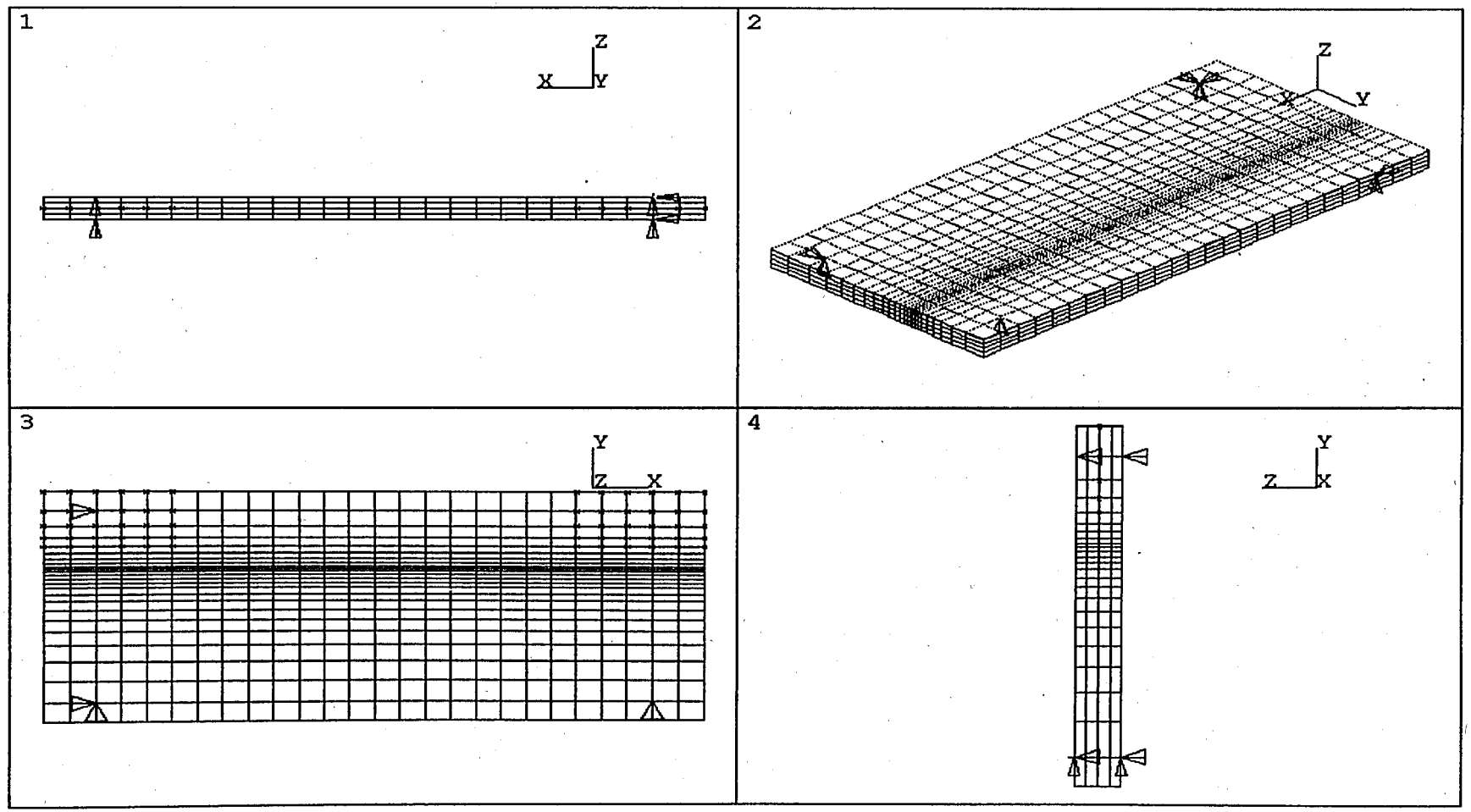

FIGURE 6.11. Finite element model of Edge crack torsion specimen with a crack to width ratio of 1/3.

6.3.1. Variation of G_{III} Percentage with Length

Various specimen having different lengths are modelled and analyzed to see the effect of specimen length. The length is the dimension parallel to the crack front. The smallest specimen has the half of the length of the specimen of Lee (1993). And the longest specimen has the double length of the original one (Figure 6.12). All the other dimensions are unchanged.

The mesh pattern remains the same but is coarser and is composed of 2288 eigth-noded-hexahedral layered elements (SOLID46) and 120 point-to-surface non-linear contact elements (CONTA49) for the specimen having the original dimensions. The element size in the longitudinal direction is kept constant. Hence the number of elements is increased with increasing length in that direction. Boundary conditions remain unchanged and the displacement load is also same for all models, and equal to 0.001m.

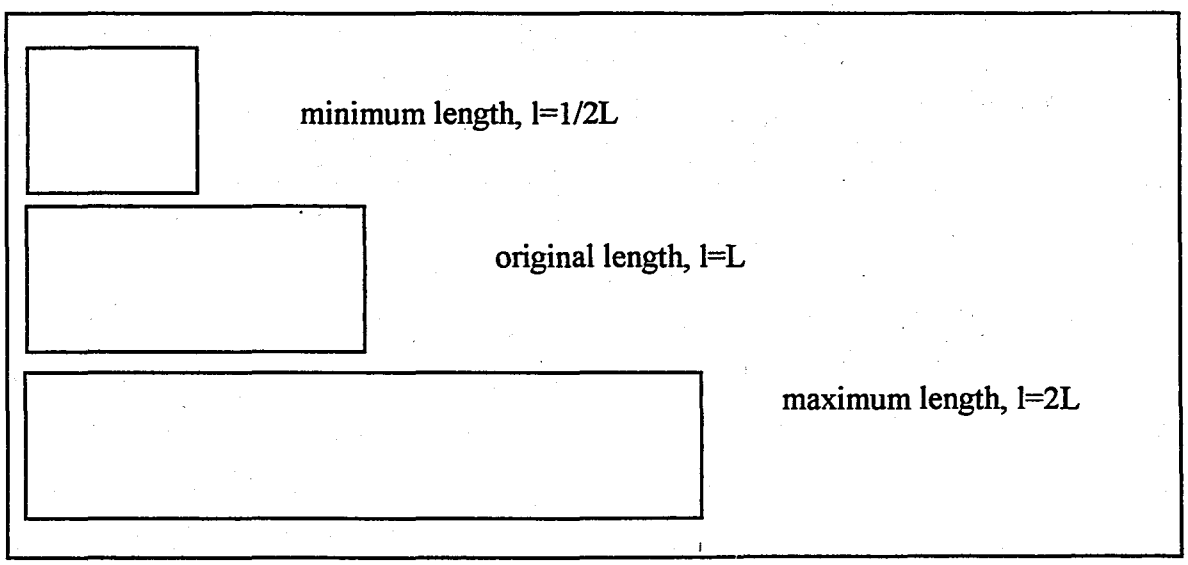

FIGURE 6.12. Comparison of the minimum, original and maximum lengths of the modelled ECT specimen.

The resulting percentage of mode III component of strain energy release rate, G_{III}, versus specimen length is listed in table 6.3 and is plotted in figure 6.13. In addition to that the total strain energy release rate, G_{total}, mode III component of strain energy release rate,

G_{III}, and the difference versus specimen length are listed in table 6.3 and are plotted in figure 6.14.

TABLE 6.3. Variation of the percentage of mode III component of strain energy release rate, G_{III}%, mode III component of strain energy release rate, G_{III}, and total strain energy release rate, G_{total}, with specimen length.

	a/B=1/2			a/B=1/3
l/l(original)	%GIII	GTOT	GIII	%GIII
		J/m^2	J/m^2	
0.500	91.31	816.634	745.657	90.5
0.625	91.25	670.68	612.021	
0.750	91.50	561.168	513.448	92.28
0.875	91.93	479.822	441.086	
1.000	92.39	418.093	386.278	92.71
1.125	92.89	370.269	343.925	
1.250	93.28	331.851	309.548	93.64
1.375	93.65	300.922	281.809	
1.500	94.02	275.195	258.74	94.4
1.625	94.35	253.245	238.947	
1.750	94.67	235.161	222.627	
1.875	94.84	218.953	207.661	
2.000	95.08	205.048	194.969	

As can be seen the percentage of mode III component of strain energy release rate, G_{III} , increases as the specimen length increases for both crack lengths. For the double length a value of 95.08 per cent is achieved for the specimen having the crack-to-width ratio of 1/2. The values for the model having crack-to-width ratio of 1/3 are slightly higher except the value for the minimum length. Excluding that data the trend is very similar.

However the magnitude of G_{III} and of G_{total} decrease. Actually the critical strain energy release rate should be independent of configuration, this shows that the critical loading for each specimen change. The critical load should increase to accommodate the decrease in the strain energy release rate. In fact, the value of G_{total} has no significance in this particular analysis, because the applied load is arbitrary and the analysis is elastic. However, the behavior is of concern.

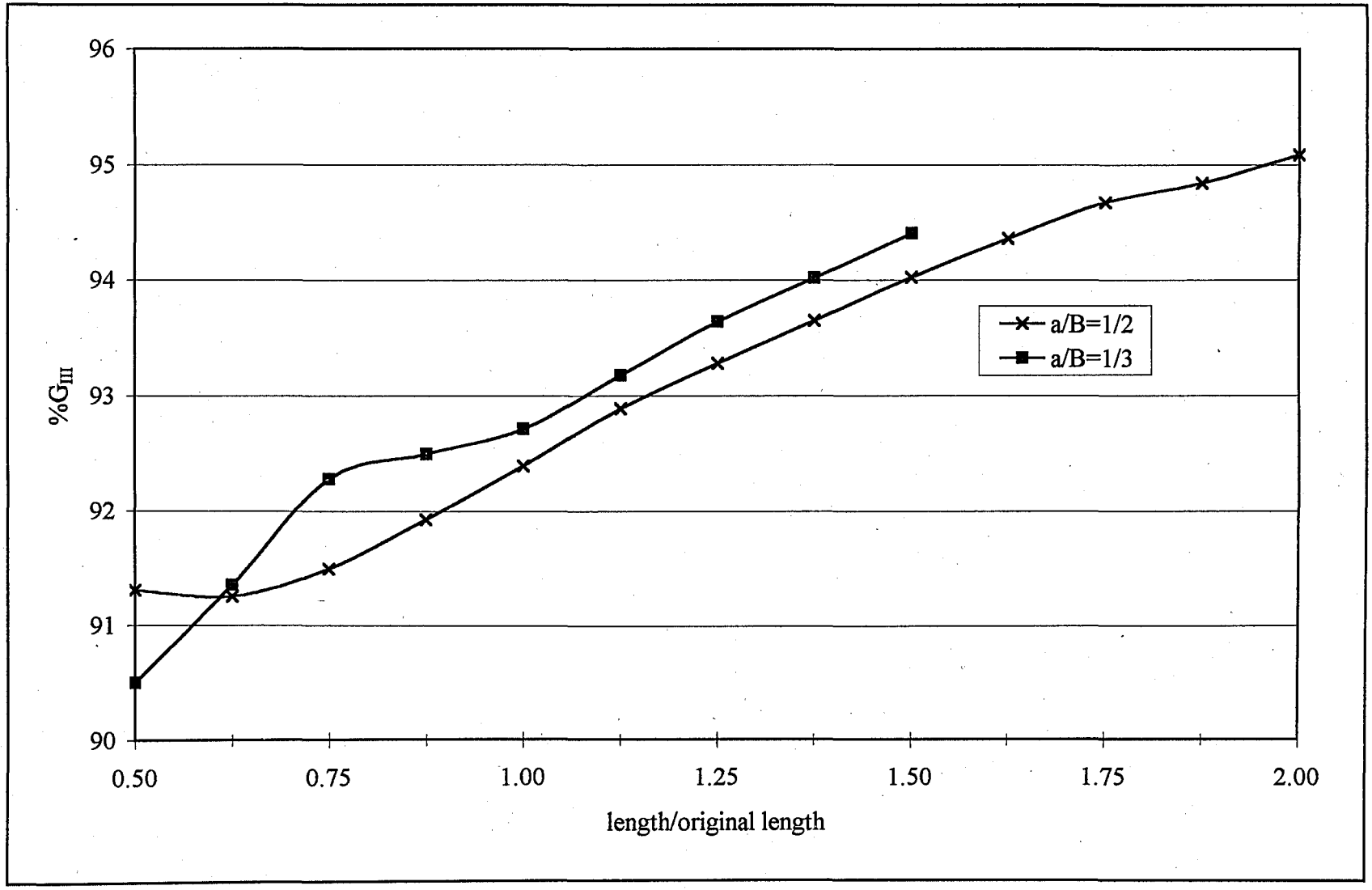

FIGURE 6.13. Variation of the percentage of mode III component of strain energy release rate, G_{III}, with specimen length, for a/B=1/2 and 1/3.

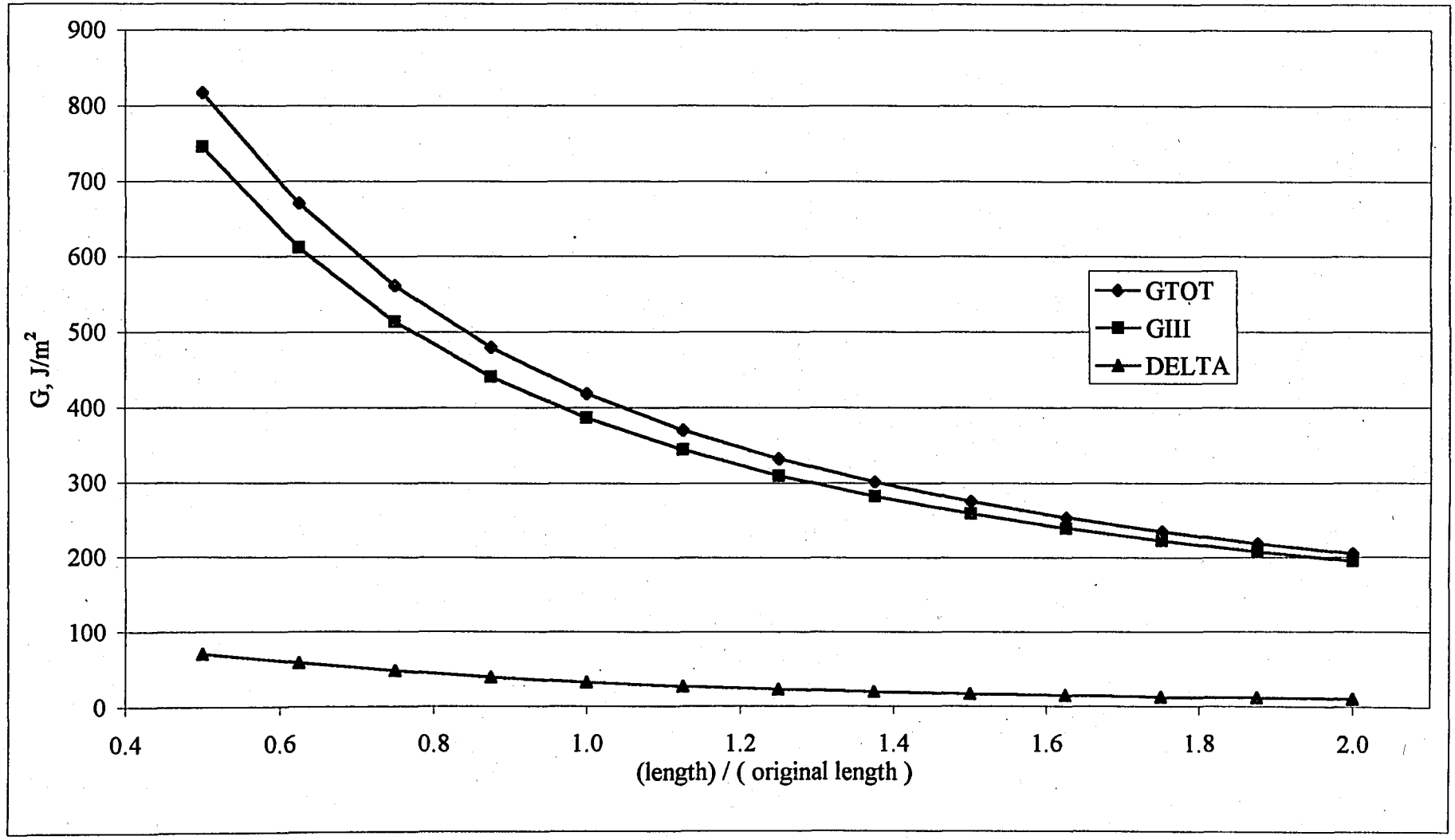

FIGURE 6.13. Variation of the percentage of total strain energy release rat, G_{total}, G_{III}, and their difference with specimen length, only for a/B=1/2.

It can be concluded that the percentage of mode III component of strain energy release rate increases with increasing length. Recalling that the region inside the loading points is in pure torsion loading, this conlusion was expected, because if the length of the specimen is increasing, the ratio of the areas inside the loading points to the remaining areas is also increasing.

6.3.2. Variation of G_{III} Percentage with Width

Similar to the specimen length, specimen width should also have an effect on the percentage of the mode III component of strain energy release rate, G_{III}. Therefore the effect of width is also investigated.

Width is the dimension perpendicular to the crack front. The width is varied from the half of the specimen of Lee to the 1.5 times the size of the original specimen (Figure 6.15) . The finite element batch file is reorganized.

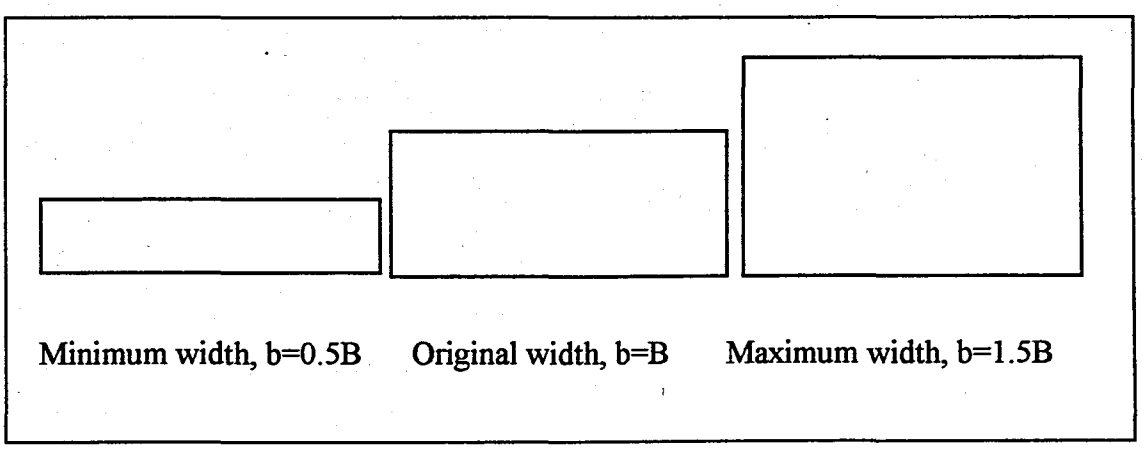

FIGURE 6.15. Comparison of the minimum, original and maximum widths of the modelled ECT specimen.

Similar to the previous analysis, behavior of G_{total} is also reported. The results can be seen in table 6.4, figures 6.16 and 6.17.

TABLE 6.4. Variation of the percentage of mode III component of strain energy release rate, G_{III}%, and total strain energy release rate, G_{total}, with normalized specimen width.

	a/B=1/2		a/B=1/3
L/L(original)	G_{tot}	%G_{III}	%G_{III}
0.5	2273.636	96.90	97.36
0.625	1281.589	96.47	
0.75	837.856	94.87	96.27
0.875	576.661	93.53	
1	418.093	92.39	92.71
1.125	314.576	91.19	
1.25	244.277	90.17	90.22
1.375	193.6187	89.37	
1.5	156.127	88.77	88.38

Unlike the effect of length, percentage of mode III component of strain energy release rate, G_{III}, decreases as the width increases. For a specimen with the half of the width of the original specimen G_{III} is 96.9 per cent. The values of the percentage of mode III component of strain energy release rate, G_{III}, for the models having a crack-to-width ratio of 1/3 are slightly higher except the last data point. The trend is very similar.

Total strain energy release rate, G_{total}, decreases as the specimen dimension increases. This means that to achieve fracture, a higher load is needed for larger specimen, knowing the fact that critical strain energy release rate or fracture toughness is constant.

It can be concluded that the percentage of mode III component of strain energy release rate, G_{III}, decreases as the specimen width increases.

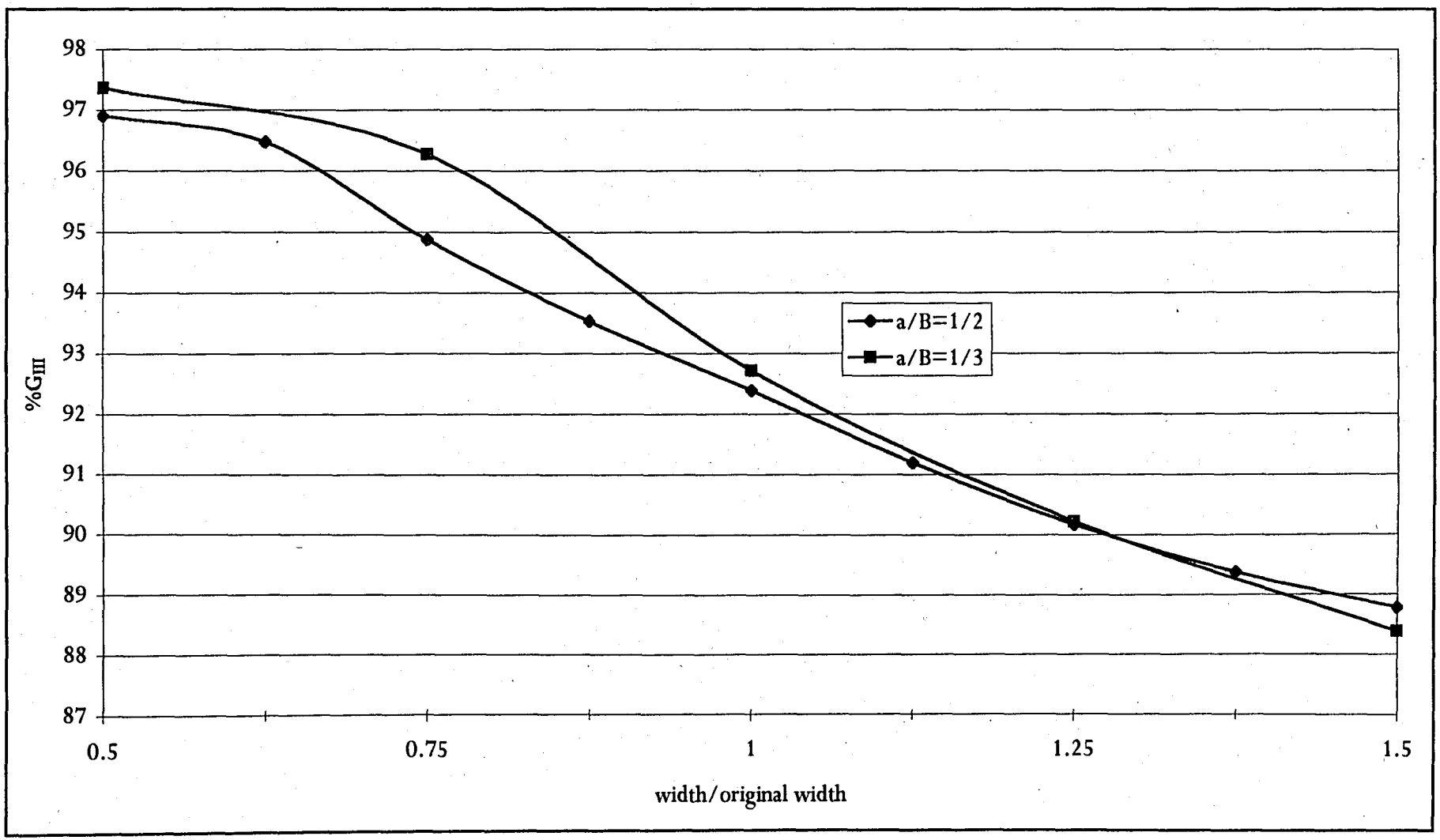

FIGURE 6.16. Variation of mode III component of strain energy release rate, G_{III}, with specimen width, for a/B=1/2 and 1/3

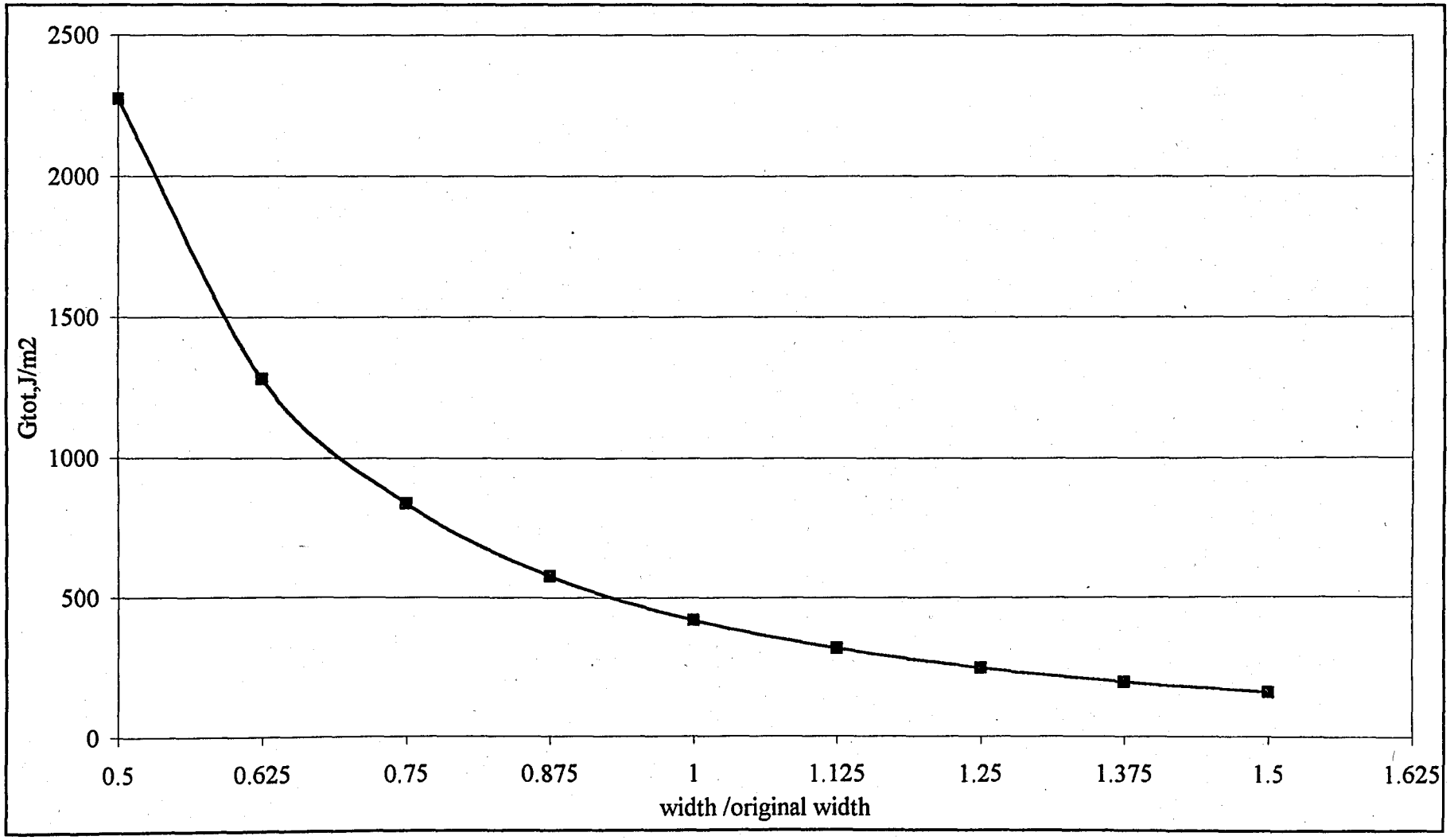

FIGURE 6.17. Variation of total strain energy release rate, G_{total}, with specimen width, only for a/B=1/2.

6.3.3. Variation of G_{III} Percentage with both Length and Width

Since the effect of specimen width and length on the percentage of mode III component of strain energy release rate, G_{III}, is contrasting, their simultaneous effect should also be examined. The size of the specimen altered from (half of the original width)x(half of the original length) to (1.5 times the original width) x (1.5 times the original length) (Figure 6.18).

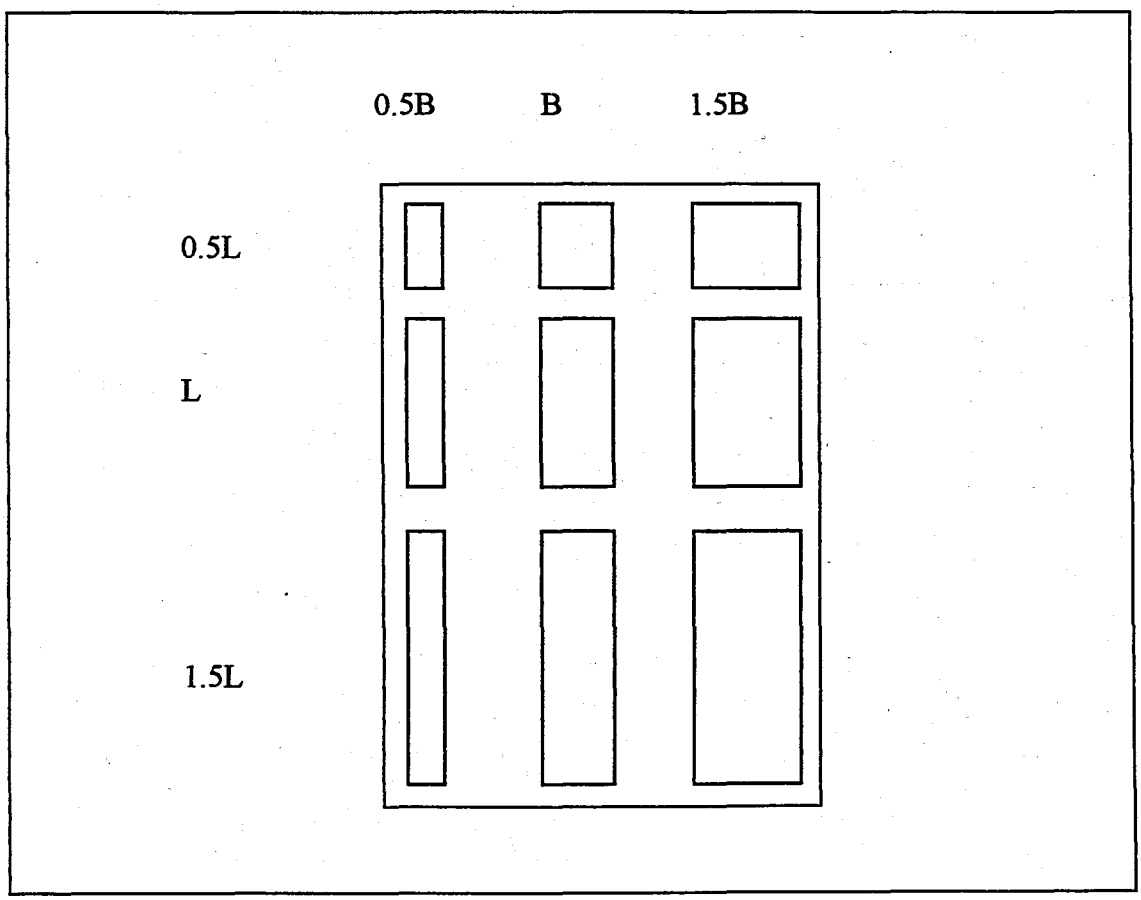

FIGURE 6.18. Comparison of the minimum, original and maximum sizes of the modelled ECT specimen.

The results are listed in table 6.5, for the specimen having crack-to-width ratio of 1/2 and 1/3. Surface plots are attained for G_{III} (for a/B=1/2 and 1/3) and G_{total} (only for a/B=1/2) in figures 6.19, 6.20 and 6.21, respectively. Besides, the same data is reorganized such that the behavior of G_{III} (for a/B=1/2 and 1/3) and G_{total} (only for a/B=1/2) can be plotted against length to width ratio in figures 6.22, 6.23 and 6.24, respectively. The L/B ratio of the original specimen is 88.9/38.1=2.333.

TABLE 6.5. Variation of the percentage of mode III component of strain energy release rate, G_{III}%, with normalized specimen dimensions for crack-to-width ratio of (a) 1/2 and (b) 1/3.

(a)	%G_{III}	WIDTH				
		0.5	0.75	1	1.25	1.5
LENGTH	0.5	94.54	92.36	91.31	90.60	89.97
	0.625	95.45	93.13	91.25	90.28	89.90
	0.75	96.07	93.83	91.50	90.01	89.41
	0.875	96.53	94.39	91.93	89.96	88.96
	1	96.90	94.87	92.39	90.17	88.77
	1.125	97.18	95.29	92.89	90.52	88.84
	1.25	97.40	95.66	93.28	90.86	88.99
	1.375	97.57	95.95	93.65	91.28	89.23
	1.5	97.74	96.18	94.02	91.61	89.51

(b)	%G_{III}	WIDTH				
		0.5	0.75	1	1.25	1.5
LENGTH	0.5	95.03	93.20	90.50	88.29	86.68
	0.75	97.30	94.55	92.28	89.30	87.49
	1	97.36	96.27	92.71	90.22	88.38
	1.25	97.94	96.28	93.64	91.13	88.99
	1.5	98.32	96.83	94.40	91.99	89.78

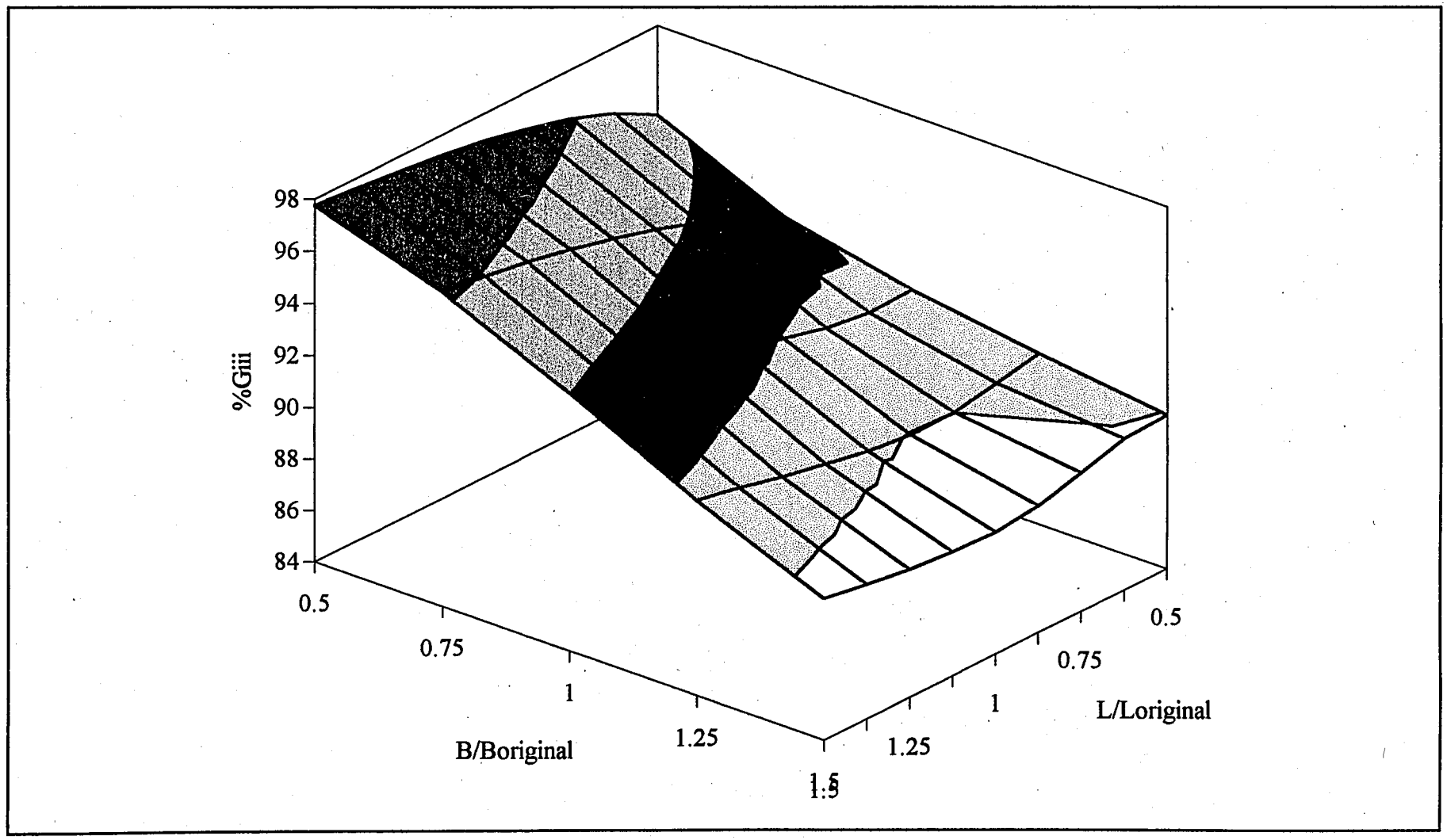

FIGURE 6.19. Variation of mode III component of strain energy release rate, G_{III}, with specimen dimensions, (both length and width), a/B=1/2.

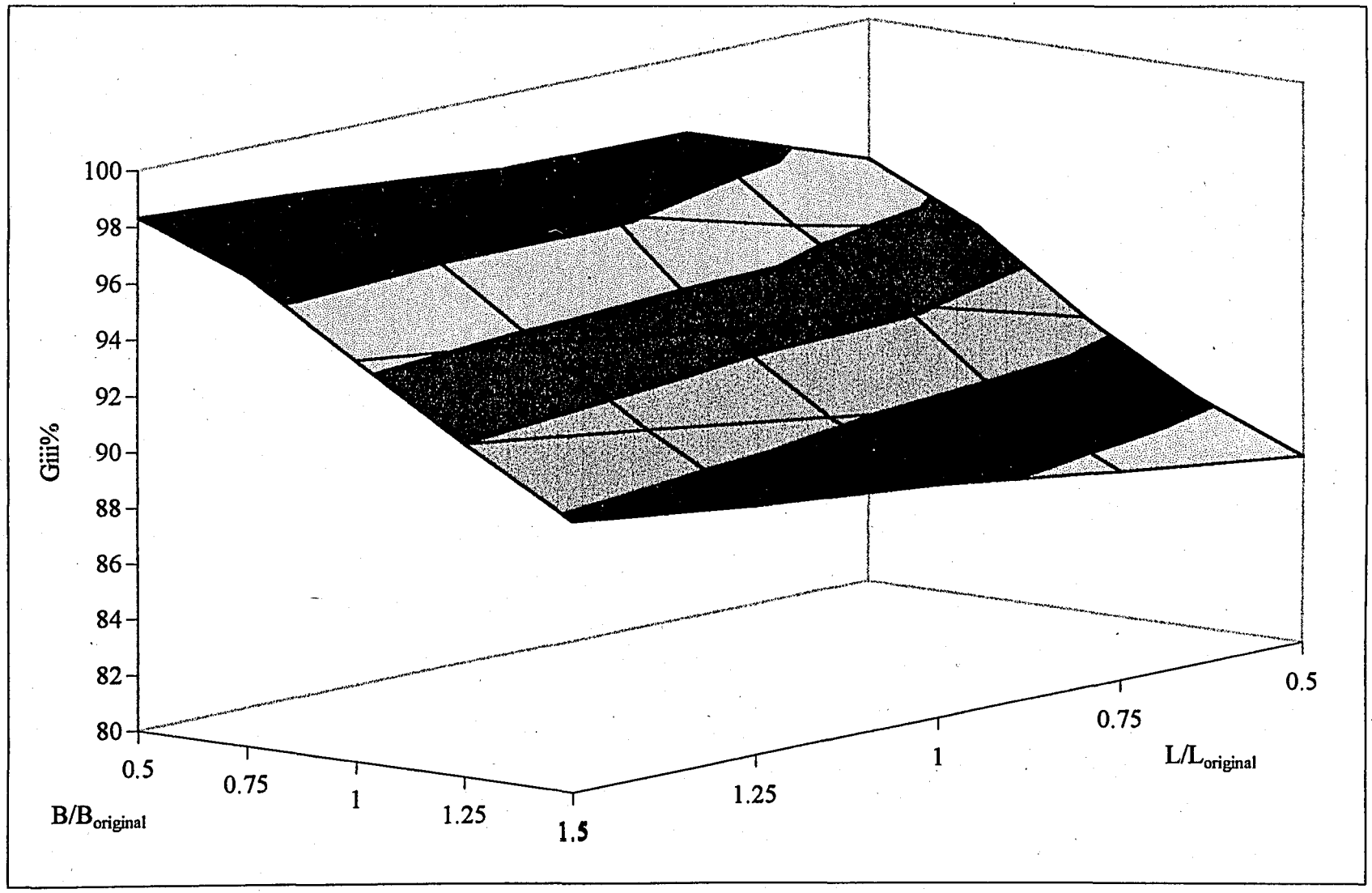

FIGURE 6.20. Variation of mode III component of strain energy release rate, G_{III}, with specimen dimensions (both length and width), for a/B=1/3.

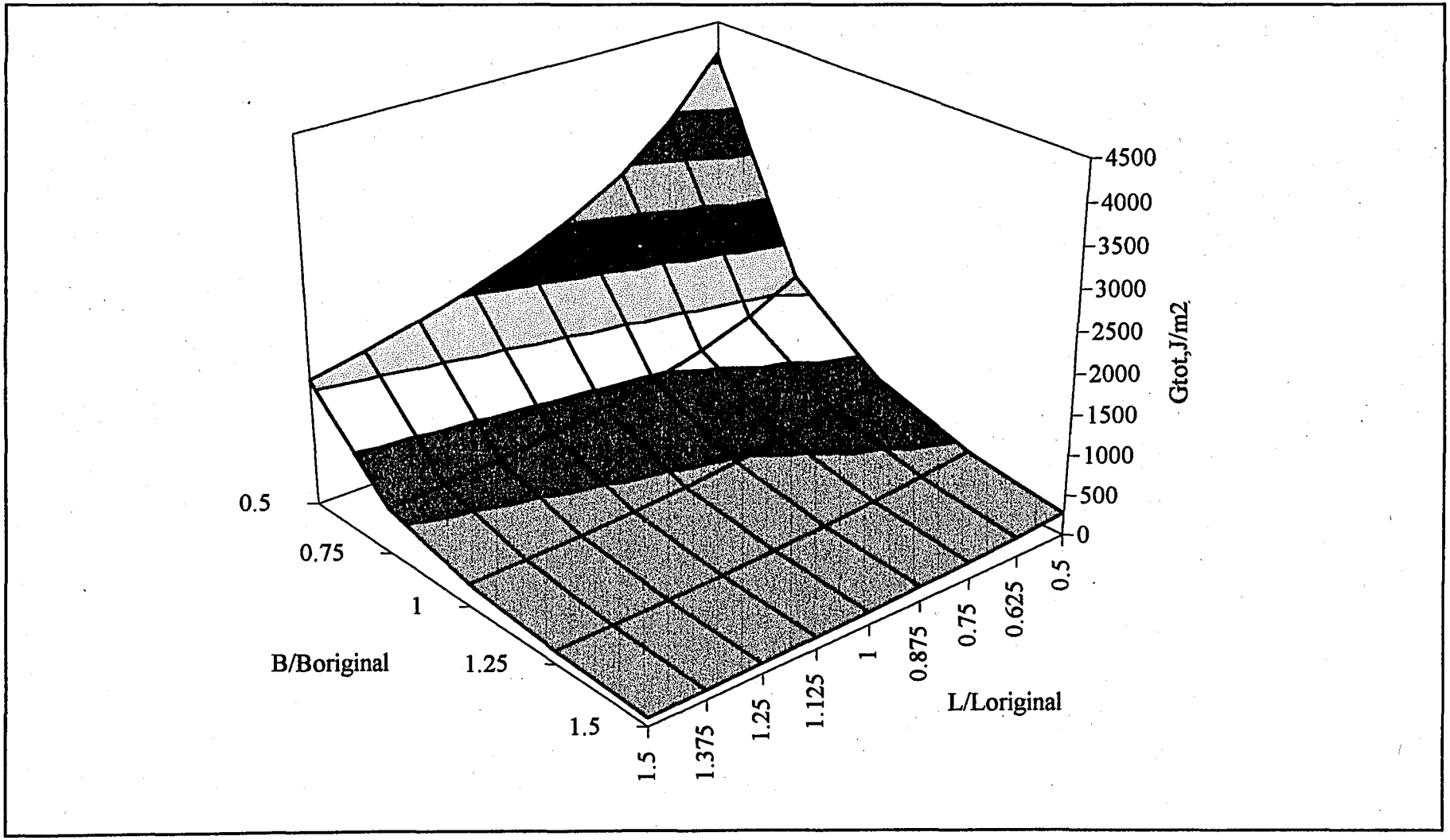

FIGURE 6.21. Variation of total strain energy release rate, G_{total}, with specimen dimensions, (both length and width), for a/B=1/2.

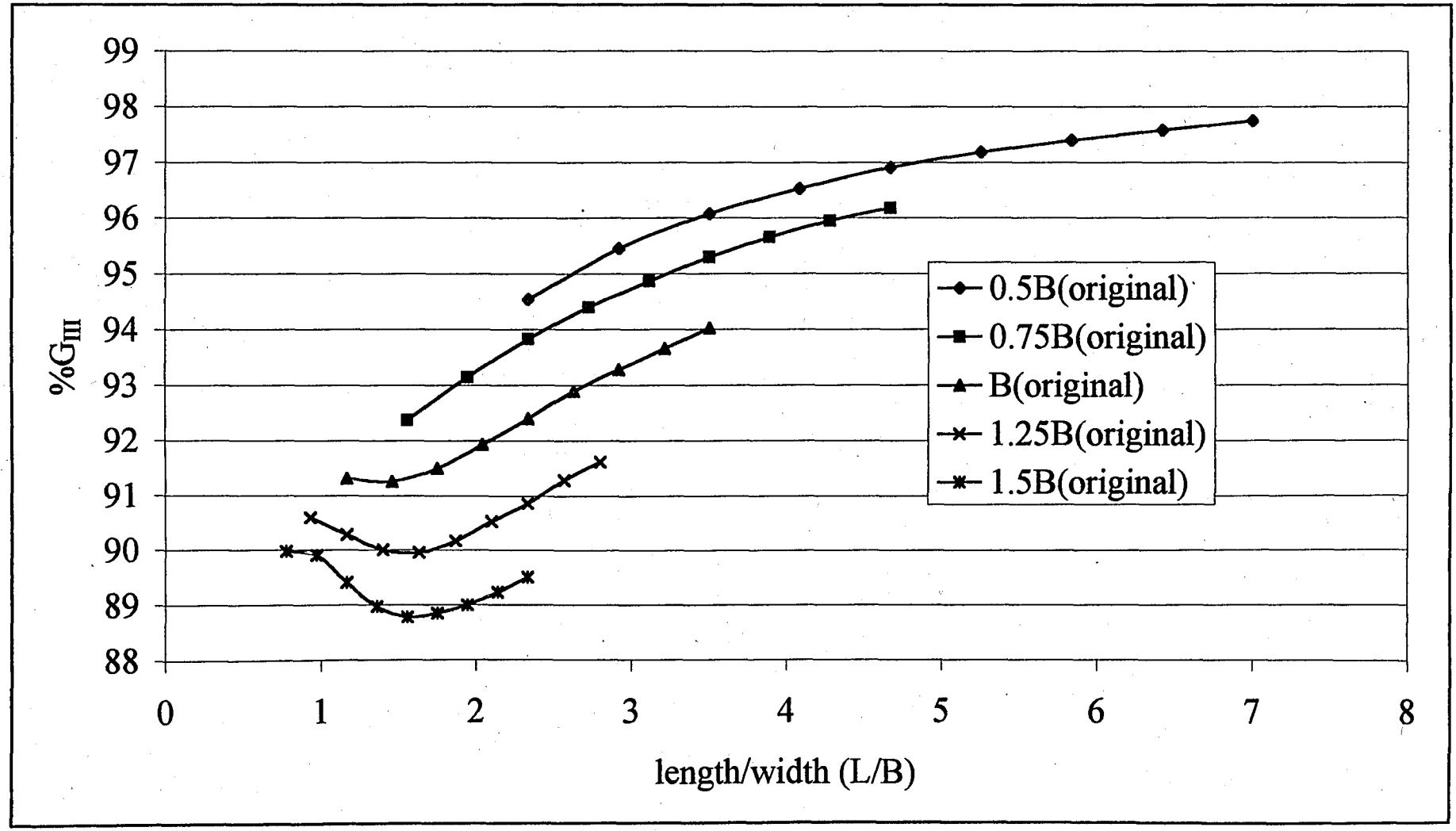

FIGURE 6.22. Variation of mode III component of strain energy release rate, G_{III}, with specimen dimensions (with length/width), a/B=1/2.

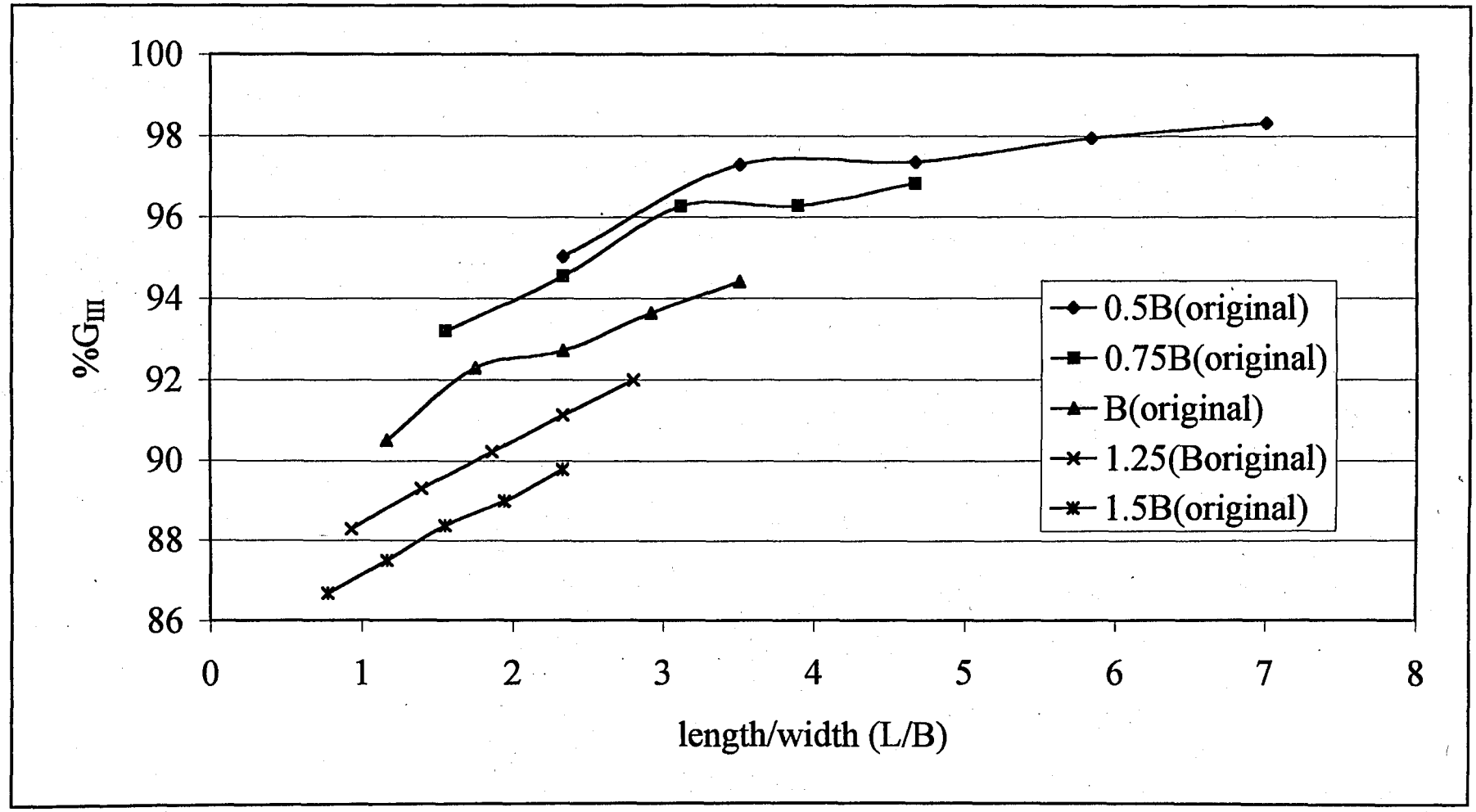

FIGURE 6.23. Variattion of mode III component of strain energy release rate, G_{III}, with specimen dimensions (with length/width), a/B=1/2.

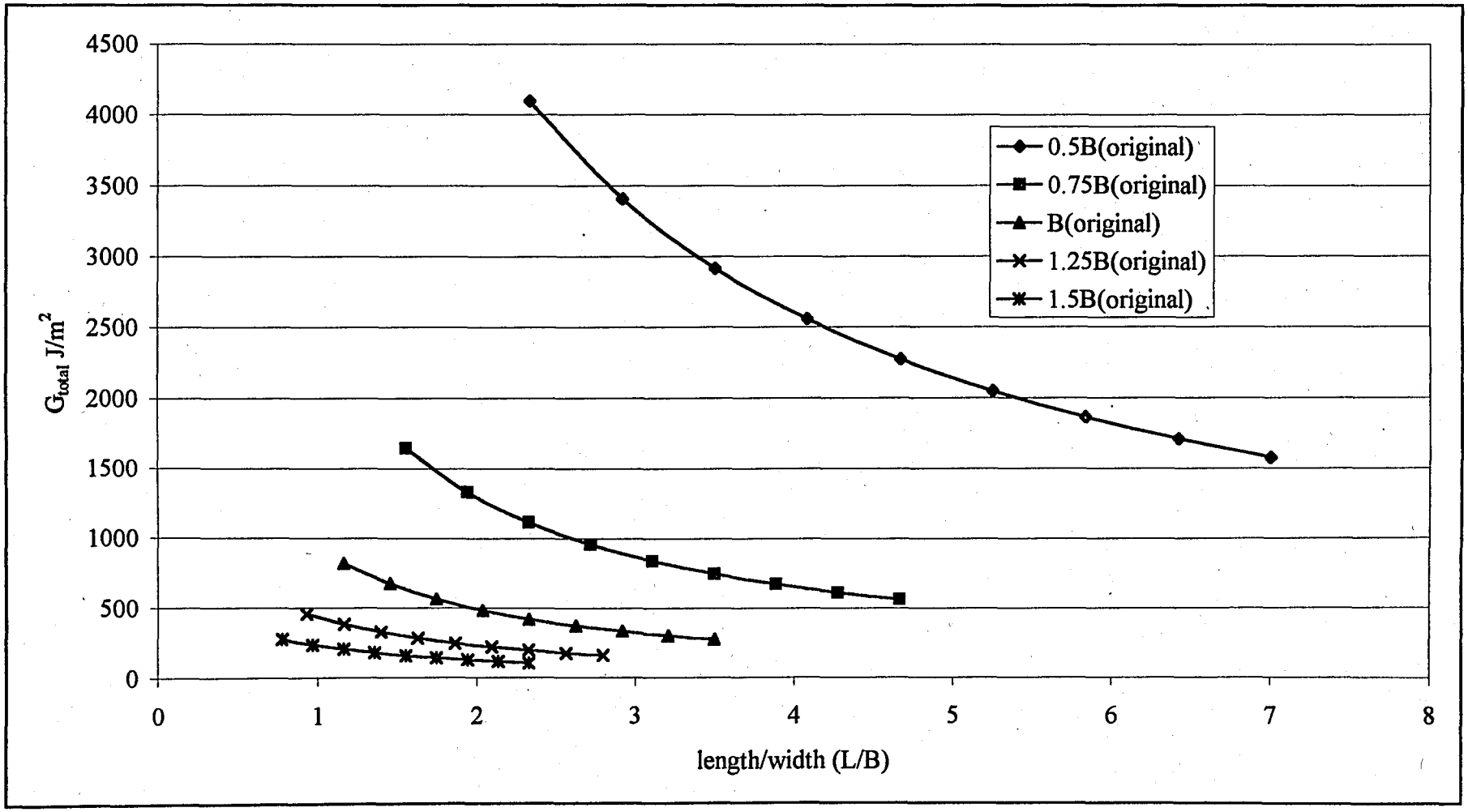

FIGURE 6.24. Variation of total strain energy release rate, G_{total}, with specimen dimensions (with length/width), a/B=1/2 .

As can be seen from the table and the figures the highest value of the percentage of G_{III} is obtained when the length is maximum ($1.5L_{original}$) and the width is minimum ($0.5B_{original}$), e.g., the model with highest length to width ratio of 7. The value the percentage of G_{III} for that configuration becomes 97.7 and 98.32 for crack to width ratio (a/B) of 1/2 and 1/3, respectively. Since for same L/B ratio different values are observed the length to width ratio is not the only independent parameter. However the plateou regions on the surface plots indicate that the percentage of G_{III} is very close to its maximum value providing that the specimen remains "plate" and does not become a "beam". It is clear that the total strain energy release rate decreases as the specimen size increases. Therefore the obtained data can be used to redesign the testing fixture of edge crack torsion specimen.

8. CONCLUSION

The purpose of this thesis is to contribute to the characterization of advanced structural composite materials. Since mode I and mode II fracture toughness tests have already been well established, the study is focused on the examination of mode III interlaminar fracture using the edge crack torsion (ECT) specimen, which proclaims the most promising configuration.

In this thesis a three dimensional finite element model of edge crack torsion (ECT) specimen is constructed. The model is verified satisfactorily with the previous studies reported in the literature (Lee 1993 and Li et al 1997).

The model is validated by reproducing the finite element analysis of Li et al. (1997). Their finite element analysis revealed that the percentage of mode III component of strain energy release rate, G_{III}, is 92 per cent, and the total strain energy release rate, G_{Total}, as 1.35 kJ/m^{-2}. The reproduced analysis gave 91.9 per cent and 1.38 kJ/m^{-2}. The experimental work of Li et al. (1997) yielded a total strain energy release rate of 1.42 kJ/m^2.

A further validation is carried out by modeling the ECT specimen used by Lee (1993). The compliance is determined from the finite element analysis. Its value is very close to the value obtained by shear deformation theory analysis of Li and Wang (1994), and has an error of 0.001 per cent.

The evaluated three dimensional finite element model is used to investigate the effect of specimen dimensions on the percentage of mode III component of strain energy release rate, G_{III}. Series of finite element analyses are done to examine models with different dimensions. Two sets of analyses are carried to model normalized crack lengths of 1/2 and 1/3. The results showed that the percentage of G_{III} increases up to 98 per cent as the specimen length increases to 133.4 mm (1.5 times the length of original specimen proposed by Lee (1993)) and as the width decreases to 19.1 mm (the half of the original specimen). The corresponding aspect ratio (length/width) changes from 2.333 to 7.

Recalling that the percentage of G_{III} of the original specimen (Lee 1993) is 92 per cent, redesigning the testing of the edge crack torsion specimen with the new dimensions will provide a much pure (around 98 per cent) mode III interlaminar fracture loading.

Although the results for both crack lengths is very close a slight deviation is observed. A further study may focus on the effect of crack size on the percentage of the mode III component of strain energy release rate. A second and important research topic may be the redesign of fixture of the edge crack torsion specimen and testing of edge crack torsion specimen for mode III interlaminar fracture toughness.

APPENDIX. FINITE ELEMENT CODES

Main.log

```
/BATCH
/COM,ANSYS REVISION  5.2                14:42:20  10/02/1997
/input,start,ans    ,/ansys52/docu/,,,,,,,,,,,,,,,,1
/TITLE,ECT OPTIMIZATION
/PREP7
 ! ANSYS BATCH FILE WRITTEN BY GOKCEN @aug 1998
!***************** !define elements
ET,1,SOLID46
ET,2,CONTAC49
!***************** !define real constants
R,1
RMODIF,1,1,7,0,0,0,
RMODIF,1,7,0,
RMODIF,1,13,1,-45,0.00013,1,45,0.00013,
RMODIF,1,19,1,-45,0.00013,1,45,0.00013,
RMODIF,1,25,1,-45,0.00013,1,45,0.00013,
RMODIF,1,31,1,90 ,0.00013,        !***************** ! stacking sequence
R,2
RMODIF,2,1,7,0,0,0,.
RMODIF,2,7,0,
RMODIF,2,13,1, 90,0.00013,1,45,0.00013,
RMODIF,2,19,1,-45,0.00013,1,45,0.00013,
RMODIF,2,25,1,-45,0.00013,1,45,0.00013,
RMODIF,2,31,1,-45,0.00013,        !***************** ! stacking sequence
R,3,2200000, , , ,.13, ,          !***************** ! contact element
!*****************!read material properties
MPREAD,ectmater,mt,
!**************
!w3          0.75*38.1E-3
!w5    full  38.1e-3
!w7          1.25*38.1E-3
!w9    1.5   1.5*38.1e-3
!*****************
*SET,L,88.9E-3 /2    !*****************!LENGTH
*set,W,0.5*38.1e-3   !*****************!WIDTH
*SET,FAC,3           !*****************!CRACK RATIO
FINISH
n=1
```

```
L=88.9E-3/2+(N-1)*8.89E-3 !****************** !LENGTH
/PREP7
VSEL,ALL
ASEL,ALL
KSEL,ALL
ESEL,ALL
NSEL,ALL
!******************!create solid model
BLOCK,     0, 6.35E-3,      0, 3.15E-3,0,1.82E-3,
BLOCK,     0, 6.35E-3, 3.15E-3, W-W/FAC,0,1.82E-3,
BLOCK,     0, 6.35E-3, W-W/FAC,W-3.15E-3,0,1.82E-3,
BLOCK,     0, 6.35E-3,W-3.15E-3,      W,0,1.82E-3,
BLOCK, 6.35E-3,L-6.35E-3,      0, 3.15E-3,0,1.82E-3,
BLOCK, 6.35E-3,L-6.35E-3, 3.15E-3, W-W/FAC,0,1.82E-3,
BLOCK, 6.35E-3,L-6.35E-3, W-W/FAC,W-3.15E-3,0,1.82E-3,
BLOCK, 6.35E-3,L-6.35E-3,W-3.15E-3,      W,0,1.82E-3,
BLOCK,L-6.35E-3,      L,      0, 3.15E-3,0,1.82E-3,
BLOCK,L-6.35E-3,      L, 3.15E-3, W-W/FAC,0,1.82E-3,
BLOCK,L-6.35E-3,      L, W-W/FAC,W-3.15E-3,0,1.82E-3,
BLOCK,L-6.35E-3,      L,W-3.15E-3,      W,0,1.82E-3,
VGEN,2,ALL, , , , ,1.82E-3, ,0                    !copy
VSEL,S,LOC,Z,1.85E-3,5E-3,,1
VGLUE,ALL                                         !glue
VSEL,S,LOC,Z,0,1.7E-3,,1
VGLUE,ALL                                         !glue
!******************!mesh
LSEL,S,LOC,X, 10E-3,L-10E-3
LSEL,A,LOC,X, 1E-3,  6E-3,
LSEL,A,LOC,X,L-4E-3,L- 1E-3,
LESIZE,ALL,3.18E-3,
LSEL,S,LOC,Y,4E-3,W/2,
LESIZE,ALL, , ,10,1/8,1
LSEL,S,LOC,Y,(w/3-3.15e-3)/2+2/3*w-0.0000001,(w/3-3.15e-3)/2+2/3*w+0.0000001
LESIZE,ALL, , ,4,6,1
LSEL,S,LOC,Z,0.5E-3,1.5E-3
LSEL,A,LOC,Z,2.0E-3,3.5E-3,
LESIZE,ALL, , ,2,1,
LSEL,ALL
LESIZE,ALL,,,1,,,
VSEL,ALL
ASEL,ALL
KSEL,ALL
ESEL,ALL
NSEL,ALL
TYPE,1,
MAT,1,
REAL,1,
VMESH,1,50,,
```

```
!*****************!modeling of crack surface
NSEL,S,LOC,Z,-.1E-3,.92E-3
ESLN,S,1
EMODIF,ALL,REAL,2                    !element attributes
NSEL,S,LOC,Z,1.8E-3,2.74E-3
ESLN,S,1
EMODIF,ALL,REAL,2                    !element attributes
NSEL,S,LOC,Z,1.81E-3, 1.83E-3
NSEL,R,LOC,Y,     0,W-W/FAC+0.2E-3
NUMMRG,NODE, , ,                     ! merge
!*****************!create components
VSEL,S,LOC,Z,2E-3,3.8E-3             !up1
NSLV,S,1
NSEL,R,LOC,Y,w-12.45e-3,50
NSEL,R,LOC,Z, 1.81E-3, 1.83E-3
NSEL,R,LOC,Y, 3*W/4,39E-1
NSEL,R,LOC,X,-.1E-1  ,.159E-1
CM,UP1,NODE
VSEL,S,LOC,Z,2E-3,3.8E-3             !up2
NSLV,S,1
NSEL,R,LOC,Y,w-12.45e-3 ,50
NSEL,R,LOC,Z, 1.81E-3 , 1.83E-3
NSEL,R,LOC,Y,  3*W/4,  39E-1
NSEL,R,LOC,X,L-.159E-1 ,L+.1E-3
CM,UP2,NODE
VSEL,S,LOC,Z,-.1E-3,1.85E-3                  !down1
NSLV,S,1
NSEL,R,LOC,Y, w-12.45e-3 ,50
NSEL,R,LOC,Z, 1.81E-3 , 1.83E-3
NSEL,R,LOC,Y,  3*W/4,  39E-1
NSEL,R,LOC,X, -.1E-1  ,  .159E-1
CM,DOWN1,NODE
VSEL,S,LOC,Z,-.1E-3,1.85E-3                  !down2
NSLV,S,1
NSEL,R,LOC,Y,w-12.45e-3 ,50
NSEL,R,LOC,Z, 1.81E-3 , 1.83E-3
NSEL,R,LOC,Y,  W*3/4,  39E-1
NSEL,R,LOC,X,L-.159E-1,L+.1E-3
CM,DOWN2,NODE
!*****************!create contact elements
VSEL,ALL
ASEL,ALL
LSEL,ALL
KSEL,ALL
ESEL,ALL
NSEL,ALL
ALLSEL,ALL
TYPE,2,
```

```
MAT,1,
REAL,3,
ESYS,0,
GCGEN,DOWN1,UP1,4, ,TOP,
GCGEN,UP2,DOWN2,4, ,TOP,
FINISH
/SOLU
!*****************!apply loads
NSEL,S,LOC,Z,-.1E-3  ,.01E-3     !bottom left
NSEL,R,LOC,X, .634E-2,.636E-2
NSEL,R,LOC,Y, W-3.15E-3
D,ALL, ,0, , , ,UX,UZ
NSEL,S,LOC,Z,3.6E-3  ,4E-3          !top left
NSEL,R,LOC,X, .634E-2, .636E-2
NSEL,R,LOC,Y, .314E-2, .316E-2
D,ALL, ,0, , , ,UX,UY,UZ
NSEL,S,LOC,Z,3.6E-3   ,4E-3         !top right
NSEL,R,LOC,Y, W-3.15E-3
NSEL,R,LOC,X,L-.634E-2,L-.636E-2
D,ALL, ,-.001, , , ,UZ
NSEL,S,LOC,Z,-.1E-3   ,.01E-3       !bottom right
NSEL,R,LOC,Y, .314E-2 ,.316E-2
NSEL,R,LOC,X,L-.634E-2,L-.636E-2
D,ALL, ,0, , , ,UY,UZ
!*****************!solve
VSEL,ALL
ASEL,ALL
LSEL,ALL
KSEL,ALL
ESEL,ALL
NSEL,ALL
ALLSEL,ALL
SOLVE
FINISH
SAVE,ectl%n%w1,db
!************************************************
```

Ectmater.mt

```
/COM,ANSYS REVISION 5.2                17:04:55   09/19/1997
!************material properties:
 MPTEMP
MPTEMP,    1, 0.0000000E+00,
MPDATA,EX ,    1 ,   1, 0.1650000E+12,
 MPTEMP
MPTEMP,    1, 0.0000000E+00,
MPDATA,EY ,    1 ,   1, 0.1030000E+11,
 MPTEMP
MPTEMP,    1, 0.0000000E+00,
MPDATA,EZ ,    1 ,   1, 0.1030000E+11,
 MPTEMP
MPTEMP,    1, 0.0000000E+00,
MPDATA,NUXY,   1 ,   1, 0.1747879E-01,
 MPTEMP
MPTEMP,    1, 0.0000000E+00,
MPDATA,NUYZ,   1 ,   1, 0.2800000E+00,
 MPTEMP
MPTEMP,    1, 0.0000000E+00,
MPDATA,NUXZ,   1 ,   1, 0.1747879E-01,
 MPTEMP
MPTEMP,    1, 0.0000000E+00,
MPDATA,GXY ,   1 ,   1, 0.5500000E+10,
 MPTEMP
MPTEMP,    1, 0.0000000E+00,
MPDATA,GYZ ,   1 ,   1, 0.5500000E+10,
 MPTEMP
MPTEMP,    1, 0.0000000E+00,
MPDATA,GXZ ,   1 ,   1, 0.5500000E+10,
 MPTEMP
MPTEMP,    1, 0.0000000E+00,
MPDATA,EMIS,   1 ,   1, 0.1000000E+01,
 MPTEMP
MPTEMP,    1, 0.0000000E+00,
MPDATA,PRXY,   1 ,   1, 0.2800000E+00,
 MPTEMP
MPTEMP,    1, 0.0000000E+00,
MPDATA,PRYZ,   1 ,   1, 0.2800000E+00,
 MPTEMP
MPTEMP,    1, 0.0000000E+00,
MPDATA,PRXZ,   1 ,   1, 0.2800000E+00,
```

Postpros.log

```
/COM,ANSYS REVISION 5.2                14:42:20   10/02/1997
/TITLE,ECT OPTIMIZATION
!SYMBOLS USED:
!N              :analysis no
!L              :length of the specimen
!Nfor           :number of the node at the crack tip
!Nmax           :node which has the higher number, near the tip
!Nmin           :node which has the lower number, near the tip
!maxux:ux of Nmax
!minux :ux of Nmin
!maxuy:uy of Nmax
!minuy :uy of Nmin
!maxuz:uz of Nmax
!minuz :uz of Nmin
!get the values of wii
!w11            :lower bound of mid-node          (do not set the exact value)
!w12            :upper bound of mid-node
!w21            :lower bound of the near-mid-node  (do not set the exact value)
!w22            :upper bound of the near-mid-node
*set,w11, 0.12699E-01
*set,w12, 0.12701E-01
*set,w21, 0.12963E-01
*set,w22, 0.12965E-01
*ask,N
L=88.9E-3/2+(N-1)*8.89E-3
/POST1
/output,res%N%,doc,/home/ect/ansys/,
/output
VSEL,ALL
ASEL,ALL
LSEL,ALL
KSEL,ALL
ESEL,ALL
NSEL,ALL
! first 3 nodes
!*****************************************************************first
node x=0
NSEL,S,LOC,Z, 1.81E-3, 1.83E-3          !nodes-tip
NSEL,R,LOC,Y,w11,w12
NSEL,R,LOC,X,0.001E-3,-0,001e-3
*GET,Nfor,NODE,0,NUM,MIN
NSEL,S,LOC,Z, 1.81E-3, 1.83E-3          !nodes-neartip
NSEL,R,LOC,Y,w21,w22
```

```
NSEL,R,LOC,X,0.001E-3,-0,001e-3
                *GET,Nmax,NODE,0,NUM,MAX
                *GET,Nmin,NODE,0,NUM,MIN
                *get,maxux,node,Nmax,U,x,
                *get,maxuy,node,Nmax,U,y,
                *get,maxuz,node,Nmax,U,z,
                *get,minux,node,Nmin,U,x,
                *get,minuy,node,Nmin,U,y,
                *get,minuz,node,Nmin,U,z,
I=1
/output,res%N%,doc,/home/ect/ansys/,append
                *VWRITE,I,Nfor,Nmax,Nmin,maxux,minux,maxuy,minuy,maxuz,minuz
(F3.0,F7.0,F7.0,F7.0,F11.8,F11.8,F11.8,F11.8,F11.8,F11.8)
/output
!*****************************************************************first
node
NSEL,S,LOC,Z, 1.81E-3, 1.83E-3          !nodes-tip
NSEL,R,LOC,Y,w11,w12
NSEL,R,LOC,X,3.174E-3,3.176e-3
*GET,Nfor,NODE,0,NUM,MIN
NSEL,S,LOC,Z, 1.81E-3, 1.83E-3          !nodes-neartip
NSEL,R,LOC,Y,w21,w22
NSEL,R,LOC,X,3.174E-3,3.176e-3
                *GET,Nmax,NODE,0,NUM,MAX
                *GET,Nmin,NODE,0,NUM,MIN
                *get,maxux,node,Nmax,U,x,
                *get,maxuy,node,Nmax,U,y,
                *get,maxuz,node,Nmax,U,z,
                *get,minux,node,Nmin,U,x,
                *get,minuy,node,Nmin,U,y,
                *get,minuz,node,Nmin,U,z,
I=1
/output,res%N%,doc,/home/ect/ansys/ ,append
                *VWRITE,I,Nfor,Nmax,Nmin,maxux,minux,maxuy,minuy,maxuz,minuz
(F3.0,F7.0,F7.0,F7.0,F11.8,F11.8,F11.8,F11.8,F11.8,F11.8)
/output
!*****************************************************************2nd node
NSEL,S,LOC,Z, 1.81E-3, 1.83E-3          !nodes-tip
NSEL,R,LOC,Y,w11,w12
NSEL,R,LOC,X,2*3.174E-3,2*3.176e-3
*GET,Nfor,NODE,0,NUM,MIN
NSEL,S,LOC,Z, 1.81E-3, 1.83E-3          !nodes-neartip
NSEL,R,LOC,Y,w21,w22
NSEL,R,LOC,X,2*3.174E-3,2*3.176e-3
*GET,Nmax,NODE,0,NUM,MAX
                *GET,Nmin,NODE,0,NUM,MIN
                *get,maxux,node,Nmax,U,x,
                *get,maxuy,node,Nmax,U,y,
```

```
                *get,maxuz,node,Nmax,U,z,
                *get,minux,node,Nmin,U,x,
                *get,minuy,node,Nmin,U,y,
                *get,minuz,node,Nmin,U,z,
I=2
/output,res%N%,doc,/home/ect/ansys/ ,append
                *VWRITE,I,Nfor,Nmax,Nmin,maxux,minux,maxuy,minuy,maxuz,minuz
(F3.0,F7.0,F7.0,F7.0,F11.8,F11.8,F11.8,F11.8,F11.8,F11.8)
/output
!*********************************************************************
! find the node distances
VSEL,ALL
ASEL,ALL
LSEL,ALL
KSEL,ALL
ESEL,ALL
NSEL,ALL
nsel,s,loc,z,1.81e-3,1.83e-3
nsel,r,loc,y,w11,w12
nsel,r,loc,x,L*2/5,L*3/5
*get,nlow,node,0,num,min
nsel,u,,,nlow
*get,nnext,node,0,num,min
nsel,all
*get,lowux,node,nlow,loc,x
*get,nextux,node,nnext,loc,x
nodedist=nextux-lowux
nodeno=(L-2*6.35e-3)/nodedist
!*********************************************************************LOOP
        *DO ,I,1,nodeno,1
                NSEL,S,LOC,Z, 1.81E-3, 1.83E-3          !nodes-tip
                NSEL,R,LOC,Y,w11,w12
                NSEL,R,LOC,X,I*nodedist+2*3.174E-3,I*nodedist+2*3.176e-3
                *GET,Nfor,NODE,0,NUM,MIN
                NSEL,S,LOC,Z, 1.81E-3, 1.83E-3          !nodes-neartip
                NSEL,R,LOC,Y,w21,w22
                NSEL,R,LOC,X,I*nodedist+2*3.174E-3,I*nodedist+2*3.176e-3
                *GET,Nmax,NODE,0,NUM,MAX
                *GET,Nmin,NODE,0,NUM,MIN
                *get,maxux,node,Nmax,U,x,
                *get,maxuy,node,Nmax,U,y,
                *get,maxuz,node,Nmax,U,z,
                *get,minux,node,Nmin,U,x,
                *get,minuy,node,Nmin,U,y,
                *get,minuz,node,Nmin,U,z,
/output,res%N%,doc,/home/ect/ansys/ ,append
                *VWRITE,I,Nfor,Nmax,Nmin,maxux,minux,maxuy,minuy,maxuz,minuz
(F3.0,F7.0,F7.0,F7.0,F11.8,F11.8,F11.8,F11.8,F11.8,F11.8)
```

```
/output
        *ENDDO

!*****************************************************************LAST node
NSEL,S,LOC,Z, 1.81E-3, 1.83E-3          !nodes-tip
NSEL,R,LOC,Y,w11,w12
NSEL,R,LOC,X,L-3.174E-3,L-3.176e-3
*GET,Nfor,NODE,0,NUM,MIN
NSEL,S,LOC,Z, 1.81E-3, 1.83E-3          !nodes-neartip
NSEL,R,LOC,Y,w21,w22
NSEL,R,LOC,X,L-3.174E-3,L-3.176e-3
*GET,Nmax,NODE,0,NUM,MAX
                *GET,Nmin,NODE,0,NUM,MIN
                *get,maxux,node,Nmax,U,x,
                *get,maxuy,node,Nmax,U,y,
                *get,maxuz,node,Nmax,U,z,
                *get,minux,node,Nmin,U,x,
                *get,minuy,node,Nmin,U,y,
                *get,minuz,node,Nmin,U,z,
I=I+1
/output,res%N%,doc,/home/ect/ansys/ ,append
                *VWRITE,I,Nfor,Nmax,Nmin,maxux,minux,maxuy,minuy,maxuz,minuz
(F3.0,F7.0,F7.0,F7.0,F11.8,F11.8,F11.8,F11.8,F11.8,F11.8)
/output
!*****************************************************************LAST node
x=L
NSEL,S,LOC,Z, 1.81E-3, 1.83E-3          !nodes-tip
NSEL,R,LOC,Y,w11,w12
NSEL,R,LOC,X,L+0.00001,L-0.00001
*GET,Nfor,NODE,0,NUM,MIN
NSEL,S,LOC,Z, 1.81E-3, 1.83E-3          !nodes-neartip
NSEL,R,LOC,Y,w21,w22
NSEL,R,LOC,X,L+0.00001,L-0.00001
*GET,Nmax,NODE,0,NUM,MAX
                *GET,Nmin,NODE,0,NUM,MIN
                *get,maxux,node,Nmax,U,x,
                *get,maxuy,node,Nmax,U,y,
                *get,maxuz,node,Nmax,U,z,
                *get,minux,node,Nmin,U,x,
                *get,minuy,node,Nmin,U,y,
                *get,minuz,node,Nmin,U,z,
I=I+1
/output,res%N%,doc,/home/ect/ansys/ ,append
                *VWRITE,I,Nfor,Nmax,Nmin,maxux,minux,maxuy,minuy,maxuz,minuz
(F3.0,F7.0,F7.0,F7.0,F11.8,F11.8,F11.8,F11.8,F11.8,F11.8)
/output
```

```
!*************************************************************************
                    ! F O R C E
!*************************************************************************
NSEL,S,LOC,Z,0.181e-2,0.275e-2
NSEL,R,LOC,Y,w11-0.02e-1,w12+0.02e-1
ESLN,S,1
NSEL,S,LOC,Z, 1.81E-3, 1.83E-3          !nodes-tip
NSEL,R,LOC,Y,w11,w12
/output,resf%N%,doc,/home/ect/ansys/ ,append
nforce
/output
!*************************************************************************
```

REFERENCES

ANSYS,Users Manual: Elements, Vol. 3, Revision 5.2, Houston, 1995

"Determination of the Mode II Delamination Resistance of Unidirectional Fiber-Reinforced Polymer Laminates Using the End Loaded Split Specimen (ELS)," Version 95-08-04, ESIS, 1995

"Making Consolidated Sheet from Aromatic Polymer Composite APC-2," Data Sheet, ICI Fiberite, 1987

Becht, G., and J. W. Gillespie, Jr, "Design and Analysis of the Cracked Rail Shear Specimen for Mode III Interlaminar Fracture," *Composite Science and Technology*, Vol. 31, pp.143-157, 1988

Becht, G., and J. W. Gillespie, Jr, "Numerical and Experimental Evaluation of the Mode III Interlaminar Fracture Toughness of Composite Materials," *Polymer Composites*, Vol. 10,No. 5, pp.293-304, 1989

Carlsson, L. A., R. B. and Pipes., *Experimantal Characterization of Advanced Composite Materials*, Prentice-Hall Inc., New Jersey, 1987

Carlsson, L.A., Gillespie, J. W. Jr., and R. B. Pipes, "On the Analysis of the End Notched Flexure (ENF) Specimen for Mode II Testing," *Journal of Composite Materials*, Vol. 20, p. 594, 1983

Crews Jr, J. H. and J. R. Reeder, " A Mixed-Mode Bending Apparatus for Delamination Testing," NASA Tech. Memo 100662, 1988

Davies, P., and M. L. Benzeggah, "Interlaminar Mode-I Fracture Testing," in K. Friedrich (Ed.), *Application of Fracture Mechanics to Composite Materials*, pp. 81-112, Elsevier Science Publishers B. V.,1989

Donaldson, S. L., "Mode III Interlaminar Fracture Characterization of Composite Materials," *Composite Science and Technology*, Vol.32, pp.225-249, 1988

Ducept, F., Davies, P.,and D. Gamby, " An Experimental Study to Validate Tests Used to Determine Mixed Mode Failure Criteria of Glass/Epoxy Composites," *Composites*, Part A, Vol. 28A, pp. 719-729, 1997.

Ersoy, N. B., "Mode II Interlaminar testing of Carbon Fiber Reinforced Plastics," FBE/ME-01/95-06, Boðaziçi University, 1994

Ersoy, N. B., "Prediction and Measurement of Residual Stresses in Layered Composites," Ph. D. Dissertation, Boðaziçi University, 1998

Garg, A. C., "Delamination -A Damage Mode in Composite Structures," *Engineering Fracture Mechanics*, Vol. 29, No. 5, pp. 557-584, 1988.

Gillespie, J. W., Jr., Carlsson, L. A., and R. S. Pipes, "Finite Element Analysis of the End-Notched Flexure Specimen for Measuring Mode II Fracture Toughness," *Composite Science and Technology*, Vol. 27, 1986, pp. 177-197.

Hashemi, S., Kinloch A. J., and J. G. Williams, "The Analysis of Interlaminar Fracture in Uniaxial Fibre-Polymer Composites," *Proceedings of the Royal Society of London*, A 427, pp. 173-199,1990

Kim, W.C.,and K. H. Dharan, "A Fracture Control Plan for Composite Structures," *Engineering Fracture Mechanics*, Vol. 34, No.2, pp. 305-324, 1989

Lee, S. M., " An Edge Crack Torsion Method for Mode III Delamination Fracture Testing," *Journal of Composites and Research*, Vol. 15, No. 3, pp. 193-201, Fall 1993.

Lekhinitski, S. G., *Theory of Elasticity of an Anisotropic Elastic Body*, Holden-Day, San Francisco, pp. 175-205, 1963

Li, J., and Y. Wang, "Analysis of a Symmetric Laminate with Mid-plane Free Edge Delamination Under Torsion: Theory and Application to the Edge Crack Torsion (ECT)

Specimen For Mode III Toughness Characterization ," *Engineering Fracture Mechanics*, Vol. 49, No. 2, pp. 179-194, 1994

Li, J., Lee, S. M., Lee, E.W.,and T. K. O'Brien, "Evaluation of the Edge Crack Torsion (ECT) Test For Mode III Interlaminar Fracture Toughness of Laminated Composites", *Journal of Composites Technology and Research*, Vol.19, No. 3, pp. 174-183, 1997

Li, J.and T. K. O'Brien,."Simplified Data Reduction Methods for the ECT Test for Mode III Interlaminar Fracture Toughness," *Journal of Composites Technology and Research*, Vol.18, No.2, pp. 96-101, April 1996

Lokman, G., "Finite Element Analysis of Interlaminar Fracture Toughness of Composite Materials," M. S. Thesis, Boðaziçi University, 1997

Martin, R. H., "Evaluation of the Split Cantilever Beam for Mode III Delamination Testing" in T. K. O'Brien (Ed.), *Composite Materials: Fatigue and Fracture*, Third Volume, ASTM 1110, pp. 243-266, ASTM, Philadelphia, 1991

Masters, John E., "Basic Failure Modes of Continuous Fiber Composites," in T.J. Reinhart (Ed.), *Engineered Materials Handbook*, Vol. 1, Composites ASM International, pp.781-785, 1987

O'Brien, T. K., "Interlaminar Fracture Toughness: The Long Winding Road to Standardization," *Composites*, Part B, 29B, pp. 57-62., 1998

Reeder, J. R and J. H. Crews, Jr, "Mixed-Mode Bending Method for Delamination Testing," *AIAA Journal*, Vol. 28, No. 7, pp. 1270-1276, 1990

Reinhart, T.J., "Introduction to Composites," in T.J. Reinhart (Ed.), *Engineered Materials Handbook*, Vol. 1: Composites, ASM International, pp. 27-34,1987

Robinson , P., and D. Q. Song, " A New Mode III Test for Composites," *Advanced Composite Letters*, Vol. 1., No. 5, pp. 160-164, 1992.

Robinson , P., and D. Q. Song, "Development of an Improved Mode III Delamination Test for Composites," *Composite Science and Technology*, Vol. 52, No. 2, pp. 217-233, 1994.

Russel, A.J., and K. N. Street, "Factors Affecting the Interlaminar fracture of Graphite/Epoxy Laminates," in T. Hayashi and S. Umekawa (Eds.), *Progress in Science and Technology of Composites*, ICCM-IV, p. 279, Tokyo, 1982

Salpekar, S. A. Raju, I. S., and T. K. O'Brien, "Strain Energy Release Rate Analysis of the End-Notched Flexure Specimen Using the Finite-Element Method," *Journal of Composite Technology & Research*, Vol. 10, No. 4, pp. 133-139, Winter 1988

Trethewey, B. R., Jr., Carlsson, L. A., Gillespie, J. W., Jr., and R. B. Pipes, "Mode II Interlaminar Fracture During Static and Fatigue Loading," CCM 86-26, Center for Composite Materials, College of Engineering, University of Delaware, Newark, DE, 1986.

Vardar, Ö., *Fracture Mechanics*, Istanbul, Boðaziçi University Publication, No:453, 1988

Wang, S. S., "Fracture Mechanics for Delamination Problems in Composite Materials," *Journal of Composite Materials*, Vol. 17, pp.210-223, May 1983

Williams, J.G., "The Fracture Mechanics of Delamination Tests," *Journal of Strain Analysis*, Vol 24, No 4, pp. 207-214, 1989